

Rowan University

Rowan Digital Works

---

Theses and Dissertations

---

9-18-2024

# Nanofiber-Hydrogel Composite Scaffold Fabrication Methods for Peripheral Nerve Regeneration

Jacob Lee Carter  
*Rowan University*

Follow this and additional works at: <https://rdw.rowan.edu/etd>



Part of the [Biomedical Engineering and Bioengineering Commons](#), [Materials Science and Engineering Commons](#), and the [Medicine and Health Sciences Commons](#)

---

## Recommended Citation

Carter, Jacob Lee, "Nanofiber-Hydrogel Composite Scaffold Fabrication Methods for Peripheral Nerve Regeneration" (2024). *Theses and Dissertations*. 3290.  
<https://rdw.rowan.edu/etd/3290>

This Thesis is brought to you for free and open access by Rowan Digital Works. It has been accepted for inclusion in Theses and Dissertations by an authorized administrator of Rowan Digital Works. For more information, please contact [graduateresearch@rowan.edu](mailto:graduateresearch@rowan.edu).

**NANOFIBER-HYDROGEL COMPOSITE SCAFFOLD FABRICATION  
METHODS FOR PERIPHERAL NERVE REGENERATION**

by

Jacob Lee Carter

A Thesis

Submitted to the  
Department of Biomedical Engineering  
College of Engineering  
In partial fulfillment of the requirement  
For the degree of  
Master of Science in Biomedical Engineering  
at  
Rowan University  
June 10, 2024

Thesis Chair: Vince Beachley, Ph.D., Professor, Department of Biomedical Engineering

Committee Members:

Sebastián Vega, Ph.D., Associate Professor, Department of Biomedical Engineering  
David Fuller, MD, Chairman and Chief, Department of Orthopaedic Surgery

© 2024 Jacob Lee Carter

## **Dedications**

I would like to dedicate this thesis to my family, who always support me in my goals and put up with all the moods I was in the past many months. I would also like to dedicate this to all my friends who helped me get out of those moods and enjoy my life. I am so thankful for everyone who supported me throughout this journey.

## Acknowledgments

I would first like to thank my advisor and thesis chair, Dr. Vince Beachley, for all his support and guidance throughout my undergraduate and graduate studies, both in research and in the classroom. His insight throughout my work was invaluable and this process would have been immensely more difficult without his knowledge. I am incredibly thankful for all his help throughout my entire college experience, and he has helped shape my experiences for years to come. I would also like to thank my committee members, Dr. Sebastián Vega and Dr. David Fuller, whose council and advice were vital throughout this project and who taught me lessons I will continue to use throughout the rest of my career.

I would next like to thank Dr. Eduard Dedkov for his assistance with this project and all the knowledge he passed to me throughout this process. I would also like to thank the other members of Dr. Beachley and Dr. Vega's lab for their help and guidance on this project, including Nikolas Belanger, Kathleen Wooster, Mohamad Keblawi, Umu Jalloh, Shrey Dalwadi, Dominique Hassinger, and Myranda Sims.

I also thank my friends, whose support was greatly appreciated throughout my research, despite often not understanding anything I would talk about. I would finally like to thank my family, who I am very lucky to have and are always helping me to become the best version of myself that I can be. None of this would have been possible without their love and support.

## **Abstract**

Jacob Lee Carter  
NANOFIBER-HYDROGEL COMPOSITE SCAFFOLD FABRICATION METHODS  
FOR PERIPHERAL NERVE REGENERATION  
2023-2024  
Vince Beachley, Ph.D.  
Master of Science in Biomedical Engineering

Nerve graft conduits (NGCs) are a rapidly advancing field for treating peripheral nerve injuries that aim to guide the growth of regenerating axons across damaged gaps. A more effective NGC can be manufactured by combining the use of nanofibers to act as guidewires within a 3-D hydrogel that imitates the extracellular matrix of nerve tissue. Several methods have been developed to embed aligned nanofibers in an ordered architecture within a hydrogel matrix. The first method involves layer-by-layer additive manufacturing to create NGCs with rows of polycaprolactone (PCL) nanofibers surrounded by a gelatin methacrylate (GelMe) hydrogel in a 3-D structure. A second method where individual films of fibers embedded in hydrogel were rolled was developed, introducing void space throughout the scaffold that allows for easier cell infiltration. The final method uses a sacrificial hydrogel scaffold template to manufacture the scaffold. The desired hydrogel is infiltrated into the template hydrogel and crosslinked before the template's removal, allowing for a much wider variety of hydrogels such as pH or ion responsive materials. It was found that GelMe and hyaluronic acid-based hydrogels limited axon infiltration in a sciatic nerve gap model at the studied weight percent and degrees of crosslinking. This result highlights how the infiltration manufacturing approach may be critical for fabricating aligned nanofiber-hydrogel composite grafts from next generation hydrogels.

## Table of Contents

Abstract .....	v
List of Figures .....	x
List of Tables .....	xii
Chapter 1: Introduction and Background.....	1
1.1 Peripheral Nerve Injury.....	1
1.2 Electrospinning Nanofibers .....	3
1.3 Polymer Hydrogel Properties.....	4
1.4 Current Treatments for Peripheral Nerve Injury.....	6
Chapter 2: Layer-By-Layer Scaffolds.....	12
2.1 Layer-By-Layer Scaffolds Introduction.....	12
2.2 Materials and Methods.....	13
2.2.1 Electrospinning Nanofibers .....	13
2.2.2 Hydrogel Fabrication .....	15
2.2.3 Frame Fiber Density .....	15
2.2.4 Layer-By-Layer Additive Manufacturing.....	16
2.2.5 Large Stack Innovation.....	19
2.2.6 In-Vitro Model.....	20
2.2.7 Sterilization Techniques .....	23
2.2.8 In-Vitro Cell Culture and Imaging.....	23

## Table of Contents (Continued)

2.2.9 Rat Sciatic Nerve Gap Study .....	25
2.2.10 Scaffold Implantation .....	26
2.2.11 Scaffold Explantation and Electrophysiological Evaluation .....	27
2.3 Statistical Analysis.....	28
2.4 Results and Discussion .....	28
2.4.1 Frame Fiber Density .....	28
2.4.2 Sterilization Study.....	29
2.4.3 In-Vitro Cell Migration and Alignment.....	30
2.4.4 Sciatic Nerve Gap Model Results .....	32
Chapter 3: Rolled Film Scaffolds .....	36
3.1 Rolled Film Scaffold Introduction .....	36
3.2 Materials and Methods.....	36
3.2.1 Rolled Film Scaffold Fabrication .....	36
3.2.2 Rat Sciatic Nerve Gap Model .....	39
3.2.3 Scaffold Implantation .....	40
3.2.4 Scaffold Explantation and Electrophysiological Evaluation .....	41
3.2.5 Normal Sciatic Nerve Harvesting .....	42
3.2.6 Paraffin Embedding and Sectioning .....	43
3.2.7 Histological Staining.....	45

## Table of Contents (Continued)

3.2.8 Fluorescent Staining .....	47
3.2.9 Resin-Embedding and Sectioning.....	48
3.2.10 Resin-Embedded Axon Staining.....	50
3.2.11 Slide Imaging.....	51
3.2.12 Axon Quantification and Analysis.....	51
3.3 Statistical Analysis.....	53
3.4 Results and Discussion .....	53
3.4.1 Electrophysiological Muscle Testing.....	53
3.4.2 Histologically Stained Image Analysis.....	55
3.4.3 Fluorescently Stained Image Analysis.....	58
3.4.4 Axon Measurement and Quantification.....	63
Chapter 4: Sacrificial Gelatin Template Scaffold Infiltration.....	71
4.1 Introduction.....	71
4.2 Materials and Methods.....	71
4.2.1 Alginate Infiltration Process .....	71
4.2.2 Alginate Time Infiltration .....	74
4.2.3 Alginate Scaffold Structure Maintenance .....	76
4.2.4 Hyaluronic Acid Scaffold Infiltration.....	77
4.3 Statistical Analysis.....	78

## Table of Contents (Continued)

4.4 Results and Discussion .....	78
4.4.1 Alginate Infiltration and Sacrificial Template Removal.....	78
4.4.2 Alginate Time Infiltration.....	82
4.4.3 Sacrificial Scaffold Template Structure Maintenance .....	87
4.4.4 Sacrificial Scaffold Template HANor Infiltration.....	90
Chapter 5: Conclusions and Future Work.....	95
5.1 Conclusions.....	95
5.2 Future Work .....	96
References.....	99

## List of Figures

Figure	Page
Figure 1. Electrospinning Schematic and Experimental Setup.....	14
Figure 2. Layer-By-Layer Scaffold Assembly Schematic .....	17
Figure 3. In-Vitro Model Assembly and Cell Seeding Schematic.....	22
Figure 4. Surgical Scaffold Placement of LBL-Scaffolds In-Vivo Rat Models .....	27
Figure 5. Electrospun Nanofiber Frame Densities for Different Spin Times .....	29
Figure 6. Sterilization Study Results for Different Concentrations of HCl. Part A is a schematic emphasizing the results seen in Part B.....	30
Figure 7. In-Vitro Model Testing Cell Migration, Infiltration, and Alignment Over 14 Days .....	32
Figure 8. LBL-Scaffold Anterior Tibialis Muscle Weights After Scaffold Explantation .....	35
Figure 9. Rolled Film Scaffold Manufacturing Schematic .....	37
Figure 10. Rolled Film Scaffold Location at Explantation.....	41
Figure 11. Normal Rat Sciatic Nerve Harvesting .....	43
Figure 12. Axon Metrics Quantification Techniques .....	52
Figure 13. Explanted Scaffold-NF Longitudinally Stained Section .....	56
Figure 14. Explanted Scaffold-RF Longitudinally Stained Section .....	57
Figure 15. Explanted Scaffold-RF Cross-Sectionally Stained Section.....	58
Figure 16. Immunofluorescent Stained Regenerating Axons and Schwann Cells in Scaffold-NF.....	60
Figure 17. Neurofilament Visualization in Normal Sciatic Nerve and Experimental Groups.....	61
Figure 18. Schwann Cell and Neurofilament Visualization in Cross-Sectional Imaging .....	62

**List of Figures (Continued)**

Figure	Page
Figure 19. Axons Regenerating Through Remaining Hydrogel in GelMe-RF .....	64
Figure 20. Normal Sciatic Nerve Axons Compared to Experimentally Regenerated Axons .....	65
Figure 21. Axon Metric Quantifications for Normal Sciatic Nerve and Regenerated Sciatic Nerve.....	66
Figure 22. G-Ratio and Nerve Fiber Density of Normal and Regenerated Sciatic Nerve.....	67
Figure 23. Sacrificial Puck Manufacturing and Infiltration with Alginate Schematic .....	73
Figure 24. Sacrificial Template Removal Evidenced by Genipin Crosslinking .....	80
Figure 25. Sacrificial Puck Weights Before, During, and After Infiltration and Removal .....	81
Figure 26. Time Infiltration of Alginate into Varied Weight Percent Sacrificial Gelatin Templates.....	83
Figure 27. Densities of Remaining Infiltrated Alginate Hydrogel after Removal of Varied Weight Percent Gelatin Templates .....	84
Figure 28. Time Infiltration of Alginate into Variously Treated Sacrificial 10% Gelatin Templates.....	85
Figure 29. Swell Capacity of 10 Weight Percent Gelatin Sacrificial Template Pucks.....	86
Figure 30. Scaffold Structure Before and After Alginate Infiltrated and Sacrificial Template Removal .....	88
Figure 31. Scaffold Dimensions Before and After Alginate Infiltrated and Sacrificial Template Removal .....	90
Figure 32. Scaffold Structure Before and After HANor Infiltrated and Sacrificial Template Removal .....	92
Figure 33. Scaffold Dimensions Before and After HANor Infiltrated and Sacrificial Template Removal .....	93

## List of Tables

Table	Page
Table 1. LBL-Scaffold Anterior Tibialis Electrophysiological Muscular Testing Results.....	34
Table 2. Rolled Film Scaffold Anterior Tibialis Electrophysiological Muscular Testing Results.....	54
Table 3. Summary Table of Axon Quantification Metrics for Normal and Regenerated Nerve.....	67

# Chapter 1

## Introduction and Background

### 1.1 Peripheral Nerve Injury

Peripheral nerve injury, often abbreviated PNI, is a broad term that covers many different types of damage to the peripheral nervous system. Over twenty million people in the United States are currently suffering from a form of PNI, with 100,000 of these patients requiring surgery every year [1]. Peripheral nerve injuries can occur from stretching, compressing, or lacerating the nerve, with stretching being the most common form of injury. The upper body is most frequently injured in peripheral nerve injuries, making up 73.5% of PNIs. Motor vehicles accidents are the most commonly seen method of serious nerve injury [2].

Peripheral nerves are responsible for communication between the central nervous system (brain and spinal cord) with the many different systems of the body. These nerves are responsible for maintaining homeostasis within the body, as well as providing sensation and the ability of movement [3]. Sensory neurons are responsible for transmitting signals from the environment to the central nervous system, while motor neurons send signals from the central nervous system to create a contraction within a muscle or muscle system. Autonomic peripheral nerves are responsible for maintaining involuntary systems in the body. There are five degrees of nerve injury, ranging from segmental demyelination (grade I) to axon, endoneurium, and perineurium damaged (grade IV) or complete nerve transection (grade V) [4].

For peripheral nerve injury, there are two main methods for natural recovery. In injuries where only 1/3 or less of the nerve fibers are damaged, the nerve can undergo collateral branching to recover. However, in injuries where most of the nerve fibers are damaged, particularly in instances of crushing or laceration, axonal regeneration is the main mechanism for recovery. Axons within the peripheral nervous system are capable of spontaneously regenerating after injury. An important stage of axonal regeneration is Wallerian degradation. In this process, the distal end of the nerve, now disconnected from the proximal nerve and no longer receiving signals, begins degradation. Glial cells, particularly macrophages, enter the distal nerve area and break down and clear the debris there. However, Schwann cells remain within their basal laminal tubes, referred to as bands of Büngner. Without this process, scarring would occur within the tissue, blocking the regenerating axons from reintervening and recovering [4-6].

Schwann cells are a type of glial cell that provide support for the peripheral nervous system and play a crucial role in the guidance of axon growth. When looking at regenerating axons after an injury, myelinating Schwann cells (MSCs) are crucial for healthy, organized growth [7]. MSCs wrap around all large diameter axons (diameters > 0.1µm), helping to produce the myelin sheath. In addition to myelinating the axons, Schwann cells guide the regeneration of axons by producing longitudinal microchannel structures called bands of Büngner. These tunnels are the basis for the directional growth of the axons and are crucial in recovering from PNI [8]. In the distal end of a nerve injury, these Schwann cells remain to guide the regenerating axons once they bridge the damaged gap.

## 1.2 Electrospinning Nanofibers

Electrospinning is a method commonly used to produce polymer fibers with diameters less than 1  $\mu\text{m}$ , referred to as nanofibers. Electrospinning has gained a lot of traction in recent years due to its ability to consistently form fibers of this size, provide controllability over the produced fiber size and dimensions, and it offers a wide versatility of polymer materials with which it can produce nanofibers from [9].

Nanofibers have become widespread in their applications, particularly in the biomedical field. One particular application is in tissue engineering scaffolds, where nanofibers are used for their ability to greatly promote cell adhesion and infiltration in these scaffolds. Other applications for nanofibers in the biomedical field include blood vessel grafts, engineering bone tissue, controlled drug release, air and liquid filters, and wound healing [10].

During electrospinning, liquid polymer droplets destabilize and elongate in the presence of an electrical field. In many setups, a high voltage system is connected to a needle that is attached to a syringe pumping liquid polymer solution. If the repulsion from the electric field on the droplet becomes great enough, the tension keeping the droplets shape will be overcome and the droplet will form into a Taylor cone shape. As the jet spreads further, the solution gradually dries, leading to the formation of very fine fibers that are then deposited in a tray beneath for collection [11, 12]. Many of the fibers produced during electrospinning begin overlapping and are typically collected in meshes. These meshes contain layers of randomly aligned fibers. If solvent is still present when new fibers are layered atop old ones, the fibers may link together forming more attached meshes [13].

One of the many benefits of nanofibers is their high surface-to-volume ratio that makes them great for concepts in biomedical engineering like cell interactions, attachment, proliferation, or drug loading. Functionalization on the surface of the fibers can then be performed after the electrospinning is complete [14]. When working with nanofibers that will be used in a biological system, different biologically active molecules can be bonded to the polymer nanofibers, allowing for increased proliferation or control over phenotypical differentiation. Therapeutic agents can be functionalized directly onto the surface of fibers to provide controlled release of the drug during degradation of the polymer fibers [15].

Polycaprolactone (PCL) is a common synthetic polymer used in electrospinning nanofibers, specifically for biomedical applications. It is characterized as having great biocompatibility and a long degradation time. Since PCL is a polymer that contains ester groups, it will degrade over time due to the process of hydrolysis. Studies have shown that PCL can take from 1-3 years to fully degrade in-vivo [16-18]. PCL is widely available and is considered highly manipulable, resulting in its use in a great degree of different biomedical platforms [19].

### **1.3 Polymer Hydrogel Properties**

Hydrogels are a wide category of different polymers, both natural and synthetic, that share hydrophilic properties, allowing them to hold large amounts of water in interconnected 3-D structures without dissolving. One property that makes this possible in hydrogels is crosslinking. Multifunctional monomers or polymers have their reactive groups bound together through a series of different reactions that results in a 3-D network capable of resisting dissolving in solution and slowing degradation significantly [20].

Many different types of hydrogels have been developed, with many new ways to crosslink the polymer or monomer chains. One common method for crosslinking seen is through free radical polymerization. Another method for crosslinking hydrogels is through changes in the environment, such as temperature or pH, to induce a chemical reaction within the polymer chains, linking them. Another form of this reaction is exposure to ions [21].

Gelatin methacrylate (GelMe or GelMa) is a hydrogel with highly tunable characteristics that make it useful for designing biomedical systems. One potential application of GelMe is using it to mimic the extracellular matrix (ECM) of cells for tissue engineering. Gelatin, one of the major components of GelMe, is comprised mostly of a form of degraded collagen, an abundant protein within the body and a large component in making up ECMs [22]. The most common method for GelMe hydrogel formation is through photoinitiated radical polymerization. In this process, GelMe in the presence of a photoinitiator is exposed to ultraviolet (UV) light, leading to formation of bonds within the polymer chains crosslinking them together [23, 24]. GelMe has been shown to have great properties for promoting cell adhesion and proliferation, due to arginine-glycine-aspartate (RGD) peptides present on the collagen molecules. RGD is highly effective at promoting cell attachment [25]. GelMe degrades in the body via collagenase, an enzyme used to break down the ECMs of cells. GelMe has been shown to degrade in a few weeks in the presence of collagenase [26, 27]. Hyaluronic acid modified with norbornene (HANor) is another hydrogel that is used to mimic the naturally occurring ECM of cells. Hyaluronic acid is a molecule abundant in the ECM. HANor is

crosslinked in the same fashion as GelMe, in the presence of photoinitiators and UV light [28, 29].

#### **1.4 Current Treatments for Peripheral Nerve Injury**

For PNI in which the damaged nerve gap is less than 5 mm, the current standard for treatment is through a process called end-to-end coaptation, in which the proximal end of the nerve stump is sutured directly to the distal end. For distances greater than 5 mm, attempts at this method would result in too great a tension placed on the nerve itself [30]. For injuries of this distance, commonly seen in grade IV or V nerve injuries, nerve guidance conduits (NGCs) are used [4].

The “golden standard” for PNI repair using NGCs is through the use of autologous nerve grafting (autograft), in which a patient’s native peripheral nerve is harvested from a different area and transplanted into this nerve defect. Problems with this method include donor site morbidity and differences in the dimensions and structure of the transplant nerve from the injured nerve. Allografts are another common treatment, in which the donor nerve is removed from a cadaver and transplanted into a patient. This method removes the negative effects that come from removing a functioning nerve from the body, however, immunological issues become largely present with these types of transplants. Immunosuppressants would be necessary to prevent an adverse reaction to the transplant [30-32].

Tissue engineering NGCs are typically cylindrical or rectangular prism shaped structures that bridge the gap between the two damaged nerve stumps. NGCs have yet to make it to market as an improved solution over auto and allografts. NGCs primarily

choose either a mechanical cue or a chemical cue to assist in nerve regeneration. Mechanical cues include methods such as using guidance channels, aligned fibers, or grooved hollow tubes. Chemical cues include conductive substrates, biochemical growth factors, or support cells throughout the substrate. Some NGCs use a hydrogel filler to imitate a native ECM [32].

The use of a hollow tube NGC prevents the formation of scar tissue or fibroblasts that could prevent the progress of regenerating axons. Longitudinally guided growth is maintained by creating an open area for the proximal nerve to regenerate through towards the distal end of a nerve gap. A hollow tube NGC also creates a buildup of fluid containing nerve growth factors that are released by Schwann cells in both the distal and proximal end [33]. Hollow tubes as NGCs have been approved for clinical use in peripheral nerve repair but are limited to distances of 3 cm or less. NeuroGen® (Integra Life Science Corp.), approved by the FDA in 2001, is a biodegradable collagen type 1 nerve guidance tube that was one of the first NGCs to be used clinically. [34, 35]. By combing neural growth factors or changing the topography of the internal wall of the tube, studies seek to enhance hollow tubes as NGCs to increase the distance and ability to regenerate peripheral nerves [36].

One area of NGC research seeks to decrease the downsides of required immunosuppression after allograft implantation while maintaining the high recovery rate through the use of decellularized extracellular matrices (dECM). By taking a nerve allografts and removing the genetic material, the three-dimensional structure can be utilized while the risk of immunorecognition and rejection is decreased [37]. The remaining structure would also contain important growth factors and native proteins that

would encourage the regeneration of peripheral nerves [38, 39]. Decellularized extracellular matrices are also being incorporated into NGCs in ways other than decellularized allografts. After undergoing the decellularization process, which often requires submersion in detergent and solvents followed by washing and lyophilization, the dECM can be dissolved and reconstituted to form into a hydrogel structure. This allows for the dECM to be shaped and modified to fit different NGC needs, such as varied topography or microchannel formation [40].

Attempts to fabricate NGCs out of protein hydrogels to mimic the ECM for peripheral nerve recovery have shown promise in animal models. Hill et al. found that when comparing hollow nerve guidance tubes with ones containing a keratin hydrogel, the axons regenerating through a rabbit sciatic nerve defect of 2 cm were more developed in the group containing the hydrogel [41]. Wei et al. conducted a similar study in which a silicon hollow tube group was compared to the tube filled with a silk fibroin peptide hydrogel or a type I collagen hydrogel in 10 mm rat sciatic nerve gaps. It was seen that the tubes filled with hydrogel to mimic the ECM had significantly higher electrophysiological signal traveling throughout the recovered scaffold as well as recovered axons with larger diameters and thicker myelin sheaths, indicating a more progressed recovery [42].

Another promising area for peripheral NGCs is through the use of nanofibers to promote the growth of recovering axons. Wang et al. fabricated randomly aligned nanofibrous scaffolds made of electrospun silk fibroin fibers coated in graphene oxide to promote conductivity and simulate electrical impulses to guide axon recovery. In 10 mm long rat sciatic nerve defects it was found that the nanofibrous scaffolds coated with

graphene oxide resulted in recovered axons with significantly higher axon diameters and myelin thicknesses than nanofibrous scaffolds containing only the silk fibroin. The graphene coated scaffold performed similarly to the autograft group in this model [43]. Zhan et al. fabricated self-assembling nanofibrous scaffolds out of RADA16-I peptide within a rat aorta tube. The scaffold group was capable of recovering a peripheral nerve gap of 10 mm in rat sciatic nerve models. The recovery of the gastrocnemius muscle of the nanofibrous group was significantly greater than both the negative control and an empty aorta group (simulating a hollow tube) [44].

By longitudinally aligning nanofibers within NGCs, contact guidance seeks to improve the ability to recover axons a further distance in a decreased amount of time. Wang et al. manufactured a hollow tube NGC consisting of longitudinally aligned Poly(l-lactide-co- $\epsilon$ -caprolactone) (P(LLA-CL)) or silk fibroin/P(LLA-CL) nanofibers by electrospinning the polymer onto a rotating drum collector, allowing the direction of the nanofiber alignment to be controlled. Both scaffold groups were implanted in 10 mm rat sciatic nerve defects along with an autograft group. It was found that the silk fibroin/P(LLA-CL) significantly outperformed the P(LLA-CL) group by coating the fibers in a bioactive molecule (silk fibrion), promoting cell attachment and proliferation. However, morphological assessment revealed both groups had significantly less mature regenerated axons than the autograft group [45].

As mentioned, many studies are being performed that attempt to encourage peripheral nerve repair using NGCs that combines multiple recovery strategies. Zilong et al. found that NGCs manufactured with dECM hydrogel from porcine sciatic nerve and longitudinally aligned microchannels were effective at promoting recovery across 15 mm

defects in rat peripheral nerve models. Axon morphology found that scaffolds also fabricated with neural growth factor had regenerated axon with thicker myelin sheaths than scaffolds fabricated without neural growth factor, indicating the nerve was more mature. The NGCs were found to still have significantly smaller myelin sheaths and smaller axon diameters than the autograft group [40].

By combining aligned nanofibers into a 3-dimensional hydrogel scaffold, McMurtrey developed an NGC that both promoted directional growth while mimicking the natural nerve environment. When electrospun PCL nanofibers were embedded within a HA hydrogel, the distance that neurite outgrowth occurred in vitro significantly improved over hydrogel only groups. It was also found in vitro that PCL nanofibers significantly improved neurite guided growth when functionalized with laminin proteins then when left untreated [46]. Similar results were found in studies conducted by Zheng et al., in which aligned and randomly oriented electrospun poly(lactic acid) (PLLA) nanofibers were embedded in a decellularized porcine nerve matrix hydrogel and implanted in 5 mm rat sciatic nerve gap models. Aligned nanofiber scaffolds were found to have a lower sciatic functional index (indicating a higher success rate) and improved histological assessment of axons when compared to randomly aligned nanofibers, however, both groups performed significantly worse than the autograft group [47].

Smith et al. developed a method to provide contact guidance for axon recovery through the use of stretch grown longitudinally aligned axons. Living porcine axons were embedded in an ECM hydrogel consisting of type I collagen and neural growth factor. These living axons provided bioactive signals that encouraged the regeneration of host axons and maintained Schwann cell activity in 5 cm porcine deep fibular nerve gaps.

After 12 months post implantation, no significant difference could be found in axon morphology between control, autograft, or experimental groups [48].

## Chapter 2

### Layer-By-Layer Scaffolds

#### 2.1 Layer-By-Layer Scaffolds Introduction

As seen in the previously mentioned literature, to bridge the gap between damaged ends of a peripheral nerve, a nerve guidance conduit (NGC) is used to promote axon growth and alignment, and to protect the nerve path by preventing the ingrowth of surrounding tissues. Many conduits rely on porous hydrogels for structure or fibrous structures for contact guidance. By combining both materials into a hydrogel-nanofiber composite scaffold, a more effective conduit can be manufactured to bridge damaged peripheral nerve gaps.

One of the most prevalent problems faced when bridging peripheral nerve damage gaps is time. By using highly aligned nanofibers that run from the proximal stump of healthy nerve to the distal stump, nerves will have a surface to attach to that will provide a contact guidance route in the most efficient path. By growing in this aligned pattern, nerves will regenerate faster than undirected axons. Healthy peripheral nerve tissue is highly aligned, growing in directional bundles. By using aligned nanofibers to direct growth, the natural pattern that nerve grows in is mimicked.

A porous hydrogel environment surrounding the aligned nanofibers will encourage cell infiltration by mimicking the 3-D environment of native tissue. The combination of both types of methods of nerve regeneration conduits into a single graft will greatly reduce the time it takes to repair peripheral nerve damage, and therefore increase the distance that damaged nerves can regenerate through.

Assembling and maintaining a 3-D, low density, aligned nanofiber structure within a porous hydrogel is highly challenging. A layer-by-layer assembly method was chosen to design the scaffolds to allow for in-depth control over the dimensions and orientation of fibers throughout the scaffold. To embed each layer of fibers within the hydrogel, fiber arrays are dipped into a liquid hydrogel which is then crosslinked using UV light. The amount of crosslinking that each layer receives can be adjusted on a per layer basis by adjusting the duration and intensity of UV light exposure the hydrogel receives at each layer. The thickness of each layer can be controlled by changing the weight percent of the hydrogel, the temperature each frame layer is dipped at, and the number of dips each layer receives. Fiber orientation could be changed at each layer if a tissue type would require an alternating direction of growth. By using layer-by-layer additive manufacturing, scaffolds can be produced to allow manufacturers fine control over the scaffold's properties.

## **2.2 Materials and Methods**

### ***2.2.1 Electrospinning Nanofibers***

To produce polymer nanofibers in an aligned fashion, a parallel track electrospinning technique is used. In this form of electrospinning, two metal-chain tracks rotate in opposite directions parallel to each other [49]. Electrospinning solution is dispensed from a charged, blunt tip needle (Probe Needles, McMaster) positioned above the gap between these rotating tracks. The solution orients into a thin fiber with either end attached to one of the rotating tracks. The needle is charged through the connection via wire from the end of the needle to a voltage box. The rate at which solution is dispensed is controlled by a syringe pump connected to the needle (Figure 1A-B). The speed at

which the tracks rotate is controlled by a stepper motor. The entire electrospinning systems resides in a humidity chamber, where the internal humidity can be controlled through attached humidifiers.

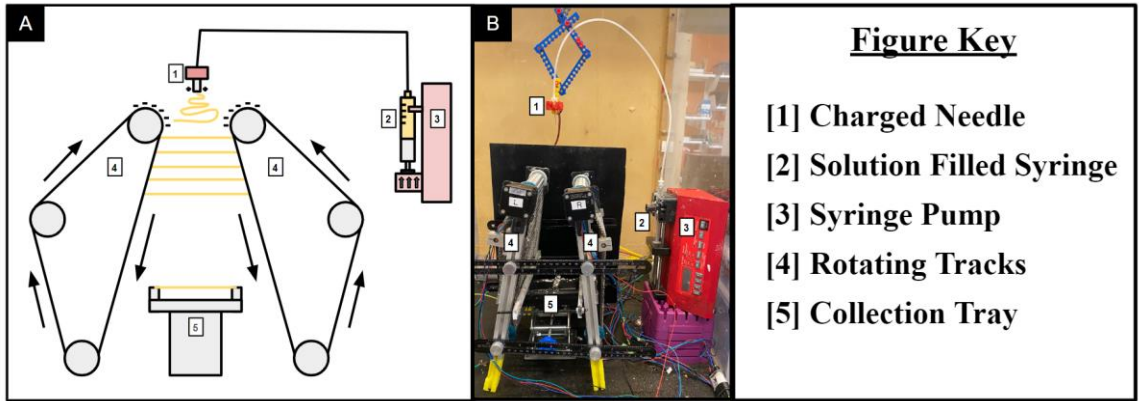


*Figure 1.* Electrospinning Schematic and Experimental Setup

The distance that the tracks are separated by can be increased as the distance from the needle increases, creating an effect on the fibers called post-drawing. As the track rotates and the fiber is moved further from the dispense needle, it elongates as the tracks widen. Post-drawing results in fibers that have higher mechanical properties, such as Young's modulus, ultimate strength, and toughness, and creates fibers with smaller radii [49]. The ratio that a fiber is post-drawn depends on the ratio of distance between tracks at the top of the device to the distance between tracks at the point of collection. This ratio will affect the fiber properties by altering their molecular alignment and mechanical strength. At the bottom of the parallel tracks is a collection tray. This collection tray attaches to either end of the fiber using double-sided tape, preserving the fibers and their

dimensions. Once the desired density of fibers is achieved on the collection tray, the tray can be removed.

Fibers for peripheral nerve scaffolds use polycaprolactone (PCL, 115,000 MW, Sigma-Aldrich, United Kingdom) fibers. To produce a solution capable of being electrospun, 18% w/v solutions of PCL were used. PCL was dissolved in dichloromethane (DCM, BeanTown Chemical, USA) and dimethylformamide (DMF, BeanTown Chemical, USA) in a 3:1 ratio, respectively. This solution was dispensed at a rate of 1 mL/hr with the needle having an applied voltage of 10 kW. The ideal humidity within the chamber for spinning this solution is between 50% and 60% relative humidity. The fibers were post-drawn in a 2:1 ratio of final length to initial length. The PCL fibers were transferred from the collection tray onto plastic frames of internal dimensions of 30 mm by 20 mm. Fibers are left to fully evaporate out the organic solvents for 24 hours before use.

### ***2.2.2 Hydrogel Fabrication***

For scaffold manufacturing, a 4% w/v solution of gelatin methacrylate in phosphate buffered saline (1X PBS, Gibco) is used. This solution also contains 20 mM concentration of Irgacure 2959 (I2959, Sigma-Aldrich, USA) to allow photoinitiation when exposed to UV light.

### ***2.2.3 Frame Fiber Density***

The density of fibers on each frame is dependent on the duration of time that electrospinning occurs over one collection tray. Increasing the amount of time that the collection tray is in the electrospinner accumulates more fibers on one two-dimensional

frame. If the density of fibers is too low, a full film will not form during dip coating, and therefore the frame cannot be used for nanofiber-hydrogel composite scaffold manufacturing. To determine the minimum density of fibers required to create a film on a frame of fibers, fibers were collected for three lengths of spinning time (1-, 3- and 5- minutes). Six frames of fibers were imaged on a brightfield light microscope (AxioVert A1, Hitech Instruments) at four random locations throughout each frame. Three 300  $\mu\text{m}$  lines were drawn perpendicular to the fibers in each photo using the software ImageJ (Version 1.54d, Java 1.8.0\_345). The number of fibers that crossed this line were counted and recorded as a value of fibers per 300  $\mu\text{m}$ . These values were used to determine an average and standard deviation of fibers per 100  $\mu\text{m}$ .

#### ***2.2.4 Layer-By-Layer Additive Manufacturing***

In the hydrogel-nanofiber composite scaffold, PCL nanofibers are embedded within a gelatin methacrylate (GelMe) hydrogel, with each fiber running parallel to the others. Fibers are separated into layers with a three-dimensional geometry. To achieve this, frames of two-dimensional fiber arrays are dip coated in hydrogel solution and stacked layer-by-layer in an additive manufacturing process to create a structure with aligned nanofibers that are dispersed throughout the structure. By manufacturing these scaffolds layer-by-layer, the individual properties of the structure, such as distance between the fibers, the thickness of each layer, and the total amount of crosslinking time the scaffold receives, can be highly controllable.

The first step in scaffold manufacturing is to embed a single frame of fiber in hydrogel. *Figure 2A* displays a schematic of the dip coating manufacturing process. The GelMe solution is heated to 50°C in a 50 mL conical tube (Cellstar, USA) in an oven

(VWR International, USA) to create a viscous liquid solution. A frame of fibers is dipped into this solution, creating a film of hydrogel solution completely coating the fibers. This film is set onto a plastic holding tray within a small humidity chamber that keeps the sample hydrated while the stacking process is undergone. Another frame of fibers repeats this process and is carefully positioned directly on top of the previous frame, starting on one side and gradually laying down to prevent air from being trapped between. The film is added matching the orientation of the fibers from the previous film. The stack is then exposed to UV light at  $10 \text{ mW/cm}^2$  for 15 seconds to begin crosslinking the GelMe hydrogel. Another frame is then coated in GelMe and layered on top of the stack. The stack receives another 15 seconds of UV light after each layer is added up to 10 layers in total. By crosslinking in small intervals, the liquid hydrogel of each additional layer will mix with that of the previous layer, limiting the rate that the delamination of layers will occur. Once all of the layers are added, the scaffold receives one minute of UV light on either side of the scaffold, resulting in at most 255 seconds of crosslinking and at minimum 135 seconds, depending on the location of the layer.

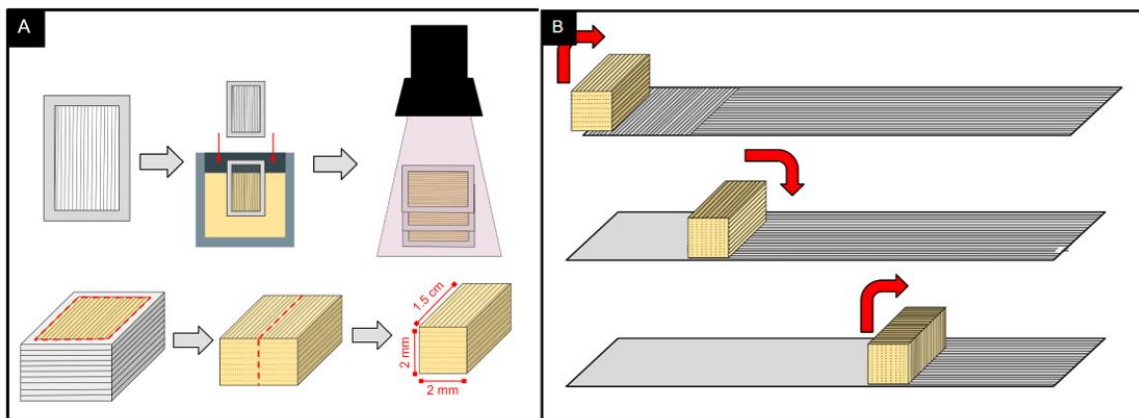


*Figure 2.* Layer-By-Layer Scaffold Assembly Schematic

Once the stack has finished receiving UV light, it will be fully crosslinked and capable of remaining in a solid state at 37°C. The stack is then cut away from the frames along the interior edge using a scalpel blade. Using a razor blade, the stack is cut into strips approximately 2 mm wide, 2 mm in height, and 10 mm long. At this point the stack is now referred to as a composite scaffold and is stored in PBS at 4°C until use.

Scaffolds are then wrapped in a nanofiber sheath for protection and to create an attachment site for suturing to in-vivo nerves, as seen in *Figure 2B*. When implanting the scaffold in a living system, the interface between healthy nerve and scaffold needs to remain in contact or close proximity. A sheath of nanofibers allows the nerve to be surgically stitched to the end of the scaffold on either side, ensuring the nerve does not drift away from the scaffold post implantation. To create the sheath, a roll of nanofibers two feet long and 14 mm wide on parchment paper (Baker's Signature, USA) is manufactured. The scaffold is positioned on one end of this roll, with the internal fibers of the scaffold perpendicular to the length of the roll. The scaffold is carefully rotated down the length of the roll, gradually becoming wrapped in the fibers situated on the roll. The fibers do not attach to the parchment paper, and therefore transfer to the moist hydrogel surface when the scaffold rotates over them. Since the width of the nanofiber roll is greater than the length of the scaffold, a hollow overhang of nanofibers is created on either side. This acts as an insertion point for a patient's nerve to situate into and be attached. The first six inches of the roll of nanofibers run parallel to the nanofibers within the scaffold. This is done so that cells along the interface between scaffold and sheath can follow these external fibers. After six inches, the nanofibers on the roll switch from

parallel to a perpendicular alignment. The tension in the nanofibers keep the wrap tight to the scaffold and help maintain its cylindrical structure.

### ***2.2.5 Large Stack Innovation***

While the layer-by-layer additive manufacturing technique was capable of creating a stack that was 10 layers high, a larger height would be beneficial and more versatile when treating peripheral nerve injuries. Once the stack reaches 10 layers, the weight of the GelMe coating the fibers begins to bow the stack downward. The frames remained rigidly locked in place, creating a meniscus shape in the stack. After ten layers, the distance between the edge of the frames and the center of the stack becomes too large and large air bubbles begin to accumulate between layers.

Attempts to cut this scaffold free from the frames before continuing the stacking process results in various issues. Some layers once cut lose too much tension and the fibers become wavy, pulling away from the end of the hydrogel. The interface between layers after cutting the stack off of the frames showed delamination of the layers, coming apart once stored in PBS.

An adjusted manufacturing method was made to the stacking process to reduce the rates of delamination and maintain the layered fiber structure within the stack. The first frame used in the stack has a decreased internal dimension compared to the rest of the stack (18 mm by 28 mm), which allows for a base to support the stack when subsequent frames are removed. Once a height of 10 frames were stacked and cross-linked, the frames were cooled in a refrigerator at 4°C for 8 minutes. If the stack remains out of the humidity chamber for too long, the hydrogel will dry out. After 8 minutes the

scaffold is brought back to the humidity chamber for 1 minute. GelMe is a hydrogel that will gelate at room temperature or colder if given the time to cool, even without the UV crosslinking. By cooling the stack, the fully solidified hydrogel will help to maintain the fiber structure while the razor blade is used to remove the frames. All frames are removed except for the first frame of the stack with the smaller internal dimensions. This frame remains to be a base for the next frames of dip coated fibers added.

Once the 9 top frames are removed the stack is returned to the humidity chamber for 1 minute before being moved to an oven set to 37°C for 3 minutes. By reheating the stack, the layers that received low to no crosslinking will return to liquid phase, creating an optimal interface for the next frame of dipped fibers to be added. When the stack is not allowed to return to liquid phase before stacking continues, large rates of delamination between the interface layers occur. The solidified layer would not attach well to the newly added layer, and the scaffold would come apart in solution.

This stacking, cooling, cutting, and reheating process continues for every 10 frames added, until a height of 50 frames is reached. At this point, the scaffold is complete and ready to be wrapped in a nanofiber sheath. To further ensure delamination rates would be reduced, the 10<sup>th</sup> frame added at each interval did not receive any UV crosslinking before being cooled. This ensured that the layer added after cutting would fully mix with the top layer before crosslinking continued.

### ***2.2.6 In-Vitro Model***

To test the scaffold for cell infiltration and alignment in-vitro, a holder was created to position the scaffold in an upright position. The design for the holder is a

cylinder with a hollow central shaft where the scaffold sits. The scaffold will remain vertical, with the fiber layers running from top to bottom. Cells can be seeded on the top surface of the scaffold, simulating attaching a healthy nerve to the end of the scaffold. The cells' ability to penetrate into the hydrogel, locate the fibers, and align onto them can then be studied.

The holder is made from polydimethylsiloxane (PDMS), a non-toxic silicone polymer that will prevent cell infiltration. A 14 mm tall plate of PDMS is made using a 100 x 20 mm petri dish. PDMS curing agent (Sylgard 184 Silicone Elastomer Curing Agent, Dow Chemical Company) is mixed well with PDMS polymer agent (Sylgard 184 Silicone Elastomer Base, Dow Chemical Company) in a 1:10 ratio in the petri dish. Once manually mixed thoroughly, the petri dish is placed in a vacuum chamber for 45 minutes, or until all trapped bubbles are released. After all the trapped air is removed from the PDMS mixture, the petri dish is transferred to an oven set to 37°C for 24 hours to fully cure. Once complete, the PDMS will have fully solidified into an easily cuttable but structurally stable polymer.

Figure 3 provides a schematic for the manufacturing and assembly of the in-vitro model. A cylinder is then cut from the PDMS using a 5 mm diameter metal punch. The punch is pressed into the polymer until the bottom of the petri dish is reached. Forceps can then be used to remove the cylinder from the surrounding PDMS (Figure 3A). In the center of this cylinder, a 12-gauge needle is used to create a hollow shaft in which the scaffold will sit. The shaft is the same width as the scaffold, creating a tight fit between the wall of the holder and the edge of the scaffold, preventing cells from migrating down the edge of the scaffold rather than infiltrating into it. The PDMS is taller than the

scaffold itself to create an inlet for cells to settle into, creating an ideal interface between cells and scaffold. Finally, a razor blade is used to fully cut the cylinder vertically in half, bisecting the shaft in two (*Figure 3B*).

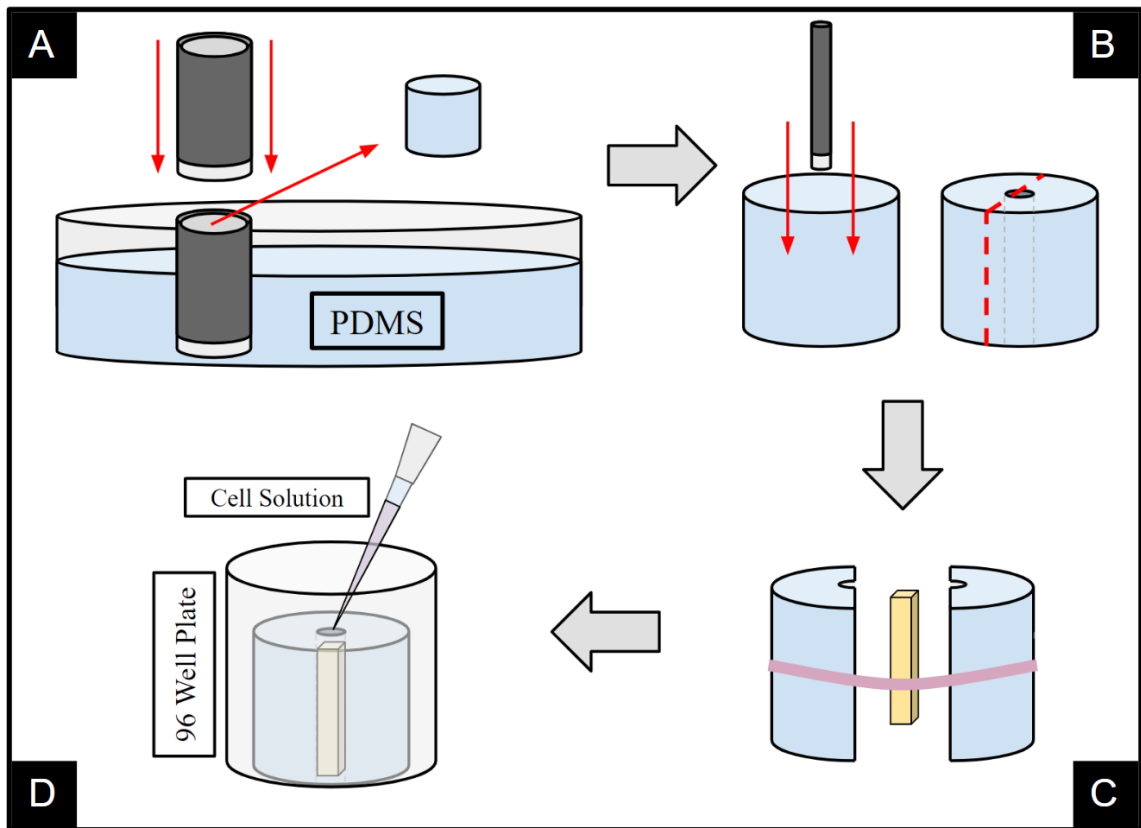


*Figure 3.* In-Vitro Model Assembly and Cell Seeding Schematic

Using forceps, a scaffold can be positioned in the center shaft leaving an inlet from the top and bottom of the cylinder. Both sides of the cylinder are then closed around the scaffold and maintained in place using a dental rubber band (*Figure 3C*). The scaffold in the holder is now ready for cell seeding and stored in PBS or cell culture media (Dulbecco's Modified Eagle Medium, Gibco, USA) until it is ready for use.

### ***2.2.7 Sterilization Techniques***

Scaffolds and holders, once manufactured, must be sterilized to avoid contamination and mold growth before use in an in-vitro or in vivo cell system. Sterilizing the scaffolds using UV light would be an impossibility due to the GelMe hydrogel system having photoinitiated crosslinking. A low pH method of sterilization using hydrochloric acid (1M HCl, Honeywell, Germany) was chosen.

Exposure of the gelatin hydrogel to a high concentration of H<sup>+</sup> ions from the HCl solution could result in its denaturing, therefore a low molarity of HCl would be ideal for sterilization. A study was conducted to determine the minimum level of HCl that would be required to sterilize a scaffold and holder to prevent contamination. Four levels of HCl molarity were chosen (0, 0.01, 0.1, 1 M) to test with 4 test samples in each group. HCl solutions were made by diluting 1 M HCL in 1X PBS. Each sample was placed in a sterile well of a 96 well plate in a cell culture hood and submerged in their respective HCl solutions (1X PBS for the control group). After 20 minutes, the solutions were aspirated out of each well and sterile PBS was used to immediately rinse the samples. Two more rinses of 20 minutes each using PBS followed the initial rinse. Finally, the samples were left in cell culture media for 14 days in an incubator at 37°C. The outer surface of the well plate was wrapped in Parafilm (Bemis) to allow oxygenation but prevent dehydration from the wells. 14 days was chosen because this is the maximum amount of time planned for any in-vitro cell culture experiments.

### ***2.2.8 In-Vitro Cell Culture and Imaging***

Each scaffold in the holder is set upright in one well of a 96 well plate. Each well has 1 ml of cell culture media added to submerge the scaffold and holder. Mesenchymal stem

cells (MSCs) from culture are passaged to prepare for cell seeding. Using a 10  $\mu$ l pipette, cells are carefully seeded in the top inlet of the holder, directly on top of the scaffold at a density of 6,000 cells per  $\text{cm}^2$ . Well plates are then stored in an incubator at 37°C for the duration of the experiment time. Media within each well is aspirated out carefully and replaced every three days. Once the full experiment has been conducted, scaffolds are carefully removed from the holder using forceps in a sterile cell culture hood and processed for imaging.

To process the scaffold for analysis, it must first be fixed and stained. The scaffold is submerged in 10% formalin for 30 minutes to fix the cells within the scaffold. Once the cells are fixed, the scaffold receives two washes in 1X PBS for two minutes each. Following this, the scaffold is submerged in a 0.1% Triton X-100 (Alfa Aesar, USA) in PBS for 10 minutes. Triton X-100 is a non-ionic surfactant, which makes it capable of dissolving the lipid layers that make up a cell's membrane. This makes the cells more permeable, allowing for stains to enter the cell and bind their appropriate targets more easily. Again, the scaffold receives two washes in 1X PBS for 2 minutes each. It is then submerged in a 3% bovine serum albumin (BSA) in PBS for 30 minutes. BSA is commonly used in cell staining as a blocking agent to reduce the non-specific binding of stains. To stain actin within the cells, Alexa Fluor 568 is used in a 1:50 ratio in the 3% BSA solution. The scaffold is submerged in this stain solution for 60 minutes. The scaffold is then washed in PBS twice for two minutes each. A 1:1000 Hoechst solution in PBS is used to stain DNA within the cells (nuclei) as well as the PCL fibers within the scaffold. Scaffolds are submerged in the Hoechst solution for 15 minutes. Finally, the scaffolds receive two more rinses in PBS for 2 minutes each.

### ***2.2.9 Rat Sciatic Nerve Gap Study***

Twenty-four Wistar rats were acquired to perform a rat sciatic nerve regeneration study using the layer-by-layer additive manufacturing scaffolds to bridge the gap (LBL-scaffolds). For this study, a 1.5 cm portion of the right sciatic nerve was removed from each rat and replaced with an LBL-scaffold. Eight of the rats received an autograft transplant.

Two different LBL-scaffold groups were manufactured. For both groups of the LBL-scaffolds, fibers were electrospun according to the procedure seen in section 2.2.1. However, the 18 wt% PCL solution also contained 10% w/v poly(ethylene glycol)-norbornene (PEGNor). The electrospinning process was performed the same way, and the fibers were collected onto frames. For 8 of the scaffolds, the frames then received UV coupling of Arginylglycylaspartic acid (RGD), YIGSR, and IKVAV peptides to the fibers. To do this, frames were soaked in a 1X PBS solution containing 1mM RGD, 1 mM YIGSR, 1 mM IKVAV, and 10% I2959. Each peptide sequence contained a cysteine at one end to enable binding of the peptide to the norbornene contained on the surface of the polymer fibers. The frames were then exposed to UV light at 5 mW/cm<sup>2</sup> for 1 minute. Each frame then received five washed in PBS for 5 minutes each. This process utilizes a UV-mediated thiol “click” reaction to functionalize the nanofibers with these peptides.

For each scaffold, 45 frames were stacked and crosslinked according to the stacking procedure found in sections 2.2.4 and 2.2.5. Eight scaffolds were manufactured using frames of nanofibers without the peptides (LBL-scaffold), and 8 were manufactured using frames of nanofibers with the peptides (LBL-scaffold-WP). Once crosslinked and wrapped in a PCL nanofiber conduit, the scaffolds underwent the

sterilization process found in section 2.2.7, using 0.1 M HCL. The scaffolds were then stored in 1X PBS at 4°C until implantation.

### ***2.2.10 Scaffold Implantation***

Twenty-four Wistar rats were chosen to undergo surgical implantation of LBL-scaffolds in a 12-week study. The rats were put under anesthesia in a gas chamber box. A mask was then put over the rat's face that connected to the anesthesia tank that ensured the rats stayed anesthetized for the full length of the surgery. After ensuring the environment and equipment was properly sterile, an incision was made into the right thigh of each rat was made directly over where the sciatic nerve is located. The surrounding tissue was carefully cut until the sciatic nerve was found. A 1.5 cm section of the sciatic nerve was then removed from the rat. For the eight rats undergoing the autograft surgery, this nerve was rotated 180° and reimplanted. The nerve stumps received a stitch to ensure the proximal and distal ends on either side were fully interfacing.

For the sixteen rats receiving scaffolds, the 1.5 cm section of sciatic nerve was removed, and a scaffold was then implanted into this region. The proximal end of the cut sciatic nerve was inserted into the overhanging hollow PCL wrap until it was interfacing directly with the surface of the scaffold. The wrap was then carefully stitched to the surface of the nerve to ensure the nerve would remain in contact with the scaffold. The same process was repeated on the distal end of the scaffold with the distally cut sciatic nerve. Once implanted, the rat's surgical incision was closed, and the rats were removed from anesthesia to begin recovery.

### ***2.2.11 Scaffold Explantation and Electrophysiological Evaluation***

After 12 weeks had passed, the rats were prepared for explantation of the scaffolds. The rats were again put under anesthesia using a gas chamber. Each rat was then removed and fitted to a gas mask that connected to the anesthesia tank that ensured the rats stayed under for the full length of the surgery. Once fully anesthetized, an incision was made down the full length of the thigh above where the sciatic nerve and implant were located. The tissue was cut carefully not to disrupt the nerve or anterior tibialis muscle until the scaffold was found, as seen in *Figure 4*.

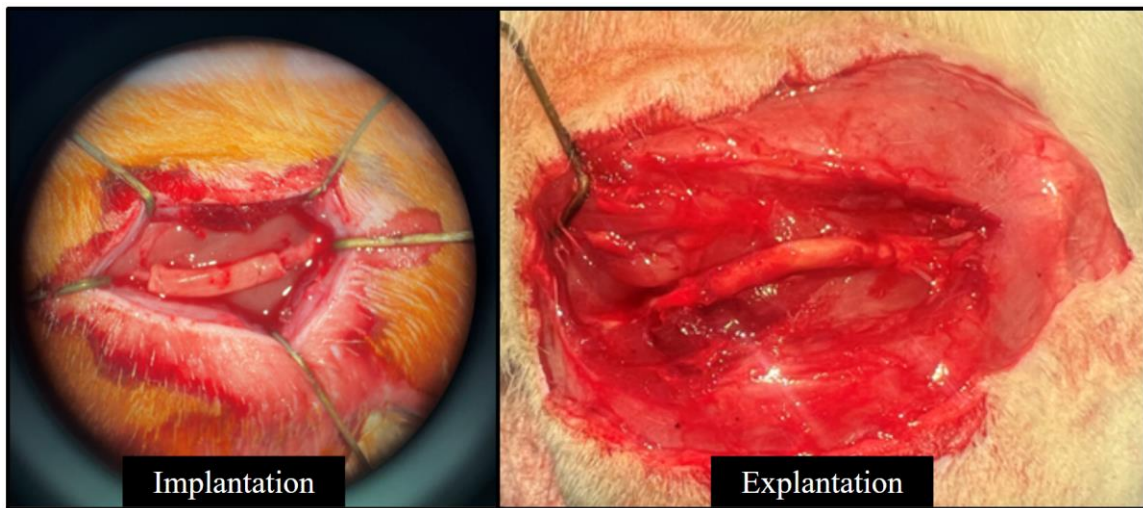


*Figure 4.* Surgical Scaffold Placement of LBL-Scaffolds In-Vivo Rat Models

An incision was then made down the length of the calf of the rats, freeing the entire anterior tibialis muscle and tibialis anterior tendon (TAT). The TAT was then cut directly above where it connected to the bones in the foot. The tendon was attached to a clamp that connected to a force sensor. Using an electrical probe, the sciatic nerve was stimulated proximally to each scaffold. The stimulation may be transmitted across the

graft to reach the muscle, causing it to contract and produce a force that was then recorded. After the scaffold underwent electrophysiological testing, the scaffold was removed by cutting into the sciatic nerve 1 mm above and below the scaffold. A stitch was added into the sciatic nerve on the proximal side of the scaffold before its removal to identify this side during histological processing. The scaffold was then stored in 10% formalin at 4°C. Rats were then removed from anesthesia and euthanized. The anterior tibialis muscle was then harvested and weighed using a scale. The left anterior tibialis was harvested and weighed as a control.

## **2.3 Statistical Analysis**

To determine statistical significance between the densities of fibers on each frame for different electrospinning time, an ANOVA was conducted using the software RStudio (Version 2023.06.2+561). A sample size of 72 observations per group was used. Significant results were analyzed with Tukey's post hoc test. Statistical significance was determined to be at an  $\alpha = 0.01$ .

## **2.4 Results and Discussion**

### ***2.4.1 Frame Fiber Density***

The 1-, 3-, and 5-minute collection times produced an average of 8, 16, and 36 fibers per 100  $\mu\text{m}$ , respectively (*Figure 5F*). Frames were then dipped in GelMe heated to 50°C to observe if a film would remain. It was observed that none of the 1-minute frames were capable of forming a film, while 3 out of the 6 frames for the 3-minute collection time were capable (*Figure 5D* and *Figure 5E*). All of the frames from the 5-minute collection time were capable of forming a film. It was determined that a density of

at least 36 fibers per 100  $\mu\text{m}$  is required on a frame to be usable in a dip coating procedure.

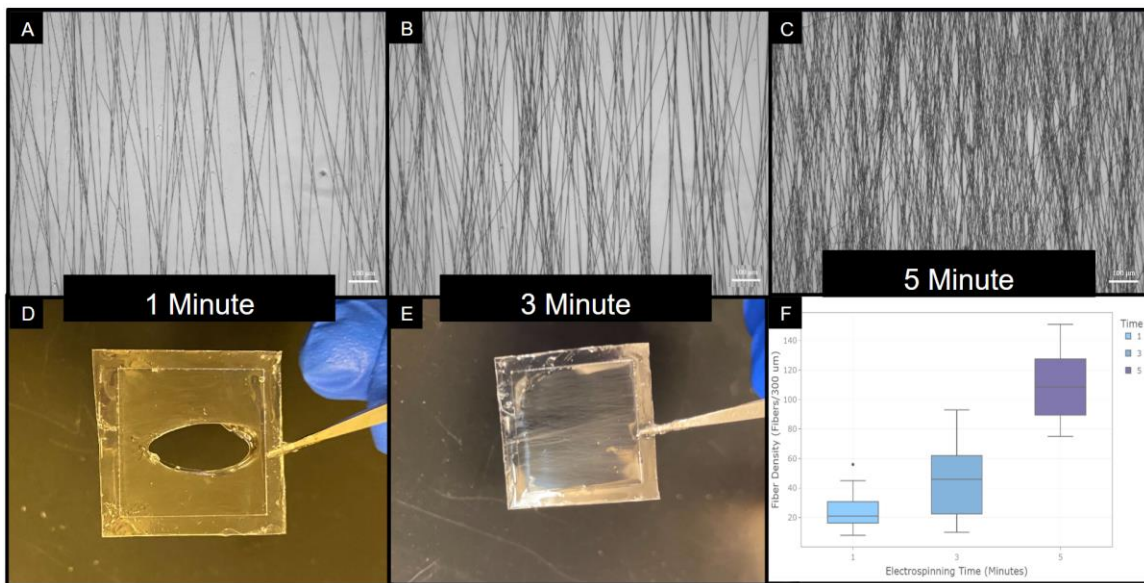


*Figure 5.* Electrospun Nanofiber Frame Densities for Different Spin Times. \* indicates significance at  $p < 0.01$ .

#### 2.4.2 Sterilization Study

After 14 days, samples were observed for contamination in each well. Clear signs of contamination would be a color change in the media (indicating a pH change of the solution caused by contaminants) or obvious mold growth. Solution samples could also be viewed under the brightfield microscope to verify if a well was suspected of contamination. *Figure 6* shows the results of the contamination study. Of the 4 control samples, three were found to have contamination, which is expected as no sterilization occurred. 2 samples out of the 4 in the 0.01 M HCl group were contaminated as well. No samples in either the 0.1 M or the 1 M HCl group were contaminated. It was concluded

that 0.01 M HCl was not of a high enough molarity to sterilize the samples in the 20-minute soaking period. 0.1 M HCl was chosen to continue sterilization for future studies as it was the lowest concentration tested that was fully successful.

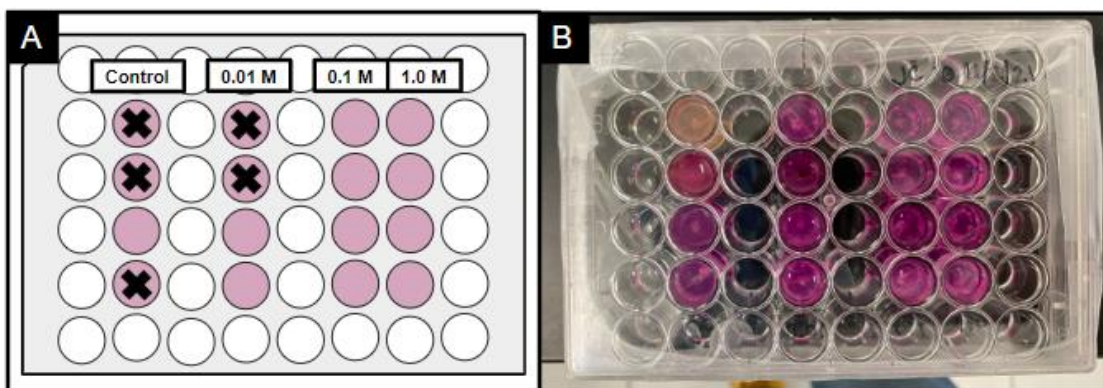


*Figure 6.* Sterilization Study Results for Different Concentrations of HCl. Part A is a schematic emphasizing the results seen in Part B

### ***2.4.3 In-Vitro Cell Migration and Alignment***

An in-vitro model of cell infiltration through an aligned nanofiber-hydrogel composite graft was designed and studied to determine if it would be an efficient model for studying cell infiltration and alignment into various formulations the scaffolds. PDMS is a highly versatile polymer that can be fabricated into many shapes by mixing the curing agent and polymer agents into a mold while the polymer still has not cured. By applying heat, the polymer solidifies to an easily cuttable yet solid material. PDMS is highly biocompatible, gas permeable, non-reactive with cells, and shows difficulties with cell adhesion over time [50, 51]. By seeding the cells directly on top of the scaffold where they are surrounded on all sides by PDMS, the cells would be expected to attach to

the top surface of the scaffold, where they would be in a position to infiltrate into it. This would mimic the path regenerating nerves would take in the body. The scaffold can easily be removed from the in-vitro model which allows for easy imaging once the experimentation is complete.

*Figure 7* shows scaffolds that underwent cell seeding in the in vitro model. Scaffolds were removed from their PDMS supports at their designated timepoints, stained, and fluorescently imaged using a confocal microscope. Cells can initially be seen atop the scaffold, stained red using Alexa fluor. The nuclei of cells and nanofibers of the scaffolds are both stained blue using Hoechst. By day 14, cells can be seen infiltrating into the scaffold and elongating on the fibers. This study demonstrates that cells are able to attach to the top face of the cylindrical graft and migrate and align along the graft in the direction of the fibers. However, it was not determined whether cells were infiltrating into the interior portions of the graft or migrating only on the outer surface of the graft.

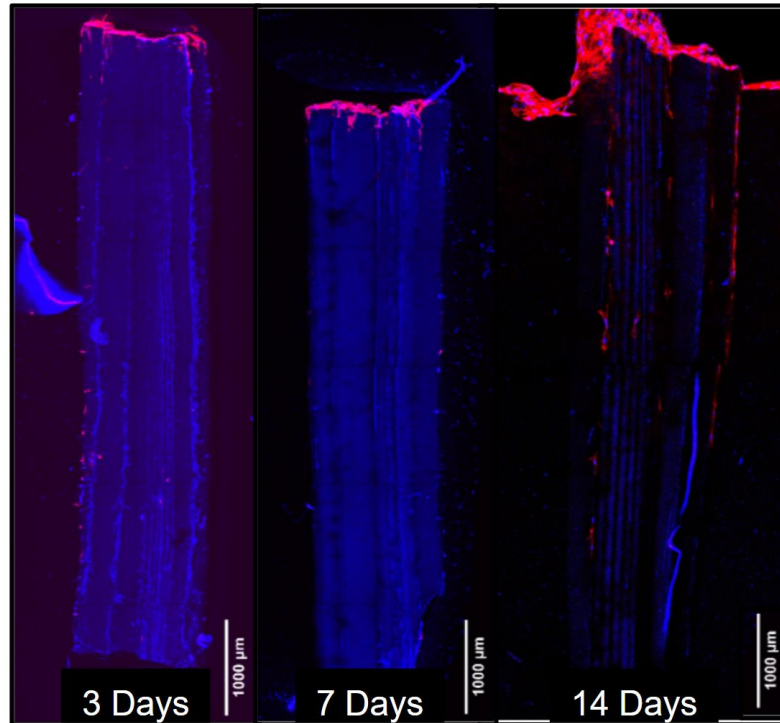


*Figure 7. In-Vitro Model Testing Cell Migration, Infiltration, and Alignment Over 14 Days*

#### ***2.4.4 Sciatic Nerve Gap Model Results***

The goal of the LBL-scaffold design is to manufacture scaffolds with specific controllable parameters such as layer thickness and degree of crosslinking. GelMe was the chosen hydrogel for this study due to it being thermosresponsive and UV cross-linkable. These are ideal properties to undergo the layer-by-layer assembly method as temperature and UV exposure time can be used to adjust the single film properties during stacking. By using 4% GelMe, the hydrogel would ideally degrade as cells infiltrate and remodel the scaffold and damaged nerve gap, being nearly completely degraded by the week 12 timepoint [26, 27].

The LBL-scaffold-WP group had functionalized nanofibers to enhance axon regeneration. By incorporating PEGNor into the nanofibers during electrospinning, peptides were given a location to be covalently bound to the fibers. RGD is a synthetic peptide that has been shown to enhance cell adhesion by imitating ECM fibronectin binding proteins [52]. YIGSR is another synthetic peptide shown to also promote cell adhesion by imitating ECM laminin binding proteins, commonly found in basement membranes [53]. IKVAV was the final synthetic peptide added, another laminin-1 based peptide that has been shown to increase cell adhesion, neurite outgrowth, and angiogenesis [54]. By incorporating these peptides onto the nanofibers, the ability of regenerating axons to have improved attachment to the fibers would increase the efficiency of the fibers as guidewires, decreasing the amount of time it would take for an axon to regenerate across a damaged nerve gap.

During explantation of the scaffolds at week 12, a muscle contraction test was conducted on the anterior tibialis muscle on the right leg of the rats, distal to the scaffold. The sciatic nerve directly innervates into this muscle and is responsible for its stimulation and contraction. The anterior tibialis connects to bones in the foot via the TAT and when stimulated results in dorsiflexion of the foot. While the rats were under anesthesia, the TAT was detached from the bone and instead attached to a force sensor via a clamp. When an electrical current is used to stimulate a healthy nerve, a signal would be passed through the nerve into the muscle causing it to contract, producing a measurable force. For this study, an electrical stimulation is introduced proximal to the scaffold. If nerves had successfully fully regenerated through the scaffold, the muscle should contract with the same force as the healthy nerve.

Before the electrophysiological muscular testing was conducted, the anterior tibialis muscle was qualitatively analyzed. In both LBL-scaffold groups, complete muscular atrophy was observed. If the nerve is unable to send a message to the muscle to contract, over time the muscle will be degraded by the body due to lack of use. Muscular atrophy is a sign that the nerve regeneration in these scaffolds was unsuccessful. Electrophysiological analysis of the scaffold groups further confirmed this result. No contraction of the muscle was seen or measurable using the force sensor. No signal was able to be passed through the scaffold, indicating there was no infiltration of axons throughout (Table 1).

**Table 1**

*LBL-Scaffold Anterior Tibialis Electrophysiological Muscular Testing Results*

<b>Scaffold Type</b>	<b>LBL-Scaffold</b>	<b>LBL-Scaffold-WP</b>
<b># of Samples</b>	<b>8</b>	<b>8</b>
<b>Muscle Observation</b>	Complete Atrophy	Complete Atrophy
<b>Muscle Force Generated</b>	No Contraction	No Contraction

Muscular weight analysis further confirmed the qualitative conclusion that complete muscular atrophy occurred. Qualitative results can be seen in *Figure 8A*, where the control anterior tibialis of the untreated leg is visualized next to the experimental anterior tibialis. Overall, the autograft recovery can be seen to be far greater than that of both scaffold groups, with the autograft recovering to an average 62% of the total control muscle mass, whereas the LBL-scaffold and LBL-scaffold-WP both recovered on average only 20% and 15% respectively (*Figure 8B*).

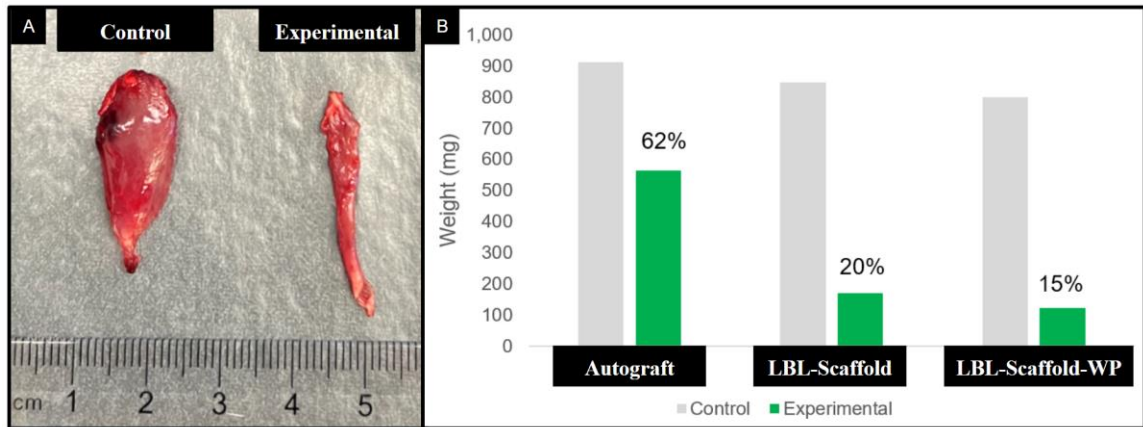


*Figure 8.* LBL-Scaffold Anterior Tibialis Muscle Weights After Scaffold Explantation

It is hypothesized that regenerating nerves were unable to penetrate into the LBL-scaffolds due to the scaffold having too little open space. The axons did not seem to be able to degrade the hydrogel at a sufficient rate, if at all. The layer-by-layer assembly method may have produced a biochemical environment that discouraged axon infiltration, even with the functional peptide attachment. The hydrogel mesh was too small for axon infiltration and could not be degraded to allow axon infiltration.

## Chapter 3

### Rolled Film Scaffolds

#### 3.1 Rolled Film Scaffold Introduction

Through the layer-by-layer additive manufacturing method, it was hypothesized that axon penetration into the hydrogel was not occurring. A new technique of scaffold manufacturing was proposed to increase the amount of porous space within the hydrogel, allowing for easier axon penetration into the scaffold. A new scaffold manufacturing technique that creates open space between films of hydrogel coated nanofibers was created to greatly increase the ability of nerve cell maneuverability throughout the scaffold and improve overall effectiveness. This method for scaffold manufacturing is referred to as the rolled film method.

#### 3.2 Materials and Methods

##### *3.2.1 Rolled Film Scaffold Fabrication*

To prepare a rolled film scaffold, nanofibers must first be spun onto frames with internal dimensions of 30 mm by 20 mm. The fibers are oriented so that they are attached across the shorter distance of the frame, with fibers of length 20 mm. These frames should have a minimum density of around 36 fibers per 100  $\mu\text{m}$  in order to make a complete film once dipped in hydrogel. The GelMe or HANor hydrogel solution is heated to 50°C in a 50 mL conical tube using an oven to create a viscous solution. 20 wt% gelatin (Type A, MP Biomedicals, France) in distilled water is also prepared and heated to 50°C.

When the GelMe or HANor hydrogel solution and the gelatin solution have reached temperature, the tubes are moved to a bead bath set to 50°C. One frame is dipped into the GelMe or HANor hydrogel solution within the conical tube, ensuring the entire frame is coated and a full film is formed. It is immediately exposed to UV lights at 10 mW/cm<sup>2</sup> for 3 minutes on either side of the frame, for 6 minutes total. Using surgical scissors, the film is cut off of the frame for the entire length of either side parallel to the fibers. This results in a film still attached at the top and bottom of the frame, but sides that are unattached. The top and bottom of the film are gradually cut where the film meets the plastic frame, starting from the outer edge and working towards the center. This is done a few millimeters at a time alternating between the left and right sides. The top and bottom of either side are always cut the same distance at the same time. Gradually, the film will begin to roll in on itself. This cutting pattern continues until there is 2 mm of film still attached to the frame on the top and bottom. This cutting pattern can be seen in *Figure 9A*.

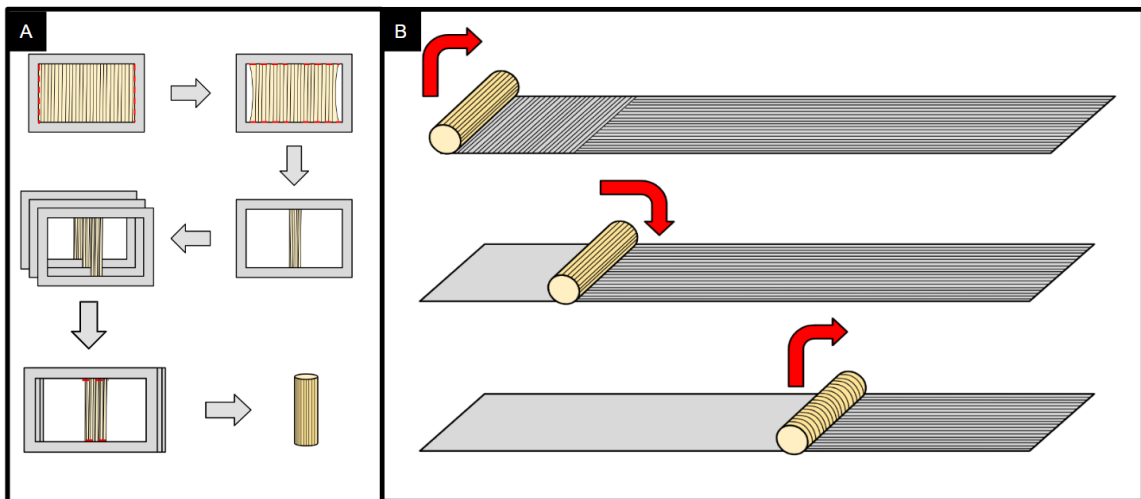


*Figure 9.* Rolled Film Scaffold Manufacturing Schematic

Five more frames are dipped, exposed to UV, and cut using this same rolling pattern until all of them are attached in the direct center of the frame. The frames are then lined up evenly so that the rolled films on each frame are bundled together using a thread tied in a knot on either end. This six-frame stack is then dipped in the 20 wt% gelatin solution and immediately moved to the refrigerator at 4°C for 3 minutes. After 3 minutes, the bundle is removed. The bundle, now cohesively held together into one structure, is removed from the frames using surgical scissors by a clean cut at the top and bottom of the frames where the bundle meets the frame. This bundle is around 2 mm in diameter. Using a razor blade, the bundle is cut to be 1.5 cm in length. The gelatin coated bundle is referred to as the scaffold.

The scaffold is wrapped in a PCL nanofiber conduit for protection and to provide guidewires along the inner surface of the conduit to guide regenerating axons, as seen in *Figure 9B*. This wrap additionally maintains the cylindrical structure of the scaffold, so the bundles of rolled films do not separate once the gelatin is removed. The scaffold is wrapped using the same process previously described in section 2.2.4. This wrap overlaps the scaffold on either side, creating a 2 mm hollow sheath in which the native nerve can be inserted and attached in-vivo to ensure a proper interface between nerve and scaffold.

The gelatin is removed from each scaffold by heating to 37°C to leave only the GelMe or HANor hydrogel. Gelatin will become a liquid at 37°C, while the photocrosslinked GelMe or HANor hydrogels will remain a solid. Scaffolds are submerged in 10 mL of 1X PBS in a 15 mL conical tube for 24 hours in an oven at 37°C. The scaffold is then removed and submerged in 10 mL of new 1X PBS for another 24 hours at 37°C to ensure all gelatin has dissolved out of the scaffold.

The final step in scaffold preparation is to sterilize the scaffolds. 0.1 M HCl in 1X PBS is used to sterilize the scaffolds in a sterile cell culture hood for 30 minutes. Each scaffold is placed in a petri dish with 5 mL of HCl solution. After 30 minutes, the HCL solution is aspirated out of the petri dish and replaced with 5 mL of sterile PBS. This PBS is aspirated out after 2 minutes and replaced with two more washed of 30 minutes each. The second wash solution is tested using a pH strip to determine whether any HCl remains within the scaffold. If the pH strip reads a value lower than around 7.4 (the pH of 1X PBS), an additional 30-minute wash is performed. Afterwards, the scaffold is inserted in a 15 mL conical tube filled with PBS and stored in a refrigerator at 4°C until use.

### ***3.2.2 Rat Sciatic Nerve Gap Model***

For an in-vivo study, 8 Wistar rats had a 1.5 cm portion of the right sciatic nerve removed and replaced with a rolled film scaffold. 4 different test groups were conducted with two rats per test group. The test groups were GelMe scaffolds with no fibers (GelMe-NF), hyaluronic acid modified with norbornene (HANor) with no fibers (HANor-NF), GelMe rolled film scaffolds (GelMe-RF), and HANor rolled film scaffolds (HANor-RF).

To manufacture the GelMe with no fibers, a 4% w/v solution of gelatin methacrylate in 1X PBS is used. This solution also contains 20 mM concentration of I2959 to allow photoinitiation when exposed to UV light. This solution was heated to 50°C in a 50 mL conical tube using an oven. Two microscope slides were attached one on top of the other using double-sided tape to create a single slide 2 mm thick. This was repeated to have identical structures. These thick slides were attached to a glass base using double-sided tape. The slides were attached to create a rectangular channel 2 mm in

width. Plastic stoppers are placed on either end of the channel to create a rectangular prism mold. Parafilm was carefully laid within this channel and pressed against all surfaces, to prevent any solution from leaking out in gaps between the slides or the base.

Once the solution has reached 50°C, a 1000 µm micro pipettor is used to transfer the heated GelMe solution to the mold, filling it completely to the top. The solution is then exposed to UV light for 10 minutes at 10 mW/cm<sup>2</sup>. Once the solution is fully crosslinked and formed into a hydrogel, forceps are used to carefully remove the hydrogel from the mold. The hydrogel is now a rectangular prism 2 mm wide by 2 mm in height. A razor blade is used to cut the hydrogel to 1.5 cm in length. This hydrogel is wrapped in a PCL fiber sheath and sterilized using the process previously described in section 3.2.1. The wrapped hydrogel is the GelMe scaffold with no fibers.

To create the HANor with no fibers scaffolds, a 3% w/v HANor in 1X PBS solution is used. This solution also contains 20 mM concentration of I2959 and 20 mM DL-Dithiothreitol (DTT, Sigma Aldrich, USA) to allow photoinitiation when exposed to UV light. The same process for creating the GelMe scaffolds with no fibers is used.

The same GelMe and HANor solutions used to manufacture the scaffolds without fibers are used to create the rolled film GelMe and HANor scaffolds. The procedure for creating the rolled film scaffolds is described in section 3.2.1. Scaffolds were sterilized and stored in PBS at 4°C until implantation.

### ***3.2.3 Scaffold Implantation***

Eight Wistar rats were chosen to undergo surgical implantation of the scaffolds. Surgical implantation followed the procedure performed for the first in-vivo rat scaffold

study, seen in section 2.2.10. All eight rats had a 1.5 cm section of their right sciatic nerve removed and replaced with a rolled film scaffold.

### ***3.2.4 Scaffold Explantation and Electrophysiological Evaluation***

After 12 weeks had passed, the rats were prepared for explantation of the scaffolds. One rat containing a HANor-NF had died at week 8, leaving 7 rats for explantation. The rats were again put under anesthesia using a gas chamber. Each rat was then removed and fitted to a gas mask that connected to the anesthesia tank that ensured the rats stayed under for the full length of the surgery. Once fully under, an incision was made down the full length of the thigh above where the sciatic nerve and implant were located. The tissue was cut carefully not to disrupt the nerve or anterior tibialis muscle until the scaffold was found, as seen in *Figure 10*.

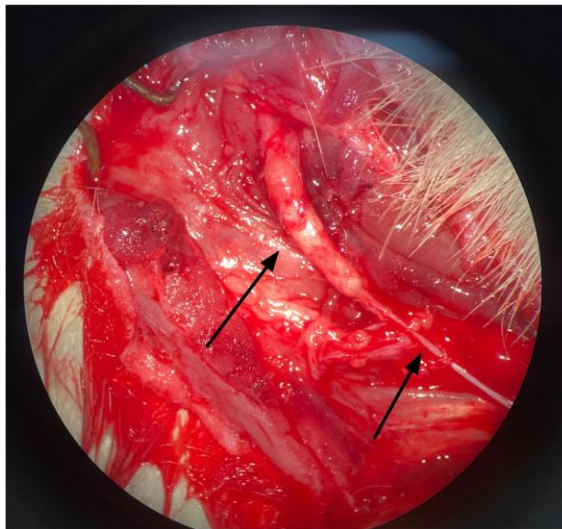


*Figure 10.* Rolled Film Scaffold Location at Explantation. The arrow on the left points to the scaffold surrounded by a fibrotic capsule, while the arrow on the right points to the distal sciatic nerve.

An incision was then made down the length of the calf of the rats, freeing the entire anterior tibialis muscle and TAT. The TAT was then cut directly above where it connected to the bones in the foot. The tendon was attached to a clamp that connected to a force sensor. Using an electrical probe, the sciatic nerve was stimulated proximally to each scaffold. The stimulation caused a signal to be sent to the muscle, causing it to contract, producing a force on the force meter that was then recorded. After the scaffold underwent electrophysiological testing, the scaffold was removed by cutting into the sciatic nerve 1 mm above and below the scaffold. A stitch was added into the sciatic nerve on the proximal side of the scaffold before its removal to identify this side during histological processing. The scaffold was then stored in 10% formalin at 4°C until it was processed. Rats were then removed from anesthesia and euthanized.

### ***3.2.5 Normal Sciatic Nerve Harvesting***

Native sciatic nerve was harvested from five deceased untreated Wistar rats (received frozen) to serve as a control to compare to regenerated nerve within the autograft and the aligned nanofiber/hydrogel nerve grafts. The rats were stored in a freezer at -80°C until the sciatic nerves were harvested. 12 hours before harvesting, the rats were moved to 4°C to begin thawing. Once fully thawed, an incision was made in the thigh of the rat down the length of the right thigh using a scalpel. The tissue was slowly cut away until the sciatic nerve was located. The surrounding tissue was cut away until the full length of the nerve was visible, as seen in *Figure 11*.

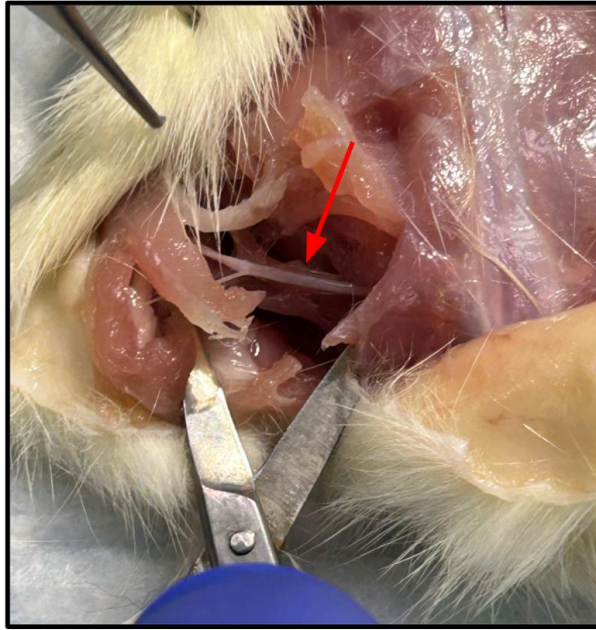


*Figure 11.* Normal Rat Sciatic Nerve Harvesting

A 15 mm length section was cut and immediately submerged in 10% formalin. This was repeated on the left leg of the rats so that 10 total normal sciatic nerves were received. The samples were stored in 10% formalin at 4°C until embedding.

### ***3.2.6 Paraffin Embedding and Sectioning***

Seven out of the eight scaffolds were chosen for paraffin embedding for histological and fluorescent staining (all except one GelMe-RF scaffold). One GelMe-RF scaffold, chosen for resin-embedding, had the proximal and distal sections removed for cross-sectional paraffin embedding. The 10 native healthy nerve samples all also underwent paraffin embedding, excluding select small sections of each of the right sciatic nerves which were chosen for resin embedding.

Scaffolds and nerves were removed from the 10% formalin solution and rinsed in 1X PB for 24 hours at 4°C. They were then transferred to their own glass scintillation

vials for tissue processing. The tissue processing procedure involves submerging the scaffolds in various solutions over various timepoints. First the scaffolds and nerves are dehydrated, replacing all the water within the tissue and scaffold with alcohol. The alcohol is then replaced with xylene, which is then replaced with paraffin wax. The solutions and submersions times are as follows: 70% Ethanol (200 proof EtOH, Pharmco) for 30 minutes, 80% EtOH for 30 minutes, two 95% EtOH cycles for 15 minutes each, three 100% EtOH cycles for 15 minutes each, two xylene cycles for 15 minutes each and one for 30 minutes. At this point, they are removed from their scintillation vials and placed in tissue embedding cassettes. The next set of submersions all occur at 55°C: 50% xylene- 50% paraffin wax for 30 minutes, 100% paraffin wax for 60 minutes, 100% paraffin wax for 60 minutes. After the scaffolds and native nerves have undergone tissue processing, they are embedded in paraffin wax on the tissue embedding cassettes and cooled using a cold plate. Once cooled, the paraffin-embedded scaffolds were stored in a refrigerator at 4°C until they were sectioned. Six of the scaffolds were embedded longitudinally while two were embedded cross-sectionally. All 10 of the native nerves were embedded longitudinally, with 3 small sections removed from the left native nerves and placed cross-sectionally.

A microtome was used to section the paraffin embedded sections. Sections were cut at a thickness of 8  $\mu\text{m}$  and placed on microscope slides. A warm water bath was used to expand samples for easier placement onto the slides. The sections on the microscope slides were heated for 24 hours at 37°C to ensure proper adhesion of the section to the slide, and then stored at room temperature until staining.

### ***3.2.7 Histological Staining***

Slides from each sample underwent either H&E (hematoxylin and eosin) staining or Masson Trichrome staining. To stain the scaffolds and tissue, the sections on the slides must first be deparaffinized and then rehydrated. To do this, slides are submerged at room temperature in the following solutions: three xylene cycles for 4 minutes each, two 100% EtOH cycles for 2 minutes each, two 95% EtOH cycles for 3 minutes each, 80% EtOH for 3 minutes, 70% EtOH for 3 minutes, and distilled water for 2 minutes.

For slides undergoing H&E staining, sections were submerged in Gill (#3) hematoxylin for 5 minutes. Hematoxylin is used to stain the nuclei of cells. After five minutes, the sections are rinsed in a bath of tap water with a continuous influx of clean water until the water is clear. To differentiate the hematoxylin, sections were then submerged in 2% glacial acetic acid in distilled water for 1 minute. Sections were again rinsed in tap water until the water was clear. To finish the hematoxylin staining, sections are submerged in a bluing solution that will change the current brown stained structures to a bright blue coloring. The bluing solution used is 0.3% NH<sub>4</sub>OH (28%) in water. The slides are then rinsed using 5 dips in distilled water before being submerged in 95% EtOH for 1 minute. Finally, slides are submerged in Eosin Y solution for 3 minutes before immediately beginning rehydration. Eosin is used to stain the cell cytoplasm pink. The Eosin Y solution is made by dissolving 1 g of Eosin Y in 20 ml of dH<sub>2</sub>O and adding 80ml of 80% EtOH. This solution is then diluted to 1 part stock to 3 parts 80% EtOH, with 0.5 mL of glacial acetic acid added per 100 mL.

For slides undergoing Masson Trichrome staining, sections were first submerged in Weigert's iron hematoxylin for 5 minutes. Weigert's iron hematoxylin is a 50/50 v/v

mix of two solutions. The first solution is made by dissolving 1 g hematoxylin in 100 mL 95% EtOH. The second solution contains 2.5 g ferric acid and 4.5 g ferrous sulfate dissolved in 298 ml distilled water and 2 ml concentrated hydrochloric acid. After staining with the Weigert's iron hematoxylin, the sections are then rinsed in a bath of tap water with a continuous influx of clean water until the water is clear. To differentiate the hematoxylin, sections were then submerged in saturated aqueous picric acid for 1 minute. Sections are then rinsed in running tap water for 10 minutes. For the second stain, slides are submerged in a 1% acid fuchsin solution for 5 minutes. To make the acid fuchsin solution, 1 g acid fuchsin is mixed in 100 mL of distilled water with 1 mL glacial acetic acid. Sections are rinsed in running distilled water until the water is clear. Slides are submerged in 1% phosphomolybdic acid for 5 minutes, before being immediately transferred to the final stain, a 2.5% aniline blue solution for 5 minutes. To make the aniline blue solution, 2.5 g aniline blue is mixed in 100 mL of distilled water with 2 mL glacial acetic acid. Finally, this stain is differentiated using 1% Acidified water for 2 minutes. Acidified water is made by adding 1 mL glacial acidified water to 100 mL distilled water.

Both sets of slides must then be dehydrated to prepare for mounting. The slides are submerged in solutions in the following order: 4 dips in 95% EtOH, 2 minutes in 95% EtOH, two cycles of 100% EtOH for 3 minutes each, one cycle of xylene for 3 minutes, and two cycles of xylene for 4 minutes each. Slides are removed from the final xylene solution and excess xylene is removed. Residual xylene on the surface of the slide will assist in evenly spreading the mounting solution. Permount mounting media is used to preserve the sections on the slides and enhance the quality of images that can be taken of

the slides. Enough mounting solution is added to the slide to completely cover the sections when a cover slip is added. The mounted slides are left to harden overnight at room temperature before imaging.

### ***3.2.8 Fluorescent Staining***

To visualize the axon growth and Schwann cell presence in the grafts, immunofluorescent staining was performed using a dual antibody staining approach. The first antibody attaches directly to the desired structure, while the secondary antibody (containing the fluorescent stain) attaches to the primary antibody. Neurofilament was stained to visualize axon growth using a chicken anti-bovine antibody neurofilament H+ stain. Schwann cells were stained using Rabbit anti-cow S100 (A and B) stain. Certain slides were also stained for laminin surrounding Schwann cells with Mouse anti-rat Laminin G1 IgG2a antibody instead of for S100.

To start, sections were deparaffinized and rehydrated following the same process previously described in section 3.2.7. The sections on each slide chosen to be stained were outlined in a hydrophobic PAP pen, to reduce the volume of stain needed. The hydrophobic outline will prevent liquid from leaking out of the desired area when staining. Sections are washed in 1X PBS three times for 3 minutes each wash. The sections are then partially digested using 20  $\mu\text{g/ml}$  proteinase K in PBS with  $\text{Ca}^{+2}/\text{Mg}^{+2}$  for 15 minutes at 37°C. By partially digesting the sections, antibody stains will have easier access to the desired structures, enhancing the quality of the stain. Slides are then washed in PBS three more times for 3 minutes each wash. Slides are submerged in 1% BSA in PBS to block non-specific binding of the antibodies. Slides were then incubated in a mixture of a chicken anti-bovine Neurofilament H IgY antibody (1:500; Cat. #

AB5539; Millipore) and a rabbit anti-cow S100 IgG antibody (1:200; Cat. # Z0311; DAKO) for 1.5 hours at 37°C. If the sections were being stained for laminin instead of S100, Mouse anti-rat Laminin G1 IgG2a antibody (1:100; Cat. # D18 or #2E8; DSHB) was used instead. This was done in a humidity chamber to reduce the rate that the stain solution will evaporate and prevent the sections from drying. Once completed, slides received three more PBS washes for 3 minutes each at room temperature. Slides received another round of blocking of non-specific binding sites using normal goat serum in PBS for 15 minutes. They were then incubated in a mixture of a donkey anti-chicken IgY AlexaFluor 488 antibody (1:1000; Cat. # A78948; Invitrogen) and a goat anti-rabbit AlexaFluor 594 antibody (1:400; Cat. # A32740; Invitrogen) for 45 minutes in the dark at 37°C in a humidity chamber. If the sections were being stained for laminin instead of S100, Goat anti-mouse IgG2a AlexaFluor 594 antibody (1:200; Cat. # A21131; Invitrogen) was used instead. Finally, the slides were given another three washes in PBS for 3 minutes before mounting.

ProLong Diamond antifade mountant containing DAPI (Invitrogene) is used to mount the fluorescently stained slides. Enough mounting solution is added to the slide to completely cover the sections when a cover slip is added. The mounted slides are left to harden in the dark overnight at room temperature before being stored at -20°C.

### ***3.2.9 Resin-Embedding and Sectioning***

Each of the right native sciatic nerve samples had a 1 mm<sup>3</sup> section of the center section of the nerve removed using a scalpel for resin-embedding. One scaffold (GelMe rolled film scaffold) was chosen for resin-embedding. This scaffold was divided into three 1 mm<sup>3</sup> sections from the center of the graft.

These samples were removed from 10% formalin and transferred to 2.5 % glutaraldehyde in 0.1M PBS for 6 hours at 4°C. A washing solution was made to rinse samples throughout the tissue processing. This washing solution consisted of 100 mL distilled water, 100 mL 1X PBS, and 8.5 g of sucrose. After processing in glutaraldehyde, the tissue was rinsed in washing solution twice for 10 minutes each time at 4°C. The tissue was then post-fixed in 1% osmium tetroxide (OsO<sub>4</sub>) in 1X PBS for 2 hours at 40°C. Post-fixation is performed to preserve the lipid structure found in the myelin sheath of axons to enhance the imaging results of the neural tissue. The tissue was again rinsed in washing solution twice for 10 minutes each time at 4°C. The samples were then dehydrated in several ethanol solutions and propylene oxide solutions at 4°C for the following times: two cycles of 50% ethanol for 5 minutes each, two cycles of 70% EtOH for 5 minutes each, two cycles of 95% EtOH for 5 minutes each, two cycles of 100% EtOH for 5 minutes each, and three cycles of propylene oxide for 10 minutes each.

Following dehydration, the samples were infiltrated with the epon/araldite solution. To prepare this solution, 25 mL of Embed 812 is mixed with 15 mL of Araldite 512, 55 mL of dodecenylsuccinic anhydride (DDSA), and 2.6 mL of 2.75% dimethylbenzylamine (BDMA) for 1.5 hours at room temperature. Samples were placed in a glass scintillation vial filled with a 1:1 v/v ratio of resin solution to propylene oxide for 1 hour at room temperature. Samples were then moved to vials containing a 2:1 v/v ratio of resin solution to propylene oxide for two hours. Samples were then moved to an uncapped vial containing only resin solution for 3 hours. Finally, samples were positioned in the embedding molds filled with resin solution so that they would be cut into cross-sectional areas when sectioning began. They remained in the molds at room

temperature for 12 hours. The molds were then moved to the oven at 60°C for 24 hours to harden. Once hardened, samples were stored at room temperature until sectioning.

To section the resin embedded samples, an ultramicrotome was used. Glass knives were prepared and prepped on the ultramicrotome. Cross-sections 1 µm thick were cut of each sample. Distilled water was used to expand the cut sections and make placement easier. A metal loop was used to transfer 10 sections to each microscope slide which was then left to dehydrate on a hot plate set to 80°C to ensure proper adhesion to the slide.

### ***3.2.10 Resin-Embedded Axon Staining***

To visualize the myelin sheath and axons of the resin-embedded sections, a toluene blue stain solution was used. Toluene blue will stain the myelin sheath of axons a dark blue color, while staining the axon center a lighter blue shade [55]. To prepare the toluene blue stain solution, 1 g of toluene blue and 1 g of sodium tetraborate were dissolved in 100 mL of distilled water. A 45 µm filter was affixed to a 10 mL syringe filled with toluene blue stain solution. The filter is used to prevent possible sediment of undissolved solute in the solution from disrupting the staining process. Solution was used to completely cover all of the sections present on the slide. The slide was then transferred to a hot plate for one minute until the edges of the drop of stain began to turn from a dark blue to a metallic green/gold color. The slide was then removed from the hot plate and rinsed using a stream of distilled water. Once the stream of water produced no more stain from the samples, the slides were returned to the hot plate until all of the water evaporated. Permount mounting media is used to preserve the sections on the slides. Enough mounting solution is added to the slide to completely cover the sections when a

cover slip is added. The mounted slides are left to harden overnight at room temperature before imaging.

### ***3.2.11 Slide Imaging***

To image the slides processed with H&E and Masson Trichrome stains, a slide scanner using a 40x magnification was used. For immunofluorescent stained sections, a fluorescent microscope was used to take fluorescent images of the appropriate color channels for each stain. These images were taken at 10x, 20x, and 40x magnification. Resin-embedded sections were imaged using the slide scanner at 63x magnification.

### ***3.2.12 Axon Quantification and Analysis***

After the stained sections were imaged, axon diameters and myelin sheaths thicknesses were quantified. Three random sections of three normal sciatic nerves, for nine total, were chosen for quantification. Nine total scaffold regenerated nerve sections were chosen to be quantified from the single embedded sample. A crosshairs technique was used to measure the inner axon diameter total myelinated axon (fiber) diameter, seen in *Figure 12B*, a commonly used method in literature [56, 57]. A line was measured across the diameter of the total fiber, and another one in the same location measuring only the inner axon diameter. The diameter of both the fiber and the inner axon were also taken directly perpendicular to the previous measurements.

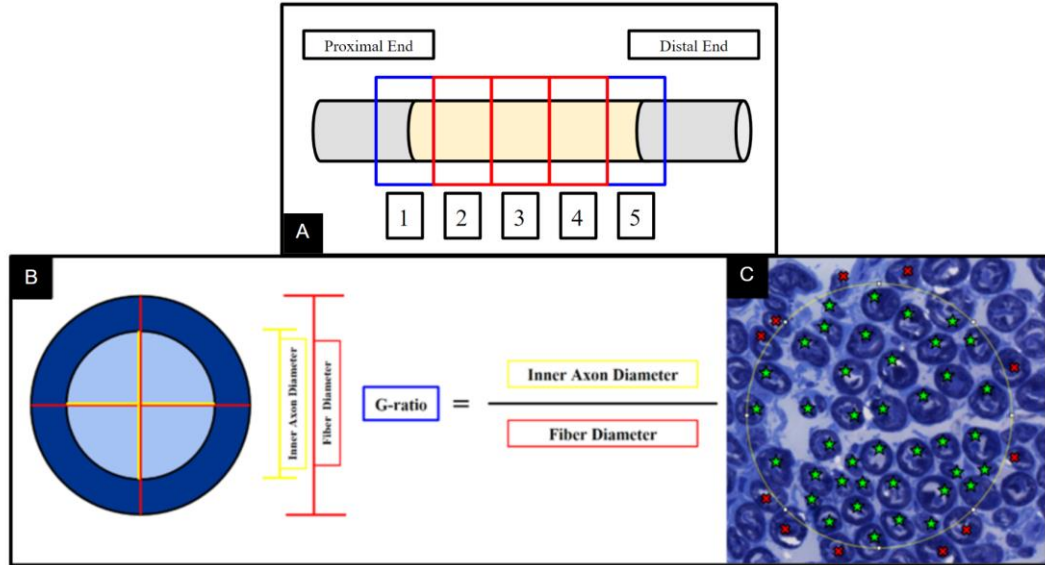


Figure 12. Axon Metrics Quantification Techniques. In Part A, blue boxes designate cut pieces used for paraffin-embedding, while red indicate pieces used for resin-embedding. In Part C, green stars are axons counted while red stars are axons not counted.

Both sets of measurements were then used to determine an average inner axon diameter and average myelinated axon diameter for each nerve measured. To determine the myelin sheath thickness, the inner axon diameter was subtracted from the fiber diameter and divided in half. To determine the G-ratio of a nerve, the inner axon diameter is divided by the fiber diameter. 287 native axons were quantified, and 200 scaffold axons were quantified.

To determine the number of axons per unit area ( $1000 \mu\text{m}^2$ ), 5 random images from the three normal nerves were selected. A circle of  $7000 \mu\text{m}^2$  diameter was drawn over the center of the picture using the ImageJ. The number of axons within this circle were then counted. For axons who overlapped with the edge of the circle, a method was devised where only axons with 50% or more of the axon was within the circle would be

counted, as seen in *Figure 12C*. This count was then used to determine the average number of axons per 1000  $\mu\text{m}$ . The same process was applied to 9 random images of regenerated nerve (3 images at 3 different locations along the graft) [55-57].

### **3.3 Statistical Analysis**

To determine statistical significance between the scaffold group and the normal nerve group for the resin embedded samples, a Welch Two Sample T-Test was conducted using the software RStudio. Statistical significance was determined to be at an  $\alpha = 0.01$ .

### **3.4 Results and Discussion**

#### ***3.4.1 Electrophysiological Muscle Testing***

Before providing the stimulation, the anterior tibialis muscle was qualitatively observed. For both hydrogel groups of scaffolds with no fibers, designated NF groups, the muscles appeared completely atrophied when compared to a healthy muscle. The same result was found in the rolled film scaffold group, designated RF groups, with the exception of one GelMe-RF scaffold. While this muscle had experienced atrophy, it was decidedly larger than the other completely atrophied muscles. Despite not experiencing complete atrophy, this initially indicated that the nerve had not successfully regenerated through the scaffold, as the muscle atrophied from lack of use because no signal for contraction was able to be passed through the scaffold.

When electrical stimulation was supplied to the sciatic nerve proximal to each scaffold, all of the scaffolds with completely atrophied muscles had no measurable force on the force sensor. Additionally, the muscles did not produce a contraction or twitch, indicating the nerve was completely disconnected. The GelMe-RF scaffold whose muscle

only exhibited mild atrophy, there was still no contraction strong enough to receive a reading from the force sensor. However, when the nerve was stimulated, contractions were visible in the muscle. This indicated that signal was being conducted down the nerve, through the length of the scaffold and into the distal nerve all the way to the muscle. A summary table of these results can be found in Table 2.

**Table 2**

*Rolled Film Scaffold Anterior Tibialis Electrophysiological Muscular Testing Results*

Scaffold Type	GelMe-NF		HANor-NF	
Sample	1	2	1	2
<b>Muscle Observation</b>	Complete Atrophy	Complete Atrophy	Complete Atrophy	N/A
<b>Muscle Force Generated</b>	No Contraction	No Contraction	No Contraction	N/A
Scaffold Type	GelMe-RF		HANor-RF	
Sample	1	2	1	1
<b>Muscle Observation</b>	Complete Atrophy	Some Atrophy	Complete Atrophy	Complete Atrophy
<b>Muscle Force Generated</b>	No Contraction	Visible Twitch	No Contraction	No Contraction

The complete atrophy of the muscles in the majority of the scaffolds indicated lack of required nerve regeneration through the rolled film scaffold design. Histological investigation was conducted to determine if any axon infiltration was present in the samples or if the structure of the scaffold was largely impenetrable. While the one GelMe-RF scaffold had a positive result, it was unclear whether the regenerating nerve had used the scaffold as designed or had traveled around the nanofiber wrapping on the outer interface of the scaffold. Axon morphology through resin-embedding and ultramicrotome sectioning was then conducted.

### ***3.4.2 Histologically Stained Image Analysis***

To visualize the initial cell distribution and the state of the scaffold, hematoxylin and eosin (H&E) staining was utilized. Hematoxylin stains the nuclei of cells a dark blue color, while eosin stains the cytoplasm of cells a light pink color. Longitudinal and cross-sectional sections from each group, excluding the GelMe-RF scaffold that produced a muscle twitch, were stained with H&E. Masson Trichrome stain utilizes three different stains to differentiate cells from connective tissue, particularly collagen. In this process, nuclei are stained a dark blue, cytoplasm is stained a red/mauve, muscle is stained bright red, and collagen is stained a bright blue [58-61].

When looking at the longitudinally cut stained sections of the scaffolds, it immediately became clear that the hydrogel of the scaffold did not fully degrade. *Figure 13* is a longitudinally cut section of one GelMe-NF scaffold. The Gelme hydrogel can be seen in both the H&E and Masson Trichrome stained centers of the section as the lighter stained core. It also was seen that a large fibrotic capsule formed around the scaffold, as seen in the tissue surrounding the scaffold. A fibrous capsule is common in inert biomaterials implanted in the body [62]. The interface between the proximal nerve stump and the scaffold (located in the red box) is magnified for visualization. It appears from histological staining that the incoming nerve was unable to penetrate into the scaffold. This result is seen across all NF scaffold groups.

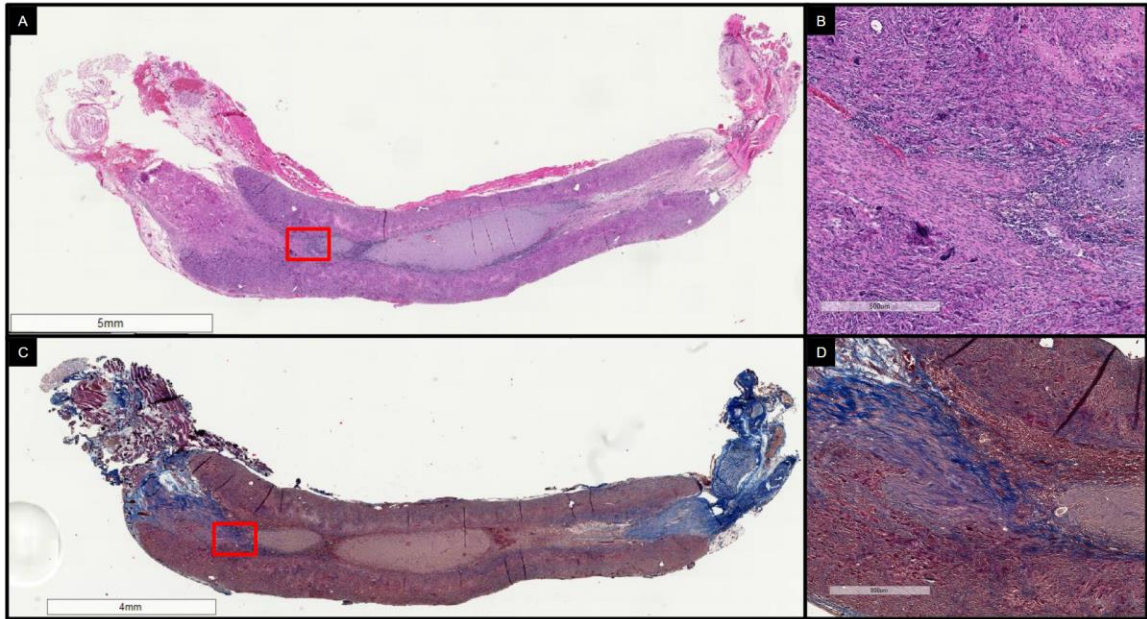


*Figure 13.* Explanted Scaffold-NF Longitudinally Stained Section. The scaffold in this photo is from the GelMe-NF group, stained in both H&E and Masson's Trichrome. Scale bar for Part A: 5 mm. Scale Bar for Parts B: 4 mm. Scale bar for Part C: 500  $\mu\text{m}$  and Part D: 800  $\mu\text{m}$ .

The same results were seen for longitudinal sections of the RF scaffolds. When viewing one sample of the HANor-RF group (*Figure 14*), the hydrogel core can be seen throughout the length of the section. The RF hydrogel visibly has a greater amount of open space than the NF scaffolds, however, it still appears that the nerve does not infiltrate through the scaffold. A fibrous capsule of approximately the same thickness formed around the rolled film scaffolds as the no fiber scaffolds. The lower crosslinking should have resulted in a higher degradation rate; however, the hydrogel is still largely abundant in the scaffold.

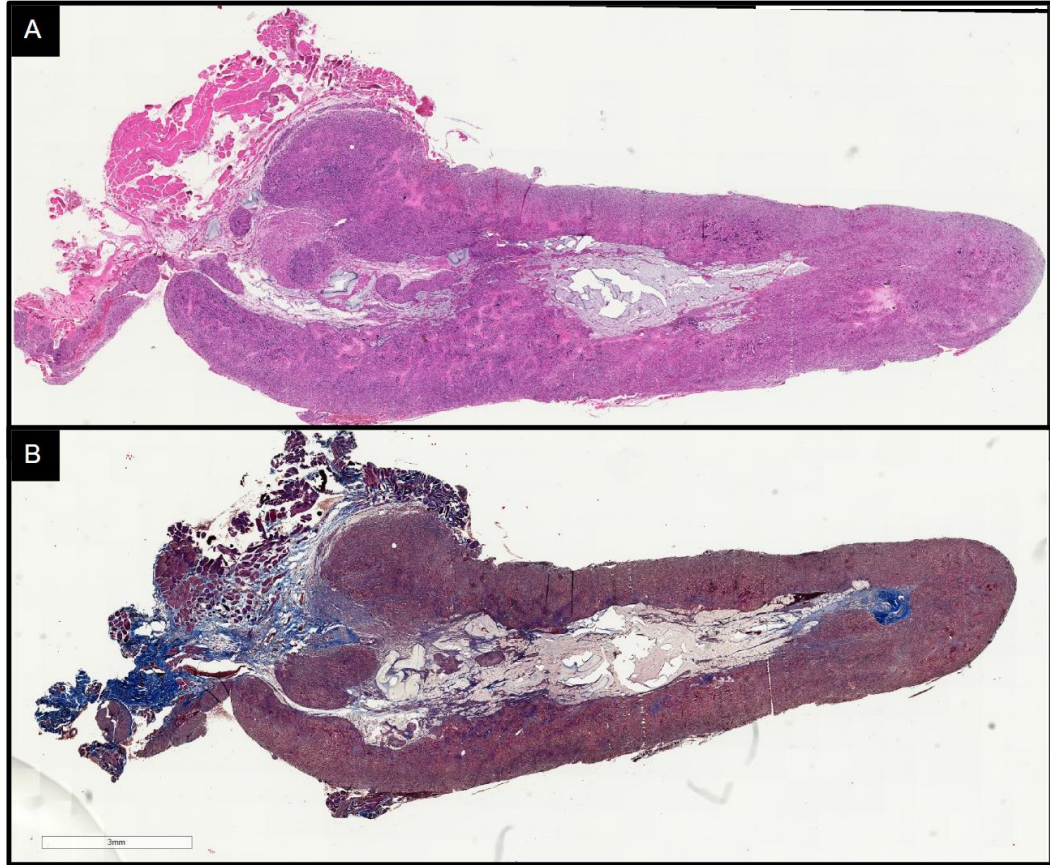


*Figure 14.* Explanted Scaffold-RF Longitudinally Stained Section. The scaffold in this photo is from the HANor-RF group, stained in both H&E and Masson's Trichrome.

Cross-sectional imaging of the GelMe-RF scaffold that did not produce a muscle twitch (*Figure 15*) further confirmed the presence of the hydrogel. It was not possible to confirm the presence and location of nanofibers within the microscopic images.

Throughout the histological images, nuclei can be seen within the hydrogel (*Figure 15D* and *Figure 15F*). There is some cell infiltration into the hydrogel, although it is unclear what type of cells are present. It appears that it is not regenerating axons that infiltrated the hydrogel, but immunofluorescence staining of nerve specific proteins provides a

better interpretation of the depth that the regenerating nerve traveled and what cells are present in the hydrogel.

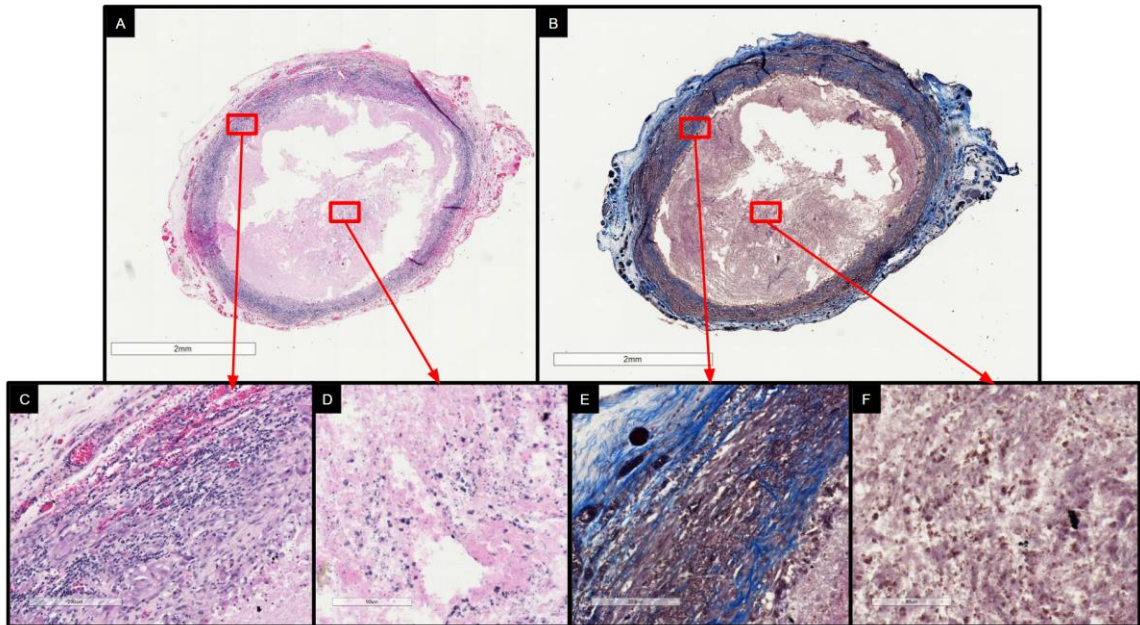


*Figure 15.* Explanted Scaffold-RF Cross-Sectionally Stained Section. The scaffold in this photo is from the GelMe-RF group that had a fully atrophied distal muscle stained in both H&E and Masson's Trichrome.

### ***3.4.3 Fluorescently Stained Image Analysis***

Fluorescent imaging was used to visualize the growth of nerves in the scaffold and fibrotic capsule. Schwann cells are a type of glial cell that provide support for the peripheral nervous system and play a crucial role in the guidance of axon growth. When looking at regenerating axons after an injury, myelinating Schwann cells (MSCs) are crucial for healthy, organized growth [7]. MSCs wrap around all large diameter axons (diameters  $> 0.1\mu\text{m}$ ), helping to produce and differentiate myelin sheath. In addition to

myelinating the axons, Schwann cells guide the regeneration of axons by producing longitudinal microchannel structures called bands of Büngner. These tunnels are the basis for the directional growth of the axons and are crucial in recovering from PNI [8].

To study the patterns of axons and Schwann cells in the regenerating nerve, an antibody staining technique was utilized to visualize the structures. To stain the regenerating axons, an antibody was used that binds neurofilament heavy chain, present abundantly in axons. This antibody was then conjugated with a secondary antibody carrying a green, fluorescent dye. To stain Schwann cells, two different structures were stained separately. The first was stained using an axon that binds S100, a protein found in the nucleus and cytoplasm of Schwann cells. The second structure that was stained for was laminin, found in the basement membrane that surrounds Schwann cells. Both of these were conjugated with a secondary antibody carrying a red fluorescent stain [58-61].

The axon and Schwann cell organization in the grafts was first explored to determine if any axons were able to go through or around the graft. *Figure 16* displays a Masson trichrome stained longitudinal section of a HANor-NF scaffold. Healthy nerve fibers, displayed in green, can be seen approaching the proximal end of the scaffold surrounded by organized Schwann cells (*Figure 16B* and *Figure 16C*). At the distal end, disorganized Schwann cells are seen in a wavy pattern as the organization dismantles after no regenerating axons are present (*Figure 16D* and *Figure 16E*). No neurofilament can be seen at the distal end as there was no infiltration across the scaffold. This result was seen for all the no fiber scaffolds and the rolled film scaffolds across both hydrogels, excluding the single GelMe-RF scaffold that conducted a muscle twitch. Axons were unable to penetrate into these scaffolds or travel along the outside of the scaffold.

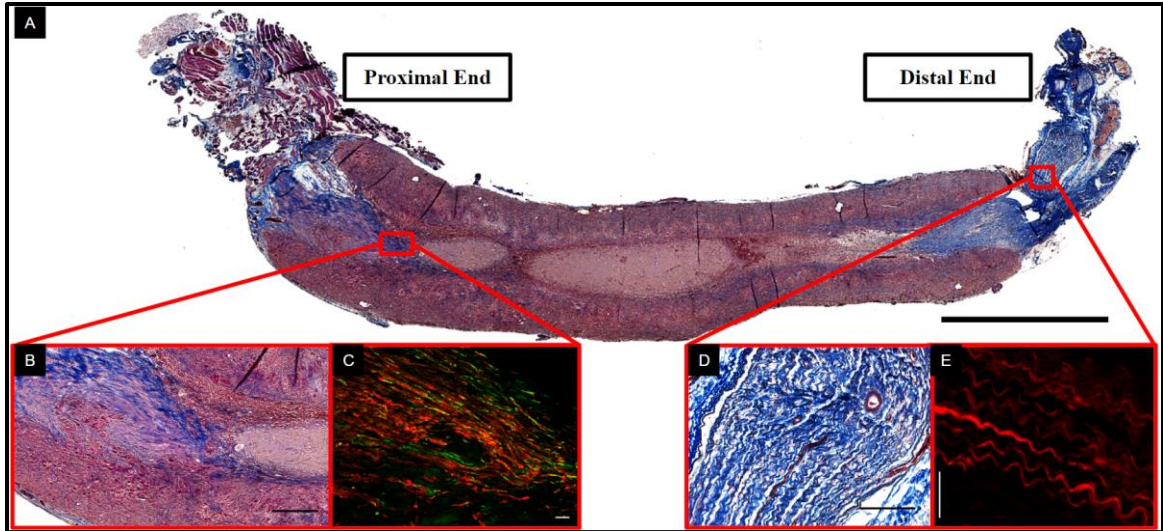


*Figure 16.* Immunofluorescent Stained Regenerating Axons and Schwann Cells in Scaffold-NF

Neurofilament at the interface between the proximal ends of the scaffolds and the center of the scaffolds was then investigated. *Figure 17A* shows neurofilament stained in a normal sciatic nerve. The neurofilament is very organized and aligned, traveling top to bottom. When visualizing the interface between the proximal sciatic nerve and the scaffold, it becomes apparent that the axons stop all infiltration upon reaching the structure. This can be seen in *Figure 17B* and *Figure 17D*, where the interface is marked with a white X. This can be seen for both no fiber and rolled film scaffolds. Fluorescent images taken at the center of the scaffolds showed no neurofilament present, further supporting the conclusion that no axons were able to infiltrate throughout the scaffolds (*Figure 17C* and *Figure 17E*).

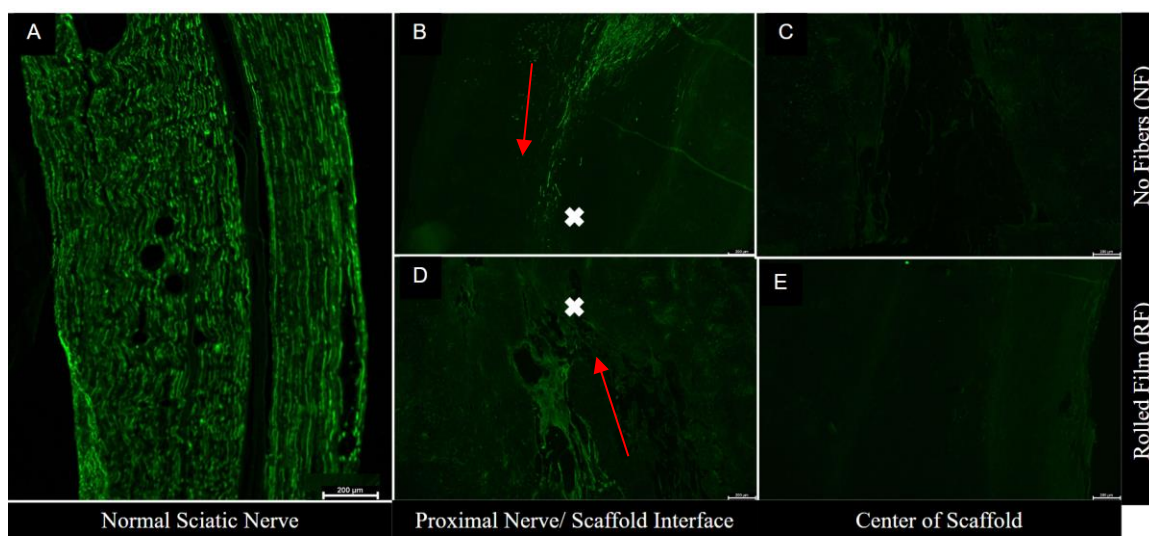


*Figure 17.* Neurofilament Visualization in Normal Sciatic Nerve and Experimental Groups. In parts B and D, the white x indicates the interface between proximal nerve and remaining hydrogel. The red arrow indicated the direction of nerve from proximal to distal. Scale bar for Part A: 200 µm. Scale Bars for Parts B, C, D, E: 40 µm.

The proximal nerve and distal nerve entering and exiting the GelMe-RF scaffold that produced a muscle twitch were imaged cross-sectionally to determine patterns of axons and Schwann cell alignment. The center of the scaffold was selected for resin-embedding to get an in depth look at axons that were suspected to infiltrate throughout, so only the very proximal and very distal ends of the scaffold were studied using fluorescent microscopy. *Figure 18* displays cross-sectional images of normal sciatic nerve next to the proximal and distal ends of the scaffold associated with incomplete muscle atrophy. In the top row of images, S100 is used to visualize Schwann cell structures, while the bottom row uses laminin to visualize Schwann cells. Normal sciatic nerve axons (green) can be seen surrounded by Schwann cells (Red) indicating healthy

nerve cells (*Figure 18A* and *Figure 18D*). The dark, unstained gap between the axon and the Schwann cell is where the myelin is present. The normal nerve has a relatively large and visible gap indicating thickly myelinated axons.

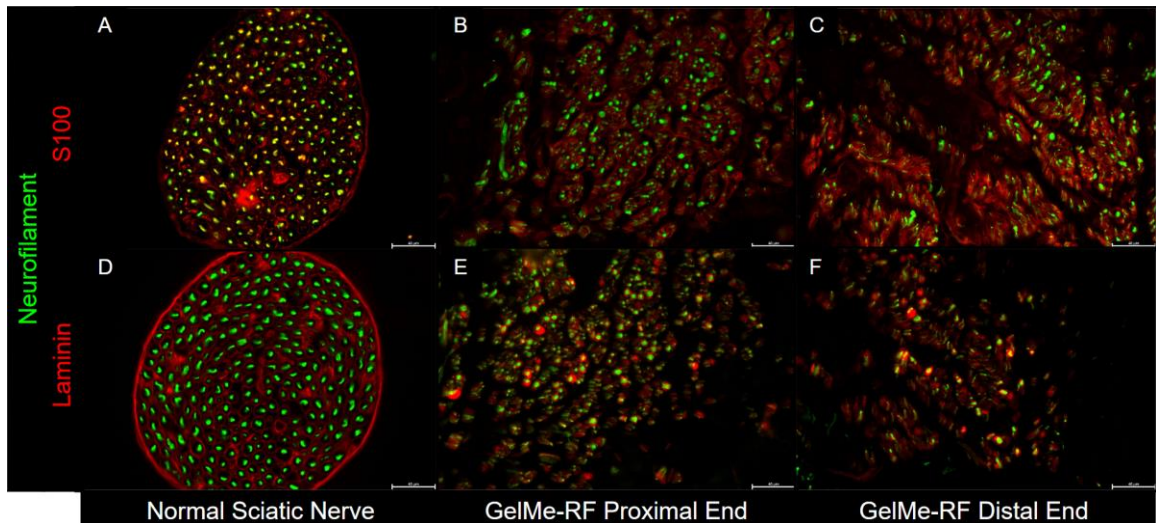


*Figure 18.* Schwann Cell and Neurofilament Visualization in Cross-Sectional Imaging

All scale bars indicate 40  $\mu\text{m}$ .

The proximal end of the GelMe-RF scaffold reveals regenerating axons surrounded by Schwann cells entering into the scaffold structure (*Figure 19B* and *Figure 19E*). These axons qualitatively appear much smaller than the normal sciatic nerve axons. The gap between the axon and the Schwann cells also appears much smaller than the normal sciatic nerve, which may indicate that the axons have thinner myelin sheaths. The axons appear to be infiltrating longitudinally through the structure as axons cross-sections give circular structures as opposed to long longitudinal lines on the cross-section. This

indicates that the axons may have found the nanofibers within the structure to align along.

At the distal end of the scaffold, axons surrounded by Schwann cells can still be seen growing through the structure (*Figure 18C* and *Figure 18F*). It appears that axons were able to regenerate throughout this GelMe-RF scaffold through the entire length. The axons are also visually seen through the center of the structure, not traveling around the scaffold, but instead infiltrating into it. To further study the growth of axons in this sample, high magnification microscopy was conducted on the center of the scaffold to quantify axon metrics.

#### ***3.4.4 Axon Measurement and Quantification***

The single GelMe-RF scaffold that was chosen for resin-embedding is referred to as “scaffold regenerated nerve” for figures in this section. Images of the resin-embedded sections of scaffold were taken at three locations down the length of the scaffold. Each of these locations revealed axon growth through the center of the scaffold area, indicating that the muscle twitch observed during scaffold harvesting was due to a signal transferred through regenerated axons. The axons that were regenerated were seen to be in close proximity to the remaining hydrogel of the scaffold. In some cases, axons could be seen regenerating in contact with the hydrogel (*Figure 19*). This processing technique did not allow for determination of whether the axons aligned along the nanofibers of the films for contact guidance to grow directionally to the other side of the scaffold. The myelin surrounding these axons is visualized as a dark blue ring, with the lighter blue center being the axon itself.

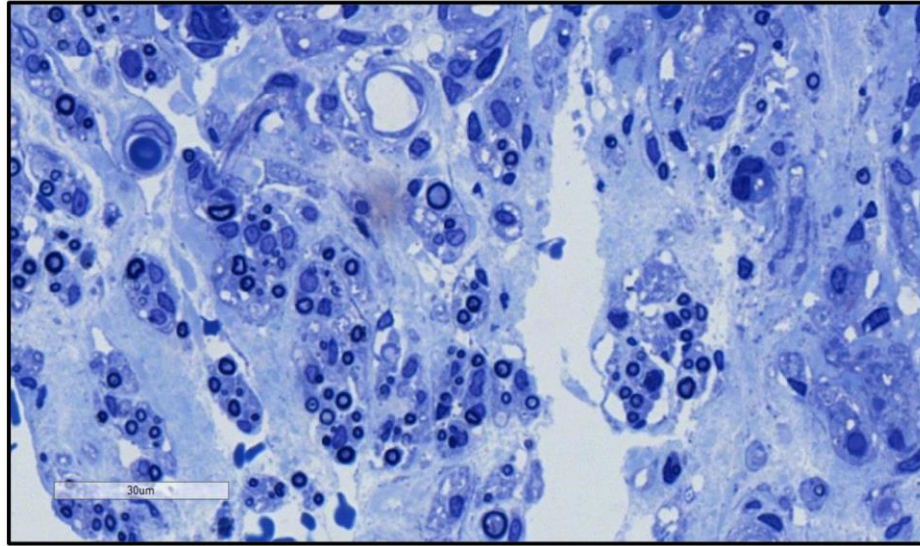


*Figure 19.* Axons Regenerating Through Remaining Hydrogel in GelMe-RF. Scale bar indicates 30  $\mu\text{m}$ .

200 regenerated axons and 287 normal axons were quantified for inner axon diameter, myelin sheath thickness, and G-ratio. Axon diameter is used as a metric for determining the health of regenerated nerve as it influences the rate of conduction properties within a myelinated axon [55-57]. Through a qualitative initial assessment of the images of both groups of nerve, the axon diameter for normal nerve was seen to be far larger than that of the regenerated nerve. *Figure 20* shows a comparison image between the normal nerve and the regenerated scaffold nerve. The myelin of these axons also appeared to be thicker upon visual assessment. In the images for the normal axons, axons are seen to be distorted in part, including in the center of the cell. This is thought to be an artifact of the freezing process of the rats. The healthy rat donors were received unfixed and frozen and therefore the healthy sciatic nerve did not react the same as the regenerated scaffold nerves throughout the embedding and staining process, resulting in

slight imaging defects. These defects did not affect the ability to quantify attributes of the nerves. G-ratio compares the diameter of the axon to the thickness of the entire fiber as a metric to determine the health of an axon [55-57].

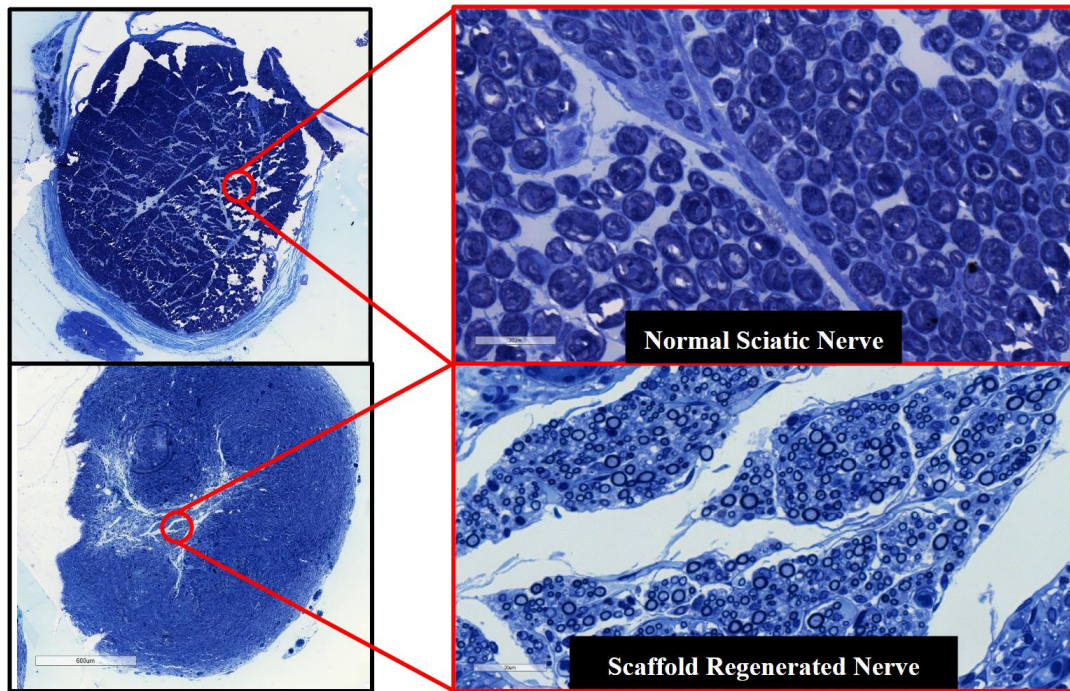


*Figure 20.* Normal Sciatic Nerve Axons Compared to Experimentally Regenerated Axons. Scale bars for zoomed out images: 600  $\mu\text{m}$ . Scale bars for zoomed in images: 30  $\mu\text{m}$ .

There appears to be a highly significant difference ( $p$ -value of  $3.64\text{E-}69$ ) in the mean axon diameter between the normal rat sciatic nerves and the regenerated scaffold sciatic nerve, with regenerated scaffold axons being far smaller than normal axons. The mean axon diameter for normal rat sciatic nerve was found to be  $4.208 \mu\text{m}$ , while the mean axon diameter for the scaffold nerve was  $1.907 \mu\text{m}$ , visualized in *Figure 21A* and

Figure 21C. It also seems that there is a highly significant difference (p-value of 1.24E-161) in the mean myelin thickness between the normal rat sciatic nerves and the regenerated scaffold sciatic nerve, with regenerated scaffold axons having far smaller myelin sheaths than normal axons. The mean myelin sheath thickness for normal axons was found to be 2.625  $\mu\text{m}$ , while the mean for scaffold axons were 0.700  $\mu\text{m}$ , visualized in Figure 21B and Figure 21D.

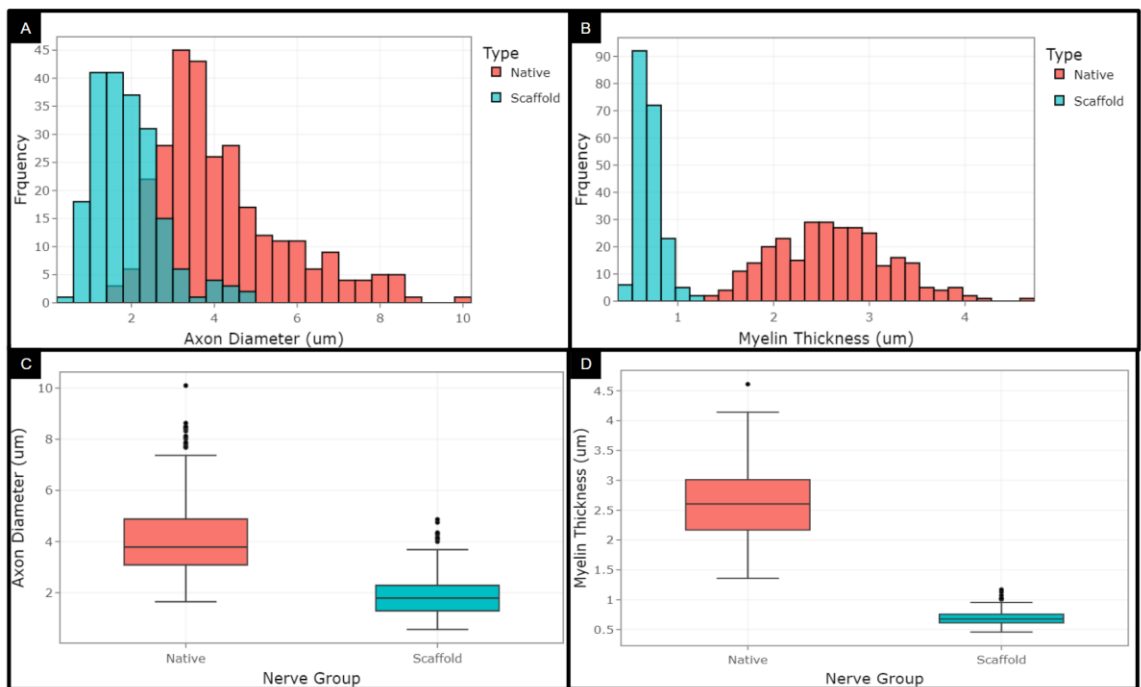
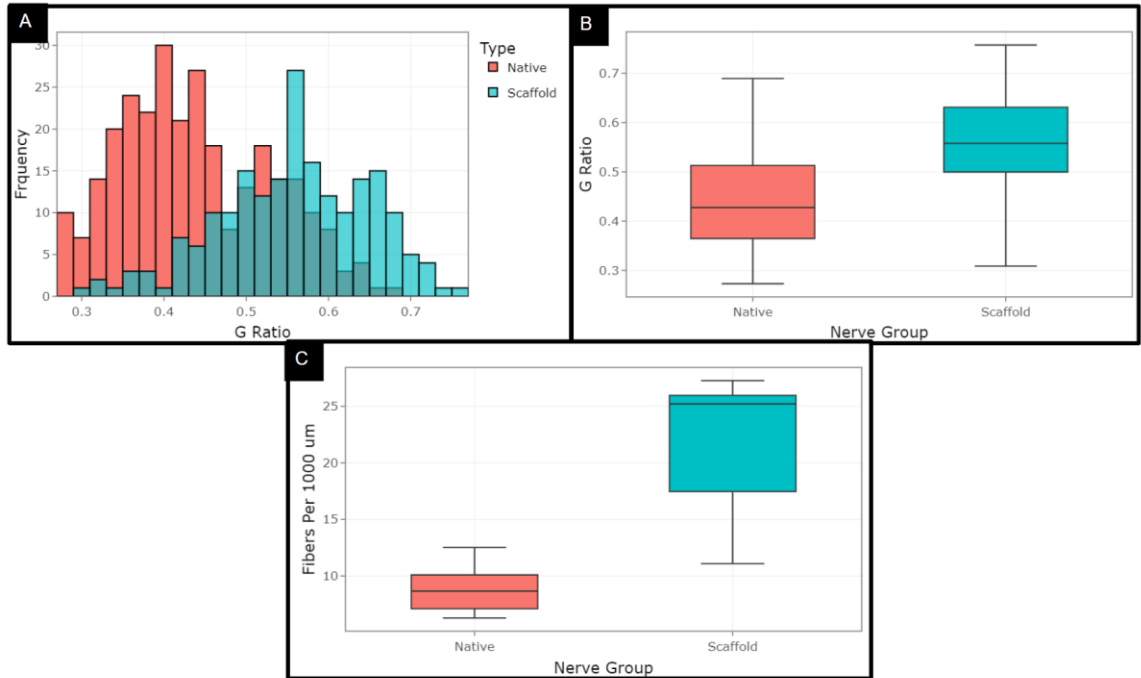


Figure 21. Axon Metric Quantifications for Normal Sciatic Nerve and Regenerated Sciatic Nerve. Circles in part c and part d indicate measurements outside of the interquartile range.

There appears to be a highly significant difference (p-value of 3.27E-38) in the mean g-ratio between the normal rat sciatic nerves and the regenerated scaffold sciatic nerve, with regenerated scaffold axons being larger than normal axons. The mean g-ratio

for normal rat sciatic nerve was found to be 0.438, while the mean g-ratio for the scaffold nerve was 0.557, visualized in *Figure 22A* and *Figure 22B*. It also seems that there is a significant difference (p-value of 1.89E-04) between the number of axons per 1000  $\mu\text{m}^2$ , as seen in *Figure 22C*. Standard deviations and p-values are recorded in Table 3.



*Figure 22. G-Ratio and Nerve Fiber Density of Normal and Regenerated Sciatic Nerve*

**Table 3**

*Summary Table of Axon Quantification Metrics for Normal and Regenerated Nerve*

Sample Type	Normal	Scaffold	P-Value
Axon Count	n = 287	n = 200	
Axon Diameter ( $\mu\text{m}$ )	4.208 $\pm$ 1.574	1.907 $\pm$ 0.823	3.64E-69
Myelin Sheath Thickness ( $\mu\text{m}$ )	2.625 $\pm$ 1.056	0.700 $\pm$ 0.484	1.24E-161
G-ratio	0.438 $\pm$ 0.091	0.557 $\pm$ 0.092	3.27E-38
Fibers Per 1000 $\mu\text{m}$	8.671 $\pm$ 1.921	21.952 $\pm$ 6.129	1.89E-04

One of the roles of a myelin sheath is to insulate the axon, preventing “leaking” of the traveling signal, maintaining its strength. By having axons with very thin myelin sheaths, more of the membrane charge traveling along the axon will be lost, decreasing its strength by the time it reaches the desired muscles. In this case the anterior tibialis muscle. Small axons are not capable of transporting as large a signal when compared to normal sized axons [63-65].

One possible explanation for the axon diameters being smaller and the myelin sheaths being thinner is that the regenerating axons need more time to develop. Another contact guidance nerve scaffold study had a similar result during in vivo studies in pigs where a muscle twitch in a sample was seen but the twitch was too weak to be measured. It was determined that the nerve had bridged the damaged nerve gap but was still immature. The muscle had been reached by the nerve but had not matured enough to have an intense enough signal to evoke a full muscle twitch. At a timepoint 2 months in the future, the regenerated nerves of the scaffolds were able to produce a full measurable muscle twitch. Histology at this late timepoint revealed large, myelinated axon that resembled native nerve [48]. The axons regenerated by the GelMe-RF scaffold could have been underdeveloped and given more time have matured into a sciatic nerve that mimicked the original host tissue and was capable of producing a measurable muscle twitch.

It is not clear why the one GelMe-RF scaffold was capable of allowing cell infiltration through the hydrogel while the other groups had no infiltration. One reason could be the low crosslinking time experienced by the hydrogel compared to the no fiber scaffolds and the layer-by-layer additive manufacturing scaffolds. The GelMe in the

GelMe-RF scaffolds only received 6 minutes total crosslinking time under UV light, while the NF scaffold received 10, and the layer-by-layer scaffolds received 13 minutes. This lower crosslinked hydrogel could allow for axons to have an easier time degrading the hydrogel and finding the fibers within. Another possible explanation is the increased open space of the scaffold. By using a RF design, there is space between the hydrogel layers and the bundles of the rolled films themselves. This space would allow axons to maneuver much easier further into the hydrogel, where it would then have more access to the fibers that would help guide growth throughout.

Neither of these explanations, however, explains why only one scaffold from one RF group showed infiltration, while the rest of the RF scaffolds had none. It was seen that the successful scaffold had significantly less hydrogel remaining than the other scaffolds. It is hypothesized that when crosslinking a single film, the hydrogel that is exposed to oxygen undergoes a reaction that prevents it from fully crosslinking. When making RF scaffolds, each layer is thin, and therefore much of the hydrogel is exposed to the air during crosslinking. It is possible that in the successful scaffold, some of the hydrogel remained not crosslinked, and therefore dissolved out once manufactured and implanted. This lower amount of hydrogel may have allowed the regenerating axons even more space to maneuver through the scaffold and find the fibers. This would not occur in the NF scaffolds or the layer-by-layer scaffolds as their thicker structure would have a lower ratio of the surface of the hydrogel exposed to the air, allowing for standard crosslinking to occur.

It is also possible that the reaction with oxygen didn't prevent crosslinking, but instead lessened its effect. This would mean that the hydrogel was not missing, just had

much lower crosslinking than previously believed. This would allow cells to break down the hydrogel faster. It is unclear why this would only happen in one scaffold. The successful scaffold may have had a greater rate of interaction with the oxygen in the air. These films may have been made immediately when the GelMe was removed from the oven, causing the films to be thinner and increasing the ratio of hydrogel exposed to air. If the films of the unsuccessful second GelMe-RF were made second, the hydrogel may have cooled slightly, increasing the viscosity of the GelMe and thickening the films. This would then increase the amount of hydrogel naturally in each film and decrease the amount that is lost due to oxygenation, increasing the overall quantity of GelMe greatly.

Overall, very few cells were seen penetrating into GelMe or HANor. These hydrogels were also expected to have a greater degree of degradation upon explantation than what was visualized. These hydrogels may be overall largely unsuccessful because they are too stiff and too crosslinked, making it uninviting for cell infiltration. While increasing the amount of open space using a RF scaffold design showed better success at cell infiltration than a layer-by-layer additive manufacturing method, more work needs to be done to promote cell ingrowth and alignment. It is possible that the biochemical environment discouraged axon and Schwann cell infiltration, as infiltration of other cell types was observed. Decreasing crosslinking time or seeking new hydrogels to use as a surrounding ECM simulating structure could be possible avenues for future scaffolds using the rolled film technique.

## Chapter 4

### Sacrificial Gelatin Template Scaffold Infiltration

#### 4.1 Introduction

Despite observing the regeneration of axons across a peripheral nerve injury, experimental results for stacked and rolled nanofiber hydrogel composite scaffolds point to the persistence of the GelMe and HANor hydrogels as an impediment to axon regeneration. Introducing more open space seems to be a positive avenue to continue exploring in future work, however, it seems that GelMe and HANor may not have the desired regenerative capabilities that are necessary for peripheral axon regeneration using a nanofiber-hydrogel composite scaffold. A method for nanofiber-hydrogel composite scaffold manufacturing was created using a sacrificial gelatin template. In this process, the thermosreversible properties of gelatin facilitate layer-by-layer stacking and stabilize 3D aligned nanofiber architecture. Another pre-hydrogel solution is infiltrated into the gelatin-nanofiber composite template, where it is then gelled. The double hydrogel composite is heated in water to remove the gelatin template, leaving only the desired second hydrogel while maintaining the 3D aligned nanofiber structure. This process allows a wider range of hydrogels to be used for scaffold manufacturing, removing the requirement of thermosreversible and photo-crosslinkable hydrogels and allowing ionic or pH sensitive gels to be used.

#### 4.2 Materials and Methods

##### *4.2.1 Alginate Infiltration Process*

Sacrificial gelatin cylinders, which will be referred to as pucks due to their shape, were first fabricated to act as a template for the infiltrating hydrogel, sodium alginate

(ChemCenter, USA). The lids of 1.5 ml microcentrifuge tubes (CellTreat Scientific Products, China) were used as a mold to make the shape of the gelatin pucks, with dimensions of 8 mm wide by 5 mm high. 10 wt% gelatin in distilled water was heated to 50°C in an oven to create a viscous liquid solution. This solution was then pipetted into the cylindrical molds at a volume of 280  $\mu$ l each. 280  $\mu$ l was an arbitrary number determined experimentally and used to have a fixed volume that filled the mold. Once the mold was filled with gelatin, it was cooled in a refrigerator at 4°C for 7 minutes, allowing the pucks to solidify. The pucks were removed from the mold by carefully using forceps around the edge of the gel and lifting.

Pucks were immediately submerged in 1.5 mL of a 2 wt% sodium alginate in distilled water solution. One puck was placed in each well of a 24 well plate (CellTreat Scientific Products, China) and sat on an agitator moving at 120 rpm. After 1 to 504 hours, depending on desired infiltration time, the samples were removed and put in 1.5 ml of a 5 wt% calcium chloride (Sigma Aldrich) in distilled water solution for 2 hours, allowing the sodium alginate to utilize the calcium ions and crosslink into calcium alginate. The samples were removed and submerged in 10 ml of distilled water in a six well plate (CellTreat Scientific Solutions, China). The well plate was placed in an oven at 37°C for 48 hours, allowing the gelatin to liquify and disperse into the distilled water, leaving only the crosslinked calcium alginate. This process is outlined in *Figure 23*.

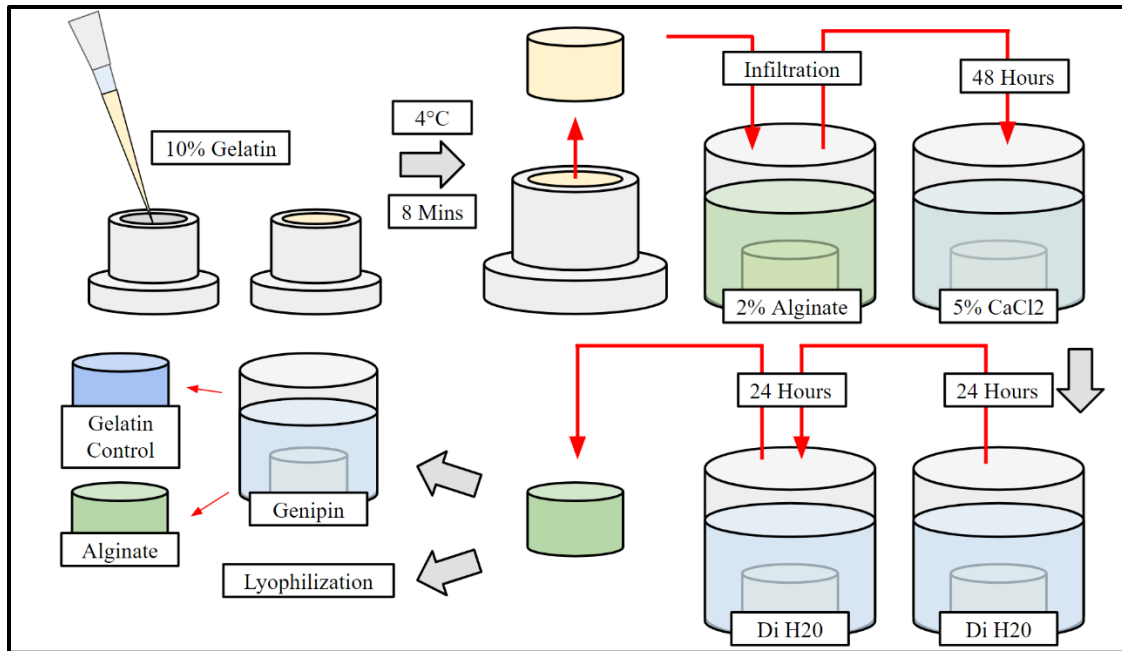


Figure 23. Sacrificial Puck Manufacturing and Infiltration with Alginate Schematic

In this preliminary proof of concept study, the properties of sodium alginate infiltration were investigated over a short time intervals (1, 3, and 5 hours). The sodium alginate solution concentration was studied at various concentrations (1%, 1.5%, 2%). 1 replicate per sodium alginate solution and time point combination.

Gelatin pucks were prepared using the same methods previously mentioned. A 2 wt% alginate sodium salt (Sigma Alrich, USA) solution in distilled water is used in place of the higher viscosity sodium alginate solution. 24 pucks are fabricated using 10 wt% gelatin, and 24 pucks are fabricated using 15 wt% gelatin. For this study, the weight of infiltrated alginate into the pucks is measured. Pucks are submerged in alginate solution for 48 hours, and then calcium chloride solution for 48 hours. 8 pucks in each gelatin group do not undergo treatment to serve as a gelatin control. Once the calcium chloride treatment is complete, 8 pucks for each group undergo gelatin removal for 48

hours, while 8 from each group do not. To ensure that all of the gelatin is removed throughout the process, the 10 ml of distilled water is replaced with fresh distilled water at 24 hours.

Once all treatments are complete, samples are frozen at  $-80^{\circ}\text{C}$  for 1 hour. Samples are then lyophilized using a freeze dryer (Labconco, USA) at 0.035 mBar and  $-80^{\circ}\text{C}$  for 4 days. Lyophilization will remove all water within the hydrogel through sublimation, leaving only the weight of the gel itself. This will allow for exact measurement of the gelatin and alginate in each puck through the use of a balance. After each lyophilized puck has been weighed, two pucks from each group were submerged in a genipin (Wako Pure Chemical Inventories) solution. Genipin is a natural compound that has a high affinity to crosslink collagen, and therefore gelatin. Once crosslinked, the gelatin will turn a dark blue color, serving as a colorimetric indicator of remaining gelatin within the scaffold. Genipin was dissolved in 200 proof ethanol at 15 mg/ml and mixed with distilled water at a ratio of 70:30 v/v genipin/ethanol to distilled water. Each puck was submerged in 2 ml of this solution for 48 hours.

For a negative control, 230  $\mu\text{L}$  of sodium alginate was submerged in 5 wt% calcium chloride solution for 48 hours. These calcium alginate pucks were immersed in the genipin solution for 48 hours.

#### ***4.2.2 Alginate Time Infiltration***

Gelatin pucks were prepared using the same methods previously mentioned in section 4.2.1 . Pucks were fabricated out of 5 wt%, 10 wt%, and 20 wt% gelatin. 2 wt% alginate sodium salt solution is used for its lower viscosity. 52 pucks for each gelatin

group were fabricated. Pucks are immersed in solution on an agitator at 120 rpm for timepoints ranging from 1 day to 21 days (1, 3, 5, 7, 10, 12, 14, 21 days). After each infiltration timepoint, the respective pucks were submerged in 5 wt% calcium chloride for 48 hours. 6 pucks for each gelatin group are lyophilized at each timepoint. Three of these pucks do not receive heat treatment to measure the weight of an infiltrated puck, while three receive heat treatment to measure the weight of alginate remaining after the gelatin is removed. 6 pucks for each gelatin wt% underwent no infiltration to act as a time zero infiltration for pucks that undergo heat treatment and those that did not undergo heat treatment. Each puck was weighed prior to infiltration to normalize the data to a fixed weight of gelatin.

Time infiltration following the same timepoints was conducted using gelatin pucks with various conditions altered. One condition altered is that the pucks were lyophilized and rehydrated previous to infiltration. 52 pucks, following the same groups seen in the previous time series infiltration, were lyophilized for 5 days, and then rehydrated in distilled water for 7 days. Alginate infiltration began after the pucks were observed to have fully rehydrated.

Another group of pucks were swollen in distilled water prior to infiltration. To determine proper swell conditions, 6 pucks made of 10 wt% gelatin were submerged in distilled water and weighed at various timepoints (1, 2.5 5.5, 20, 24, 48, 93, 52, 142 hours). The dimensions of each puck as it swelled with water were taken as well. Once the pucks were no longer changing in weight or volume, the kinetics of the gelatin swelling were plotted, and the ideal swell time was determined. 52 10 wt% gelatin pucks

were immersed in distilled water for 48 hours to allow them to fully swell, before alginate infiltration began.

A third group followed the same parameters as the time series infiltration, however, the alginate solution used was the higher viscosity alginate referred to in this paper as sodium alginate. 2 wt% of sodium alginate in distilled water was used.

#### ***4.2.3 Alginate Scaffold Structure Maintenance***

Sacrificial scaffolds were fabricated using a similar layer-by-layer additive manufacturing method described in section 2.2.4. 10% gelatin solution was heated to 50°C using an oven. 10 frames with PCL nanofibers of density of at least 36 fibers per 100 µm were prepared. Each layer was dipped in the gelatin solution to form a film and layered on top of the previous frame ensuring that the fiber orientations are the same. No UV crosslinking is performed in this process as the hydrogel is gelatin, not gelatin methacrylate, and a sacrificial template is being constructed. The stack was then cooled in the refrigerator at 4°C for 5 minutes. Once the gelatin has cooled and fully solidified, a scalpel was used to cut around the edge where the stack meets the frames. After completing this, the stack is removed from the frames and six scaffolds were cut to around 8 mm long and 2 mm wide. Initial dimensions were taken of the scaffolds using a caliper. The scaffolds were then ready to begin alginate infiltration.

Sacrificial scaffolds were submerged in 1 ml of 2 wt% alginate sodium salt solution in a 1.5 ml microcentrifuge tube. This tube was placed on an orbital shaker set to 120 rpm for 12 days. After 12 days, the scaffolds were removed, and excess alginate was removed using a paper towel. The scaffolds were then placed in a clean 1.5 ml

microcentrifuge tube and 1 ml of 5 wt% calcium chloride in dH<sub>2</sub>O was added to crosslink the infiltrated alginate solution. The tube was returned to the orbital shaker. The alginate was allowed to crosslink for 48 hours. Once complete, each scaffold was moved to 10 ml of dH<sub>2</sub>O in a 6 well plate to remove the sacrificial gelatin template. This was kept at 37°C for 48 hours. The dH<sub>2</sub>O was removed and replaced after 24 hours. Scaffold imaging was performed on a brightfield microscope at 5x and 10x magnification. Final dimensions were taken with calipers.

#### ***4.2.4 Hyaluronic Acid Scaffold Infiltration***

Infiltration into a sacrificial gelatin scaffold template using hyaluronic acid followed a similar infiltration process to the calcium alginate infiltration process described in section 4.2.3. 3 wt% HANor solution was made by dissolving 300 mg of HANor in a solution containing 1000  $\mu$ l of 0.5% I2959 solution, 1250  $\mu$ l of 20 mM of DTT solution, and 7750  $\mu$ l of PBS. A 10-layer stack of frames containing PCL nanofiber was made using the process described in section 4.2.3. Five sacrificial gelatin scaffolds were made using this method. Scaffolds were cut to around 8 mm wide by 2 mm wide. Initial dimensions were taken using a caliper.

Sacrificial scaffolds were submerged in 1 ml of HANor solution in a 1.5 ml microcentrifuge tube. This tube was placed on an orbital shaker set to 120 rpm for 12 days. After infiltration, the scaffolds were removed from the solution and excess was removed using a paper towel. Scaffold then received 5 minutes of UV light at 10 mW/cm<sup>2</sup> on each side of the scaffold, for 20 minutes total to crosslink the infiltrated HANor solution. The scaffolds were then submerged in 10 mL of 1X PBS for 48 hours at 37°C to remove the sacrificial gelatin template. At 24 hours the PBS was removed and

replaced with new PBS. The scaffolds were stored in PBS at 4°C. Scaffold imaging was performed on a brightfield microscope at 5x and 10x magnification. Final dimensions were taken with calipers.

### **4.3 Statistical Analysis**

To determine statistical significance between groups within the sacrificial template removal study and in the density of sacrificial pucks at 14 and 21 days, an ANOVA was conducted. There were 8 samples per group for the sacrificial template removal study and 3 samples per group for the density of sacrificial pucks study. Significant results were analyzed with Tukey's post hoc test. Error bars in graphs representing the density studies represent standard error of the samples. Error bars in time series data indicate a confidence interval, which was chosen to represent the error of the data as there are only three observations per group per timepoint. To determine significance in the change in dimensions of both alginate infiltration and HANor infiltration, paired sample t-tests were conducted, with 3 samples per group for alginate infiltration and 5 samples per group for HANor infiltration. All significance testing was conducted using RStudio. Statistical significance for all tests was determined to be at a  $p = 0.01$ .

### **4.4 Results and Discussion**

#### ***4.4.1 Alginate Infiltration and Sacrificial Template Removal***

Before using sacrificial gelatin scaffold templates, sacrificial gelatin pucks were used. These pucks contained no nanofibers and were comprised solely of gelatin. This decision was made as a large quantity of gelatin pucks could be manufactured in a much faster time than gelatin scaffolds could be. Additionally, the exact volume of gelatin used,

and the dimensions of pucks could be regulated more precisely than a sacrificial scaffold template. Initial experimentation was conducted to determine if sodium alginate, once infiltrated into the porous space of a gelatin template, could be then crosslinked to form a new hydrogel within the template. The ability to completely remove the gelatin template, leaving only the infiltrated alginate was also studied.

Sodium alginate, also known as alginic acid sodium salt, is a polymer that forms a viscous solution when dissolved in distilled water. When a calcium ion source is added to the solution, in this case calcium chloride, the sodium ions are replaced with calcium ions rapidly. This process binds the alginate molecules together in an organized structure, resulting in the formation of a calcium alginate hydrogel. By infiltrating the gelatin template with this polymer in solution form and then ionically crosslinking it, a hydrogel loaded with a second hydrogel should form. Alginate was chosen as the infiltrating hydrogel for a large portion of this study as it is cheap, easy to work with, and crosslinks rapidly, allowing for testing to occur using a wide range of properties. A calcium alginate hydrogel is not thermosensitive and will not melt at body temperature (37°C) as the sacrificial gelatin scaffold does.

In this study, it was found that alginate was able to infiltrate into the gelatin and crosslink to form a hydrogel. When the gelatin scaffold was sacrificed, the calcium alginate remained in the overall shape of the pucks. When the pucks were exposed to genipin, which is a crosslinking agent that in the presence of collagen, found abundantly in gelatin, with bind to is turning it blue. *Figure 24* displays the results of crosslinking gelatin template pucks, gelatin template pucks infiltrated with calcium alginate, and calcium alginate once the sacrificial template is removed. Before exposure to genipin, it

is seen that the alginate maintains the shape of a puck once the sacrificial template is removed. This is an important property for this manufacturing process to ensure that the fibers in a sacrificial scaffold template will remain in an aligned pattern once the template is removed. Once exposed to genipin, the gelatin pucks turned a dark blue as expected, as did the infiltrated gelatin. The calcium alginate remaining after infiltration did not change color, staying a clear-white color, indicating that the sacrificial gelatin template was completely removed from the infiltrated hydrogel. This was shown using both a 10 wt% gelatin template and a 15 wt% gelatin template.

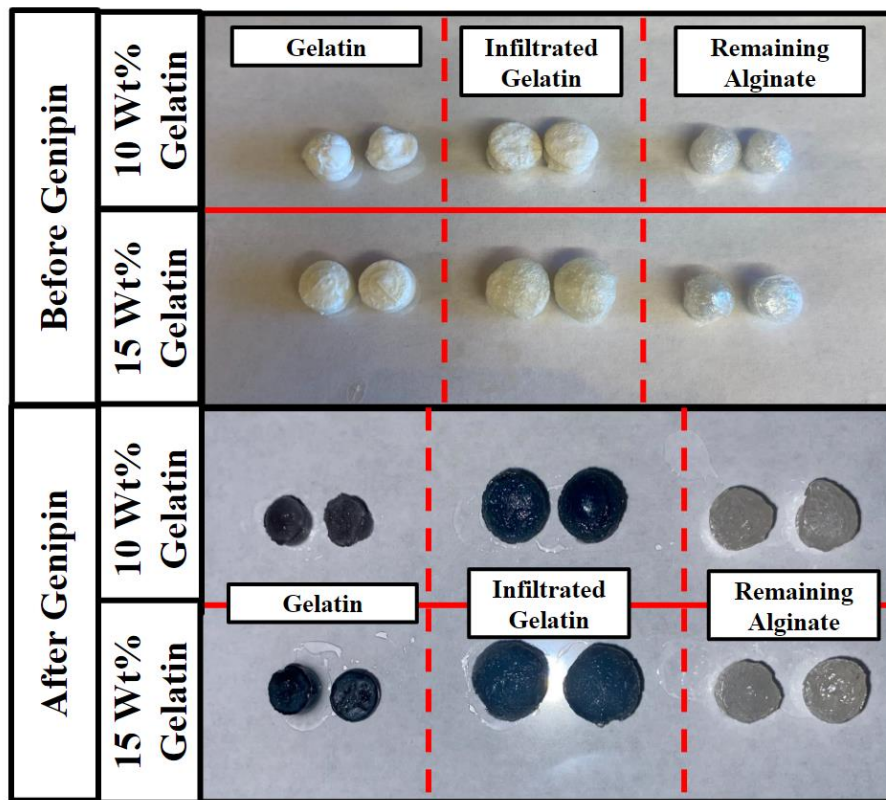
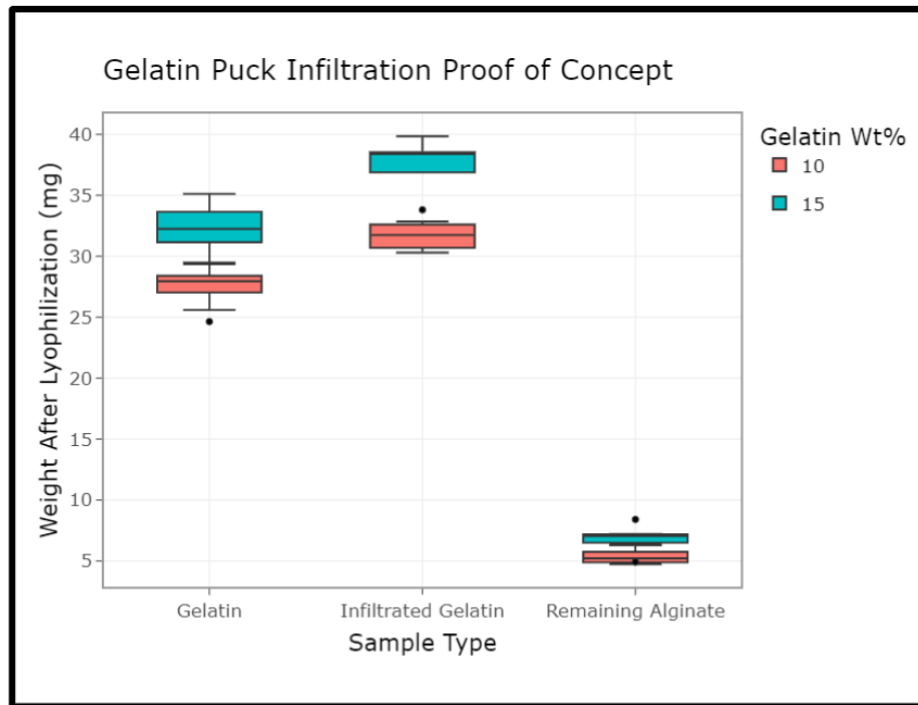


Figure 24. Sacrificial Template Removal Evidenced by Genipin Crosslinking

It was verified that the alginate was capable of infiltrating the hydrogel and crosslinking, and that the template was completely removable. The amount of infiltrated hydrogel that was present was then determined. Lyophilization was used to determine the final weights of the pucks at each stage of the infiltration process. Lyophilization was chosen because this process completely removed water through sublimation, and therefore the resultant weight will be that of only the hydrogel polymer and not the included weight of water absorbed. The resultant weight of 8 replicates of pucks at each sample type revealed that the remaining alginate weight is significantly lower than that of the initial gelatin template and the infiltrated template (*Figure 25*).



*Figure 25.* Sacrificial Puck Weights Before, During, and After Infiltration and Removal

#### ***4.4.2 Alginate Time Infiltration***

After verifying a method for removing the sacrificial template, the length of time to completely infiltrate the template was investigated. Sacrificial pucks were infiltrated over different timepoints to study the amount of alginate that will infiltrate.

Lyophilization was again used to get the final weights of the hydrogel at each time point. The weight of the remaining alginate after gelatin template removal was measured at each timepoint and plotted (*Figure 26B*). Three different weight percentages of the sacrificial template (5, 10, 15 wt%) were investigated to determine the most efficient template to use to increase the rate of hydrogel infiltration. All of the pucks received the same volume of gelatin for the template regardless of wt%. It was therefore hypothesized that the 5 wt% sacrificial templates would infiltrate the fastest, as this has the largest mesh size and thus the highest porosity, allowing alginate molecules to infiltrate at a more rapid rate. The 20 wt% templates would have the slowest and least amount of alginate infiltrated based on the same hypothesis.

It was found that over the length of the experiment, the 5 wt% templates reached their max infiltration the fastest (around 3 days), however, they were infiltrated with the least amount of alginate. The 20 wt% scaffolds were seen to still be increasing in infiltration weight at the 21-day timepoint but had the highest alginate weight remaining once the template was removed. This disagreed with the initial hypothesis that 5 wt% template would infiltrate with the highest amount of alginate hydrogel.

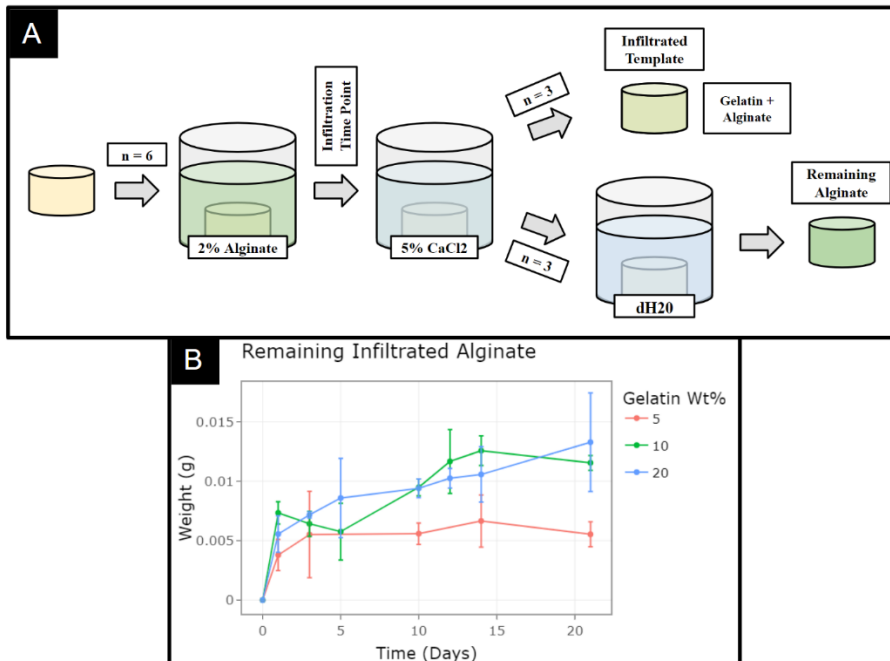


*Figure 26.* Time Infiltration of Alginate into Varied Weight Percent Sacrificial Gelatin Templates

It was observed that the 5 wt% pucks decreased in size after one day of infiltrating in the sodium alginate solution, and that the 20 wt% template slightly increased in size after 1 day. The 10 wt% template remained around the same size as when it began infiltration. The dimensions of the pucks were then taken after the gelatin template removal at timepoints 14 days and 21 days, and the density was then calculated using the measured weight. These densities are displayed in *Figure 27*. It was found that while the 5 wt% templates infiltrated the least total quantity of hydrogel, it had a higher density than the 20 wt% templates produced. The highest density at both time points was the 10 wt% templates, followed closely by 5 wt%, and significantly less was 20 wt%. A significant difference was seen between 10 wt% and 20 wt% at 14 days of infiltration (p-value of 0.00669). No significant differences were observed at 21 days of infiltration. 10

wt% was chosen as the wt% of the template moving forward as it had the highest density of hydrogel infiltrated and remained approximately the initial size of the puck. 5 wt% was also ruled out due to its very low mechanical properties, being an extremely weak gel that often fell apart while being moved from the molds into the well plate during manufacturing.

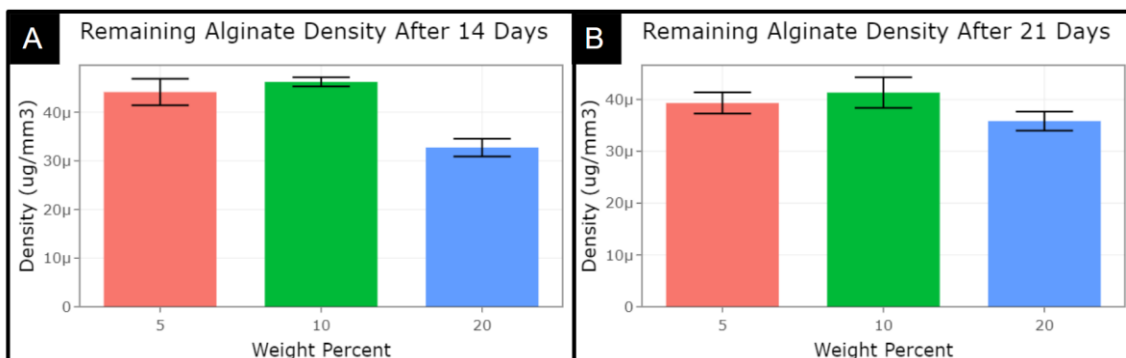
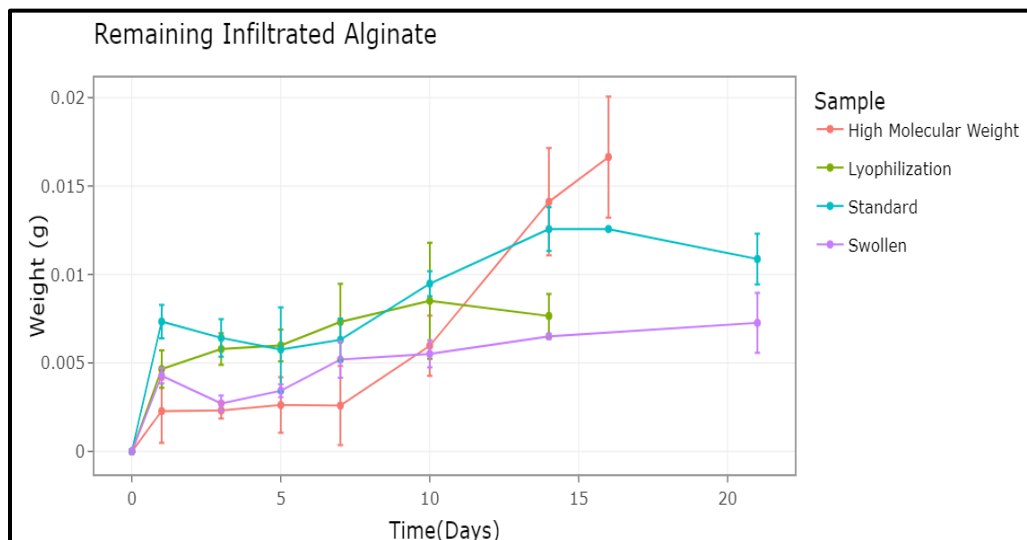


Figure 27. Densities of Remaining Infiltrated Alginate Hydrogel after Removal of Varied Weight Percent Gelatin Templates

Overall, it was seen that for a 10 wt% sacrificial template at least 12 days of soaking time was needed to fully infiltrate the template with the alginate solution. Several methods for improving the rate at which alginate would infiltrate into the template were then tested. The first method involved lyophilizing the gelatin templates and rehydrating them before alginate infiltration. It has been seen that lyophilization of a hydrogel will increase its porosity and pore size [66, 67]. The hypothesis of this test group was that increasing the pore size of the hydrogel would increase the rate at which hydrogel would enter the sacrificial template at a faster rate while still maintaining the same total hydrogel infiltration amount. It was found, however, that the rate of infiltration does not

change by a discernable value, and that the total amount of alginate infiltrated is seen to be lower than that of a standard hydrogel (*Figure 28*).



*Figure 28.* Time Infiltration of Alginate into Various Treated Sacrificial 10% Gelatin Templates

A second strategy for increasing the rate at which the alginate entered the hydrogel was by initially swelling the sacrificial gelatin templates. 10 wt% gelatin will swell when placed in dH<sub>2</sub>O. The rate at which the template pucks of this experiment swelled was investigated. It was found that after 48 hours, the gelatin pucks have swelled to their maximum weight and volume (*Figure 29*). A swollen group of pucks consisting of gels swollen in dH<sub>2</sub>O for 48 hours before infiltration was tested over time. By pre-swelling the pucks, it was hypothesized that the swelling of the gels would increase the mesh size of the template, resulting in a higher porosity and increased infiltration rate. Therefore, it was expected that there would be a rapid increase in the amount of infiltrated hydrogel between timepoints 1 day and 3 days. It was found that the swollen

gels again had a decreased rate of infiltration and a decreased of total alginate infiltrated. The pucks were observed to have decreased to their normal size after only 12 hours in the alginate solution. It is unclear why this treatment would result in a decreased total alginate infiltration as once unswollen, the hydrogel was largely unchanged from the standard group (*Figure 29*).

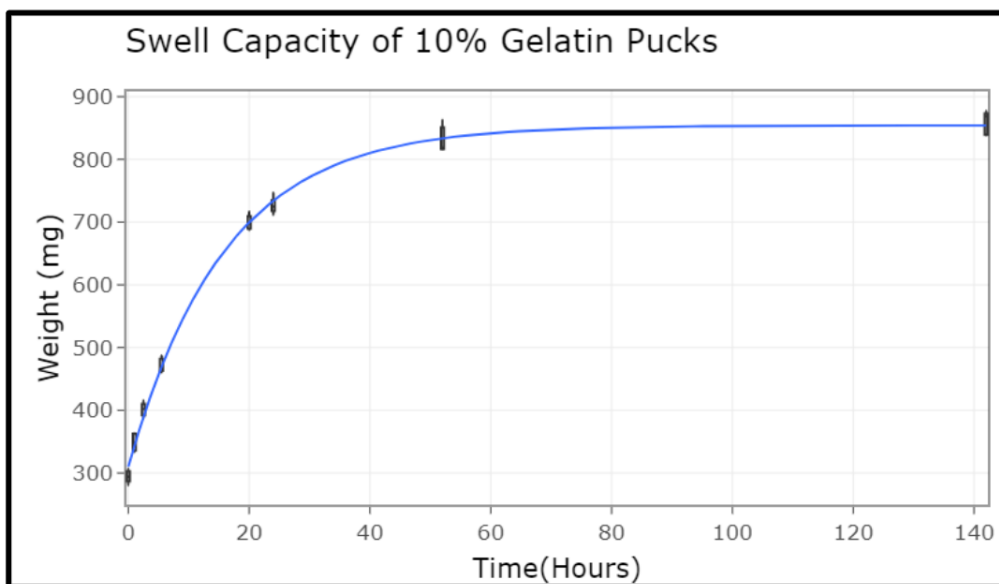


*Figure 29.* Swell Capacity of 10 Weight Percent Gelatin Sacrificial Template Pucks

The third treatment group did not change the pucks but instead increased the molecular weight of the alginate solution. An alginate polymer of significantly higher molecular weight at the same wt% was used for infiltration. It was hypothesized that by increasing the molecular weight of the infiltrating solution, the rate of infiltration would decrease, as the solution would diffuse at a slower rate. It was found that the rate of infiltration was much lower than that of the lower molecular weight sodium alginate, as expected. The total alginate infiltrated at the last timepoint was higher than that of the

standard group (*Figure 29*). While the increase molecular weight decreases the rate at which the alginate diffuses through the porous mesh of the sacrificial template, the end crosslinked value eventually became higher. It is hypothesized that a portion of uncrosslinked infiltrated alginate leaks out of the structure when the sacrificial template is removed. The amount of uncrosslinked alginate is likely higher in the lower molecular weight sample, as seen by a decreased final weight.

Overall, it was found that a 10 wt% sacrificial template in the lower molecular weight solution was the most efficient method for the purpose of infiltrating to manufacture the nanofiber-hydrogel composite scaffolds when forming an alginate hydrogel with a gelatin hydrogel template. The effect that polymer molecular weight has on infiltration was an interesting finding that could be applied to other hydrogels to increase or decrease the amount infiltrated. While alginate has a relatively high molecular weight, with polymer chains up to 700,000 Daltons [68], other hydrogels may be higher. This study showed that the time of infiltration into these sacrificial templated may need to be adjusted to match the molecular weight and viscosity properties of the infiltrating hydrogels.

#### ***4.4.3 Sacrificial Scaffold Template Structure Maintenance***

Once the ideal properties of the sacrificial hydrogel template were determined and the length of infiltration that was necessary found, the ability to infiltrate into a sacrificial scaffold template was investigated. Sacrificial scaffold templates were manufactured using 10 wt% gelatin and 10 PCL nanofiber frames using the layer-by-layer procedure described in section 2.2.4. The goal of this study was to determine if the organization of the nanofibers within the scaffold would be disrupted by replacing the gelatin template

hydrogel. This disruption could be in the 2-D plane of each frame, where the fibers would lose tension and become wavy or unaligned. The disruption could also have been in the 3-D plane, with the layered structure of the hydrogel becoming lost and fiber layers becoming overlapped. After infiltrating the sacrificial scaffolds for 12 days and removing the template, the alginate scaffolds were imaged.

For alginate scaffolds, it was found that the 2-D structure of the fiber layers were slightly distorted. The fibers of the scaffold became slightly wavy, indicating that when the template was removed, the fibers lost some tension stored while being fixed in place by the gelatin. The 3-D structure, however, remained intact and layered (*Figure 30*). The layers of fibers did not shift or distort, indicating that the benefits of using a layer-by-layer assembly method, such as layer thickness tunability and fiber distance, are still controllable while making sacrificial template scaffolds.

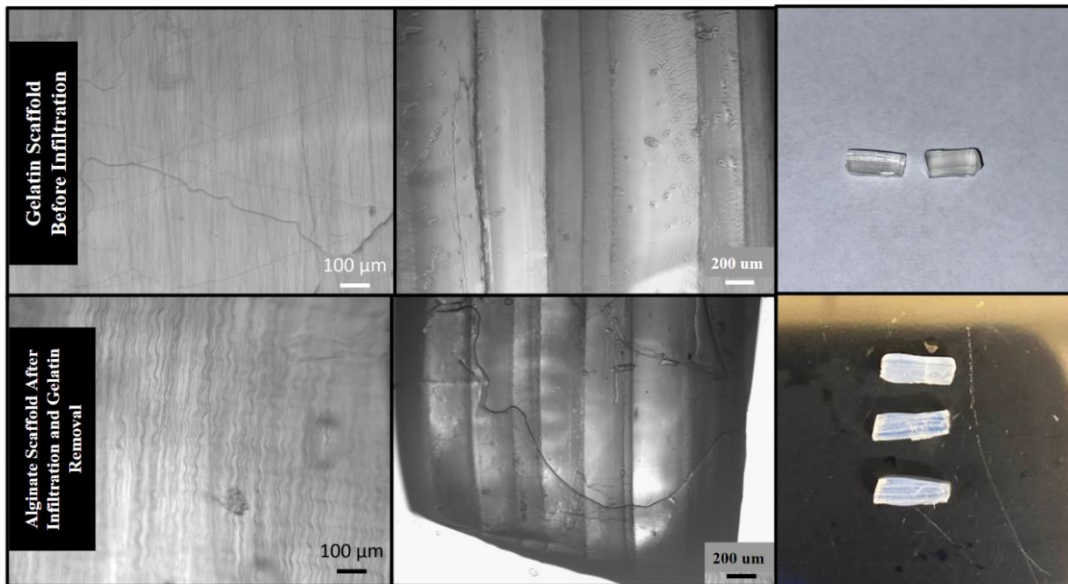


*Figure 30.* Scaffold Structure Before and After Alginate Infiltrated and Sacrificial Template Removal

It is believed that the fibers in the 2-D plane became distorted because the scaffold decreased in overall dimensions. The height, length, and width of each gelatin scaffold were taken prior to alginate infiltration and then the dimensions of the alginate scaffold after infiltration and gelatin removal were taken again (*Figure 31*). It was found that while there was no significant difference in the height, width, or volume of the scaffolds (p-values of 0.3190, 0.1487, and 0.0401, respectively), there was a significant difference in the length of the scaffolds (p-value of 0.00170). The volume of the scaffolds decreased insignificantly. When the length of the scaffolds decreased, the fibers that were previously stretched from end-to-end contracted inward, losing all tension. While this crimped orientation is not expected to be desirable, the overall alignment and layer spacing of the fibers remained unaffected, and the fibers still traveled in the direction from proximal to distal end, indicating the scaffold could still provide contact guidance of the axons. We hypothesize that fiber crimping could be reduced or eliminated by controlling the swelling of the alginate hydrogel by selecting ideal solution molarities for the hydrogel solutions and incubating liquids used during manufacturing.

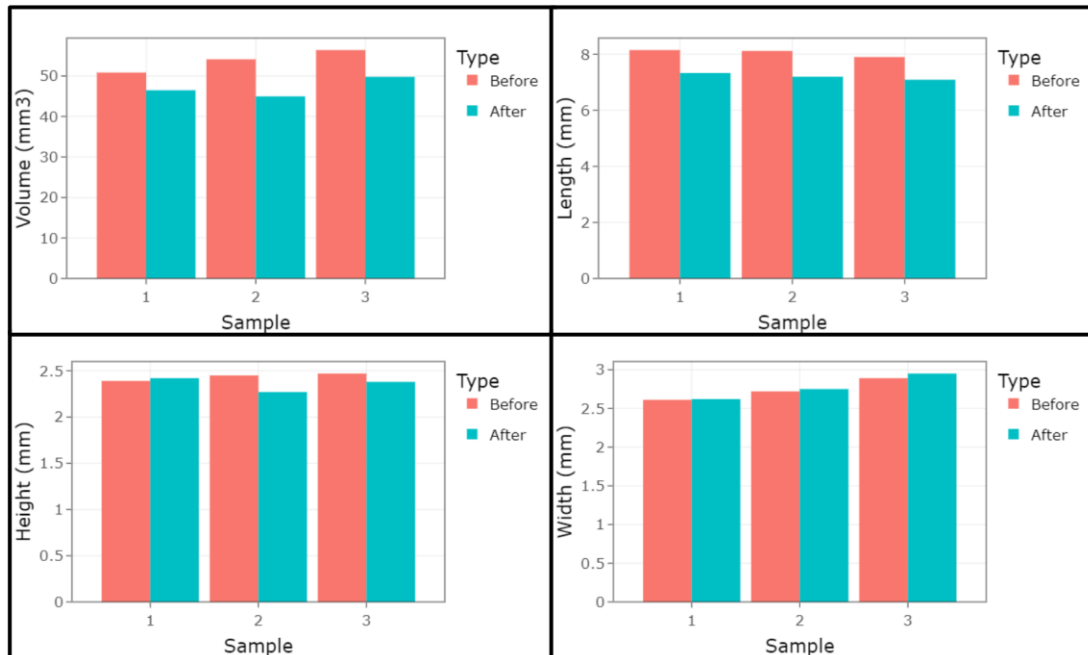


Figure 31. Scaffold Dimensions Before and After Alginate Infiltrated and Sacrificial Template Removal

#### 4.4.4 Sacrificial Scaffold Template HANor Infiltration

While calcium alginate is a versatile hydrogel with many applications, it is not necessarily the ideal polymer for a nerve regeneration scaffold. As previously mentioned, alginate was chosen for this study to be the infiltrating hydrogel because it is cheap, easy to work with, and crosslinks rapidly. It was also mentioned that calcium alginate has a relatively high molecular weight. Molecular weight was shown to have an impact on the ability to infiltrate into a sacrificial gelatin template. By choosing a hydrogel with a high molecular weight for this study, the capability for this method to work with hydrogels of lower molecular weight would theoretically be easier and more efficient. Calcium alginate is representative of the ability of this method to be functional

with an ionically cross-linkable hydrogel, however, the purpose of this manufacturing method is versatility in infiltrating hydrogels.

HANor was tested with the sacrificial gelatin template manufacturing method as a representative of UV cross-linkable polymer hydrogels. This process could then be applied to other polymer gels that are UV cross-linkable. Sacrificial scaffold templates were made and infiltrated with 3 wt% HANor hydrogel over 12 days. The scaffolds were then crosslinked using UV light instead of an ionic crosslinker as seen in alginate infiltration. The sacrificial template was then removed, and the infiltrated nanofiber-hydrogel scaffold imaged.

It was seen that both the fiber alignment and layer spacing were preserved and mimicked the original template closely (*Figure 32*). Both the layered structure and the nanofibers can be seen remaining in the same orientation and alignment. The dimensions of the HANor scaffold increased when compared to the dimensions of the sacrificial gelatin template. This is in contrast to the alginate scaffolds, which decreased in size. We hypothesize that this is why the fibers in the HANor hydrogels remained straight, while the fibers in the alginate hydrogels became crimped (*Figure 33*). The height, width, and volume of the scaffold significantly changed from the initial value (p-values of 0.000695, 0.000260, and 0.00189, respectively), whereas the length of the scaffold did not show a significant change (p-value of 0.3072). This is possibly due to the nanofiber tension fixing the HANor hydrogel to the length of the nanofibers, causing swelling to be limited to dimensions where the nanofibers would not provide a resisting force.

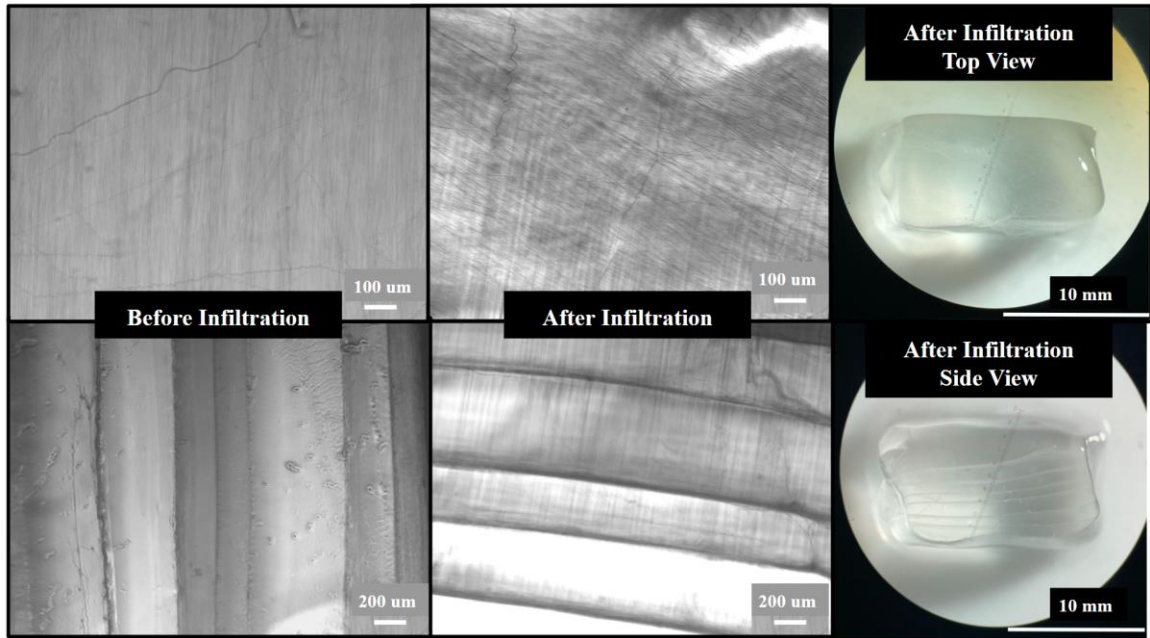


*Figure 32. Scaffold Structure Before and After HANor Infiltrated and Sacrificial Template Removal*

This result is promising for the ability to use this manufacturing method over a wide range of hydrogels, allowing for a diverse variety of hydrogel properties to be tested and optimized in the goal of improving axon infiltration into composite hydrogel scaffolds containing aligned nanofibers for axon contact guidance. One disadvantage this method has is the inability to use thermoresponsive hydrogels that are in liquid phase at the same point that 10 wt% gelatin is in liquid phase. The infiltrating hydrogel must be a liquid during infiltration while the gelatin scaffold is a solid. A hydrogel like GelMe, which becomes a liquid  $\sim 30^{\circ}\text{C}$  before crosslinking, would not be able to be used because the template would dissolve before infiltration and crosslinking could occur. However, other non-thermoreversible hydrogels such as alginate may be able to be used as the sacrificial template in the same way.

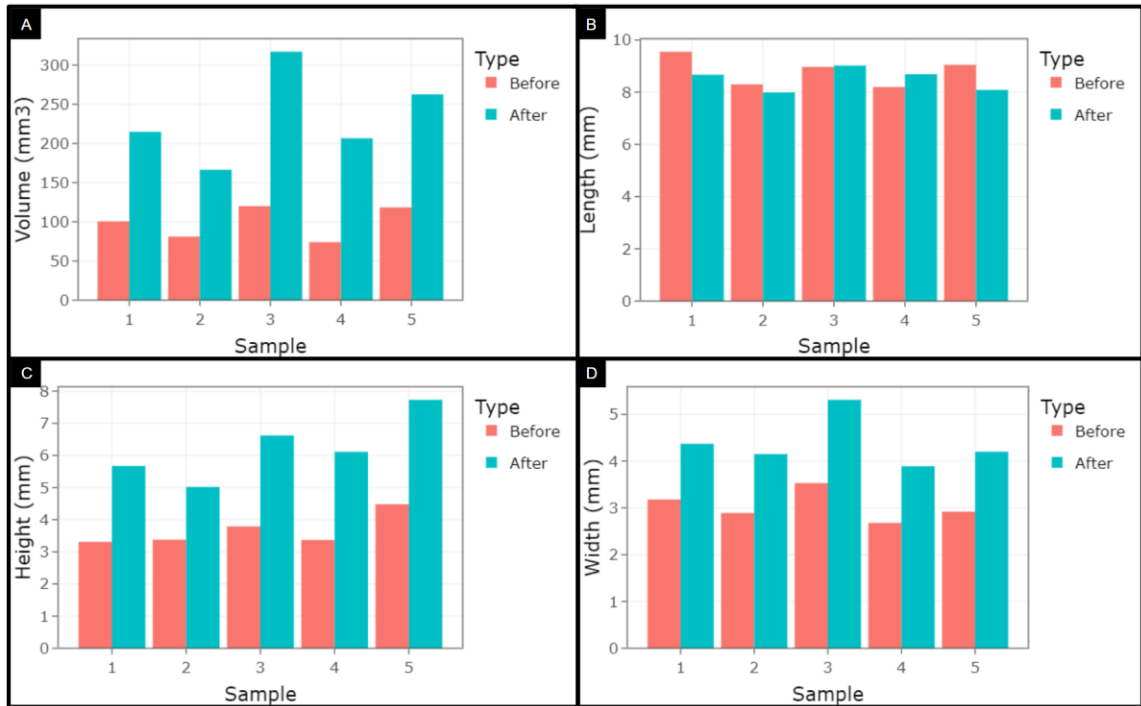


Figure 33. Scaffold Dimensions Before and After HANor Infiltrated and Sacrificial Template Removal

Another benefit of this manufacturing method is the ability to create much weaker scaffolds that are not physically durable enough to insert or wrap in a conduit. Nerve tissue and the surrounding ECM is generally much weaker than other tissues [69-71]. Mimicking the natural environment of the regenerating tissue is the goal of using a hydrogel composite scaffold. By producing a very weak gel, axons may be able to penetrate into the hydrogel with ease. This method could allow for the infiltration of weaker gels into a scaffold pre-fit into a nerve guidance conduit tube. Once the template was removed, the weaker gel can be handled and implanted due to the support of the nerve guidance conduit. For example, HANor may facilitate axon infiltration at a lower weight percent or degree of crosslinking than previously tested.

Another benefit of this method is that the quantity of hydrogel required for manufacturing is much lower. Gelatin, a cheap and easy to use polymer, is able to be used in abundance to create the template for infiltration. A much lower quantity of the infiltrating polymer is needed to achieve a scaffold with the same properties as the template. For example, 8 mL of gelatin solution is necessary to make the gelatin template, but only 500  $\mu$ L is necessary to infiltrate a 2 mm by 2 mm by 1.5 cm scaffold. Many hydrogels that could be very beneficial for a nerve guidance conduit can be highly expensive and hard to obtain in high quantities. Decellularized nerve matrix would contain the large amounts of beneficial growth factors and proteins that are found in native nerve tissue but may be hard to obtain in quantities to manufacture layer-by-layer scaffolds [38, 39].

GelMe and HANor were chosen for layer-by-layer assembly and/or rolled film assembly because their properties are easily tunable using UV light and temperature, allowing for highly controllable fiber orientation. Not every hydrogel that could be used for nerve regeneration has highly controllable properties. By using gelatin to design the ideal scaffold template, and then being able to infiltrate a final hydrogel into this template, the versatility of nanofiber-hydrogel composite scaffolds greatly increased.

## Chapter 5

### Conclusions and Future Work

#### 5.1 Conclusions

Aligned nanofiber-hydrogel composites have great potential in peripheral nerve injury regeneration. Combining the use of a nanofiber guidewire and ECM mimicking hydrogel into an NGC provides multiple strategies to advance the nerve in the regeneration process. Throughout this research, many discoveries were made about the design of aligned nanofiber-hydrogel composite scaffolds, while providing new avenues of manufacturing techniques for improvement over limitations that were encountered. The layer-by-layer additive manufacturing process resulted in a method offering fine control over the properties of the hydrogel and nanofiber alignment within a nanofiber-hydrogel composite scaffold, such as versatility with layer thickness, density of nanofibers, and degree of photocrosslinking. An in-vitro model for seeding cells and imaging NGCs was also developed that can be applied to further studies and the area of research as a whole.

In order to manufacture aligned nanofiber hydrogel composite grafts with a large percentage of porous void space, the rolled film nanofiber-hydrogel composite scaffold was developed. In this aligned nanofiber NGC, open space was introduced throughout the scaffold cross-section by rolling films of hydrogel covered nanofibers instead of stacking them, providing areas of easy access for axons. This method showed improved results in a rat sciatic gap model, leading to the successful regeneration of axons through a 1.5 cm nerve gap. However, overall results showed a slow degradation rate of the hydrogel within the living system as well as an inability of axons and Schwann cells to

infiltrate into GelMe and HANor at the hydrogel weight percent and degree of crosslinking tested. The scaffold that regenerated axons across the damaged nerve gaps showed the ability of axons to penetrate the hydrogel, which is hypothesized to be the result of a lower degree of crosslinking and decreased volume of gel due to oxidative factors during crosslinking. 10% GelMe and 3% HANor hydrogels UV crosslinked for 14 and 6 minutes respectively were determined to not be ideal for nerve regeneration and different hydrogels should be investigated or the weight percent of these hydrogels or degree of crosslinking should be decreased.

A third manufacturing method that infiltrates a sacrificial composite scaffold template with a desired hydrogel was designed to create aligned nanofiber-hydrogel composite NGCs with hydrogels that are not compatible with a layer-by-layer stacking approach. For layer-by-layer scaffold manufacturing, a thermosresponsive and UV cross-linkable hydrogel had to be used to have adhesion between each layer. By adapting the layer-by-layer assembly method, a gelatin template scaffold can be used to stabilize the aligned nanofiber architecture and design the properties of the scaffold, and then be replaced with a hydrogel with more ideal properties. This process can greatly increase the number of hydrogels that are available for use when designing aligned nanofiber-hydrogel composite NGCs.

## **5.2 Future Work**

The mechanisms associated with layer-by-layer and rolled film self assembly should be investigated further. Studying the properties of oxidation on the crosslinking of GelMe will provide insights as to how this reaction affects the degree and uniformity of crosslinking throughout the films. Understanding how this process affects the films can

allow its effects to be minimized or controlled to the scaffolds advantage. Studying the crosslinking process within a vacuum, immersed in a liquid, or in an inert gas environment should be investigated.

The sacrificial template design provided the ability to use new hydrogels in nanofiber hydrogel composites that were previously unrealistic due to cost or incompatibility with the layer-by-layer manufacturing method. Now that the practicality of using different hydrogels to infiltrate into a sacrificial template has been shown, these hydrogel properties should be tested. One hydrogel material of interest is nerve tissue extracellular matrix hydrogel. By using decellularizing nerve tissue to create a hydrogel, the genetic material that would result in an immune response is eliminated, leaving only important proteins and nerve growth factors naturally found in nerve ECM [38, 39]. The use of a hydrogel like this would be unrealistic for layer-by-layer assembly, but now is made possible through the sacrificial template infiltration. Studying cell infiltration into scaffolds made of ECM gels using the in-vitro model should be investigated to determine a new ideal hydrogel to be used for future aligned nanofiber-hydrogel composite NGCs.

While GelMe and HANor were shown to be generally unsuccessful at the properties we studied at, the prospect of decreasing the weight percent or degree of crosslinking is promising. Mechanical property requirements prevented the use of lower weight percent hydrogels throughout the layer-by-layer and rolled film scaffold assembly methods. These scaffolds would need a nerve conduit tube surrounding them to protect them and allow handling and surgical implantation without them coming apart. Inserting mechanically weak hydrogel nanofiber composite scaffolds into a conduit would be extremely challenging without destroying the scaffold itself. However, a sacrificial

template, with suitable mechanical properties, could be placed within the nerve guidance tube, and then infiltrated with a much lower weight percent of GelMe or HANor, to form a scaffold with weak mechanical properties directly within the protective conduit.

Furthermore, one of the main limitations discussed of this infiltration is the inability to use a hydrogel that is not liquid at room temperature. However, investigation into a double infiltration method would be promising to move forward with. If a hydrogel such as alginate can be used to infiltrate into a gelatin sacrificial template, a second hydrogel would then be able to infiltrate the alginate in an increased temperature environment. Once the alginate is removed through reverse-crosslinking, the final hydrogel would remain. Studying a double infiltration method could open even more possibilities of hydrogels to use in future studies.

## References

- [1] E. E. H. Clifford T. Pereira, Anastasiya Stasyuk, Neil Parikh, Andrew Li, "Molecular Basis of Surgical Coaptation Techniques in Peripheral Nerve Injuries," *Journal of Clinical Medicine*, vol. 12, 2023.
- [2] W. W. Campbell, "Evaluation and management of peripheral nerve injury," *Clinical Neurophysiology*, vol. 119, no. 9, pp. 1951-1965, 2008/09/01/ 2008, doi: <https://doi.org/10.1016/j.clinph.2008.03.018>.
- [3] M. Romero-Ortega, "Peripheral Nerves, Anatomy and Physiology of," in *Encyclopedia of Computational Neuroscience*, D. Jaeger and R. Jung Eds. New York, NY: Springer New York, 2022, pp. 2715-2719.
- [4] R. M. Menorca, T. S. Fussell, and J. C. Elfar, "Nerve physiology: mechanisms of injury and recovery," (in eng), *Hand Clin*, vol. 29, no. 3, pp. 317-30, Aug 2013, doi: 10.1016/j.hcl.2013.04.002.
- [5] R. Akram *et al.*, "Axonal Regeneration: Underlying Molecular Mechanisms and Potential Therapeutic Targets," (in eng), *Biomedicines*, vol. 10, no. 12, Dec 8 2022, doi: 10.3390/biomedicines10123186.
- [6] J. W. Fawcett and R. J. Keynes, "Peripheral Nerve Regeneration," *Annual Review of Neuroscience*, vol. 13, no. Volume 13, 1990, pp. 43-60, 1990, doi: <https://doi.org/10.1146/annurev.ne.13.030190.000355>.
- [7] M. O. V. Gabriel Corfas, Chien-Ping Ko, Nancy Ratner, Elinor Peles, "Mechanisms and Roles of Axon–Schwann Cell Interactions," *The Journal of Neuroscience*, 2004.
- [8] B. K. Victor T. Ribeiro-Resende, Susanne Nichterwitz, Sven Oberhoffner, Burkhard Schlosshauer, "Strategies for inducing the formation of bands of Bungner in peripheral nerve regeneration," *Biomaterials*, 2009.
- [9] G. S. B. Thandavamoorthy Subbiah, R. W. Tock, S. Parameswaran, S. S. Ramkumar, "Electrospinning of Nanofibers," *Journal of Applied Polymer Science*, vol. 96, pp. 557–569, 2004.
- [10] X. W. Jian Fang, Tong Lin, "Functional applications of electrospun nanofibers," *Nanofibers - production, properties and functional applications*, 2011.
- [11] J. Xue, T. Wu, Y. Dai, and Y. Xia, "Electrospinning and Electrospun Nanofibers: Methods, Materials, and Applications," (in eng), *Chem Rev*, vol. 119, no. 8, pp. 5298-5415, Apr 24 2019, doi: 10.1021/acs.chemrev.8b00593.

- [12] J. Xue, J. Xie, W. Liu, and Y. Xia, "Electrospun Nanofibers: New Concepts, Materials, and Applications," (in eng), *Acc Chem Res*, vol. 50, no. 8, pp. 1976-1987, Aug 15 2017, doi: 10.1021/acs.accounts.7b00218.
- [13] N. M. Neves, R. Campos, A. Pedro, J. Cunha, F. Macedo, and R. L. Reis, "Patterning of polymer nanofiber meshes by electrospinning for biomedical applications," (in eng), *Int J Nanomedicine*, vol. 2, no. 3, pp. 433-48, 2007.
- [14] A. Hiwrale, S. Bharati, P. Pingale, and A. Rajput, "Nanofibers: A current era in drug delivery system," (in eng), *Heliyon*, vol. 9, no. 9, p. e18917, Sep 2023, doi: 10.1016/j.heliyon.2023.e18917.
- [15] H. S. Yoo, T. G. Kim, and T. G. Park, "Surface-functionalized electrospun nanofibers for tissue engineering and drug delivery," *Advanced Drug Delivery Reviews*, vol. 61, no. 12, pp. 1033-1042, 2009/10/05/ 2009, doi: <https://doi.org/10.1016/j.addr.2009.07.007>.
- [16] M. Bartnikowski, T. R. Dargaville, S. Ivanovski, and D. W. Hutmacher, "Degradation mechanisms of polycaprolactone in the context of chemistry, geometry and environment," *Progress in Polymer Science*, vol. 96, pp. 1-20, 2019/09/01/ 2019, doi: <https://doi.org/10.1016/j.progpolymsci.2019.05.004>.
- [17] H. Sun, L. Mei, C. Song, X. Cui, and P. Wang, "The in vivo degradation, absorption and excretion of PCL-based implant," *Biomaterials*, vol. 27, no. 9, pp. 1735-1740, 2006/03/01/ 2006, doi: <https://doi.org/10.1016/j.biomaterials.2005.09.019>.
- [18] L. Van der Schueren, B. De Schoenmaker, Ö. I. Kalaoglu, and K. De Clerck, "An alternative solvent system for the steady state electrospinning of polycaprolactone," *European Polymer Journal*, vol. 47, no. 6, pp. 1256-1263, 2011/06/01/ 2011, doi: <https://doi.org/10.1016/j.eurpolymj.2011.02.025>.
- [19] V. Guarino, G. Gentile, L. Sorrentino, and L. Ambrosio, "Polycaprolactone: Synthesis, Properties, and Applications," in *Encyclopedia of Polymer Science and Technology*, pp. 1-36.
- [20] E. M. Ahmed, "Hydrogel: Preparation, characterization, and applications: A review," *Journal of Advanced Research*, vol. 6, no. 2, pp. 105-121, 2015/03/01/ 2015, doi: <https://doi.org/10.1016/j.jare.2013.07.006>.
- [21] S. Cascone and G. Lamberti, "Hydrogel-based commercial products for biomedical applications: A review," *International Journal of Pharmaceutics*, vol. 573, p. 118803, 2020/01/05/ 2020, doi: <https://doi.org/10.1016/j.ijpharm.2019.118803>.

- [22] M. A. Rahman, "Collagen of Extracellular Matrix from Marine Invertebrates and Its Medical Applications," *Marine Drugs*, vol. 17, no. 2, p. 118, 2019. [Online]. Available: <https://www.mdpi.com/1660-3397/17/2/118>.
- [23] K. Yue, G. Trujillo-de Santiago, M. M. Alvarez, A. Tamayol, N. Annabi, and A. Khademhosseini, "Synthesis, properties, and biomedical applications of gelatin methacryloyl (GelMA) hydrogels," *Biomaterials*, vol. 73, pp. 254-271, 2015/12/01/ 2015, doi: <https://doi.org/10.1016/j.biomaterials.2015.08.045>.
- [24] S. Sharifi, H. Sharifi, A. Akbari, and J. Chodosh, "Systematic optimization of visible light-induced crosslinking conditions of gelatin methacryloyl (GelMA)," *Scientific Reports*, vol. 11, no. 1, p. 23276, 2021/12/02 2021, doi: [10.1038/s41598-021-02830-x](https://doi.org/10.1038/s41598-021-02830-x).
- [25] S. L. Bellis, "Advantages of RGD peptides for directing cell association with biomaterials," (in eng), *Biomaterials*, vol. 32, no. 18, pp. 4205-10, Jun 2011, doi: [10.1016/j.biomaterials.2011.02.029](https://doi.org/10.1016/j.biomaterials.2011.02.029).
- [26] S. Heltmann-Meyer *et al.*, "Gelatin methacryloyl is a slow degrading material allowing vascularization and long-term use in vivo," *Biomedical Materials*, vol. 16, no. 6, p. 065004, 2021/09/06 2021, doi: [10.1088/1748-605X/ac1e9d](https://doi.org/10.1088/1748-605X/ac1e9d).
- [27] I. Pepelanova, K. Kruppa, T. Scheper, and A. Lavrentieva, "Gelatin-Methacryloyl (GelMA) Hydrogels with Defined Degree of Functionalization as a Versatile Toolkit for 3D Cell Culture and Extrusion Bioprinting," *Bioengineering*, vol. 5, no. 3, p. 55, 2018. [Online]. Available: <https://www.mdpi.com/2306-5354/5/3/55>.
- [28] K. A. Gultian *et al.*, "Injectable hydrogel with immobilized BMP-2 mimetic peptide for local bone regeneration," (in English), *Frontiers in Biomaterials Science*, Original Research vol. 1, 2022-July-22 2022, doi: [10.3389/fbiom.2022.948493](https://doi.org/10.3389/fbiom.2022.948493).
- [29] E. M. Plaster, M. K. Eiken, and C. Loebel, "DMTMM-mediated synthesis of norbornene-modified hyaluronic acid polymers to probe cell-hydrogel interactions," *Carbohydrate Polymer Technologies and Applications*, vol. 6, p. 100360, 2023/12/01/ 2023, doi: <https://doi.org/10.1016/j.carpta.2023.100360>.
- [30] S. Yi, L. Xu, and X. Gu, "Scaffolds for peripheral nerve repair and reconstruction," *Experimental Neurology*, vol. 319, p. 112761, 2019/09/01/ 2019, doi: <https://doi.org/10.1016/j.expneurol.2018.05.016>.
- [31] C. Raza, H. A. Riaz, R. Anjum, and N. u. A. Shakeel, "Repair strategies for injured peripheral nerve: Review," *Life Sciences*, vol. 243, p. 117308, 2020/02/15/ 2020, doi: <https://doi.org/10.1016/j.lfs.2020.117308>.

- [32] S. Vijayavenkataraman, "Nerve guide conduits for peripheral nerve injury repair: A review on design, materials and fabrication methods," *Acta Biomaterialia*, vol. 106, pp. 54-69, 2020/04/01/ 2020, doi: <https://doi.org/10.1016/j.actbio.2020.02.003>.
- [33] C. R. Carvalho, J. M. Oliveira, and R. L. Reis, "Modern Trends for Peripheral Nerve Repair and Regeneration: Beyond the Hollow Nerve Guidance Conduit," *Front Bioeng Biotechnol*, vol. 7, p. 337, 2019, doi: 10.3389/fbioe.2019.00337.
- [34] G. C. de Ruitter, M. J. Malessy, M. J. Yaszemski, A. J. Windebank, and R. J. Spinner, "Designing ideal conduits for peripheral nerve repair," *Neurosurg Focus*, vol. 26, no. 2, p. E5, Feb 2009, doi: 10.3171/FOC.2009.26.2.E5.
- [35] S. Kehoe, X. F. Zhang, and D. Boyd, "FDA approved guidance conduits and wraps for peripheral nerve injury: a review of materials and efficacy," *Injury*, vol. 43, no. 5, pp. 553-72, May 2012, doi: 10.1016/j.injury.2010.12.030.
- [36] A. Muheremu and Q. Ao, "Past, Present, and Future of Nerve Conduits in the Treatment of Peripheral Nerve Injury," *Biomed Res Int*, vol. 2015, p. 237507, 2015, doi: 10.1155/2015/237507.
- [37] D. J. Gerth, J. Tashiro, and S. R. Thaller, "Clinical outcomes for Conduits and Scaffolds in peripheral nerve repair," *World J Clin Cases*, vol. 3, no. 2, pp. 141-7, Feb 16 2015, doi: 10.12998/wjcc.v3.i2.141.
- [38] Y. S. Kim, M. Majid, A. J. Melchiorri, and A. G. Mikos, "Applications of decellularized extracellular matrix in bone and cartilage tissue engineering," (in eng), *Bioeng Transl Med*, vol. 4, no. 1, pp. 83-95, Jan 2019, doi: 10.1002/btm2.10110.
- [39] Y. Kong, D. Wang, Q. Wei, and Y. Yang, "Nerve Decellularized Matrix Composite Scaffold With High Antibacterial Activity for Nerve Regeneration," (in eng), *Front Bioeng Biotechnol*, vol. 9, p. 840421, 2021, doi: 10.3389/fbioe.2021.840421.
- [40] T. L. Zilong Rao, Shuai Qiu, Jing Zhou b, Sheng Liu a, Shihao Chen a, Tao Wang c,d, Xiaolin Liu c, Qingtang Zhu c,d,\*, Ying Bai b,d,\*, Daping Quan, "Decellularized nerve matrix hydrogel scaffolds with longitudinally oriented and size-tunable microchannels for peripheral nerve regeneration," *Materials Science & Engineering C*, vol. 120, 2020.
- [41] P. J. A. Paulina S. Hill, Jonathan Barnwell, Tom Smith, L. Andrew Koman, Anthony Atala, Mark Van Dyke, "Repair of Peripheral Nerve Defects in Rabbits Using Keratin Hydrogel Scaffolds," *Tissue Engineering*, vol. 17, Part A, 2011.

- [42] M. Y. Guo-Jun Wei, Yan-Song Wang, Chang-Wei Zhou, De-Yu Wan, Peng-Zhen Lei, Jian Wen, Houg-Wei Lei, Da-Ming Dong, "Promotion of peripheral nerve regeneration of a peptide compound hydrogel scaffold," *International Journal of Nanomedicine*, 2013.
- [43] Y. C. Juan Wang, Liang Chen, Tonghe Zhu, Kaiqiang Ye, Chao Jia, Hongjun Wang, Meifang Zhu, Cunyi Fan, Xiumei Mo, "In vitro and in vivo studies of electroactive reduced graphene oxide-modified nanofiber scaffolds for peripheral nerve regeneration," *Acta Biomaterialia*, vol. 84, pp. 98–113, 2018.
- [44] X. Zhan *et al.*, "Nanofiber scaffolds facilitate functional regeneration of peripheral nerve injury," *Nanomedicine*, vol. 9, no. 3, pp. 305-15, Apr 2013, doi: 10.1016/j.nano.2012.08.009.
- [45] C. Y. Wang, K. H. Zhang, C. Y. Fan, X. M. Mo, H. J. Ruan, and F. F. Li, "Aligned natural-synthetic polyblend nanofibers for peripheral nerve regeneration," *Acta Biomater*, vol. 7, no. 2, pp. 634-43, Feb 2011, doi: 10.1016/j.actbio.2010.09.011.
- [46] R. J. McMurtrey, "Patterned and functionalized nanofiber scaffolds in three-dimensional hydrogel constructs enhance neurite outgrowth and directional control," *Journal of Neural Engineering*, vol. 11, 2014.
- [47] Z. Y. Chushan Zheng, Shihao Chen, Fang Zhang, Zilong Rao, Cailing Zhao, Daping Quan, Ying Bai, Jun Shen, "Nanofibrous nerve guidance conduits decorated with decellularized matrix hydrogel facilitate peripheral nerve injury repair," *Theranostics*, vol. 11, no. 6, 2021.
- [48] J. C. B. Douglas H. Smith, Kevin D. Browne, Kritika S. Katiyar<sup>1</sup>, Mindy I. Ezra, John L. Dutton, Joseph P. Morand, Laura A. Struzyna, Franco A. Laimo, H. Isaac Chen, John A. Wolf, Hilton M. Kaplan, Joseph M. Rosen, Harry C. Ledebur, Eric L. Zager, Zarina S. Ali, D. Kacy Cullen, "Tissue-engineered grafts exploit axon-facilitated axon regeneration and pathway protection to enable recovery after 5-cm nerve defects in pigs," *ScienceAdvances*, vol. 8, 2022.
- [49] D. A. Brennan, D. Jao, M. C. Siracusa, A. R. Wilkinson, X. Hu, and V. Z. Beachley, "Concurrent collection and post-drawing of individual electrospun polymer nanofibers to enhance macromolecular alignment and mechanical properties," *Polymer*, vol. 103, pp. 243-250, 2016/10/26/ 2016, doi: <https://doi.org/10.1016/j.polymer.2016.09.061>.
- [50] S. Kidambi, N. Udpa, S. A. Schroeder, R. Findlan, I. Lee, and C. Chan, "Cell adhesion on polyelectrolyte multilayer coated polydimethylsiloxane surfaces with varying topographies," (in eng), *Tissue Eng*, vol. 13, no. 8, pp. 2105-17, Aug 2007, doi: 10.1089/ten.2006.0151.

- [51] E. Pedraza, A. C. Brady, C. A. Fraker, and C. L. Stabler, "Synthesis of macroporous poly(dimethylsiloxane) scaffolds for tissue engineering applications," (in eng), *J Biomater Sci Polym Ed*, vol. 24, no. 9, pp. 1041-56, 2013, doi: 10.1080/09205063.2012.735097.
- [52] S. L. Bellis, "Advantages of RGD peptides for directing cell association with biomaterials," *Biomaterials*, 2011.
- [53] S. S. L. Samuel Y. Boateng, William Mosley, Thomas J. Hartman, Luke Hanley, Brenda Russell, "RGD and YIGSR synthetic peptides facilitate cellular adhesion identical to that of laminin and fibronectin but alter the physiology of neonatal cardiac myocytes," *American Journal of Physiology Cell Physiology*, vol. 288, no. 1, 2004.
- [54] W. B. Soheila Kazemi, Karl Schilke, Hadi Mansouri, John Enrique Mata, "IKVAV-linked cell membrane-spanning peptide treatment induces neuronal reactivation following spinal cord injury," *Future Science OA*, 2015.
- [55] G. Ronchi, F. Fregnan, L. Muratori, G. Gambarotta, and S. Raimondo, "Morphological Methods to Evaluate Peripheral Nerve Fiber Regeneration: A Comprehensive Review," *International Journal of Molecular Sciences*, vol. 24, no. 3, p. 1818, 2023. [Online]. Available: <https://www.mdpi.com/1422-0067/24/3/1818>.
- [56] J. Isaacs, S. Mallu, and M. Batchelor, "Modification of commercially available image analysis software for semi-automated qualitative analysis of axon regeneration and myelination in the rat sciatic nerve," *Journal of Neuroscience Methods*, vol. 233, pp. 45-49, 2014/08/15/ 2014, doi: <https://doi.org/10.1016/j.jneumeth.2014.05.032>.
- [57] L. M. Orfahli *et al.*, "Histomorphometry in Peripheral Nerve Regeneration: Comparison of Different Axon Counting Methods," *Journal of Surgical Research*, vol. 268, pp. 354-362, 2021/12/01/ 2021, doi: <https://doi.org/10.1016/j.jss.2021.06.060>.
- [58] V. Carriel, I. Garzon, M. Alaminos, and M. Cornelissen, "Histological assessment in peripheral nerve tissue engineering," *Neural Regen Res*, vol. 9, no. 18, pp. 1657-60, Sep 15 2014, doi: 10.4103/1673-5374.141798.
- [59] O. D. Garcia-Garcia, T. Weiss, J. Chato-Astrain, S. Raimondo, and V. Carriel, "Staining Methods for Normal and Regenerative Myelin in the Nervous System," *Methods Mol Biol*, vol. 2566, pp. 187-203, 2023, doi: 10.1007/978-1-0716-2675-7\_15.

- [60] J. A. Kiernan, "Histochemistry of Staining Methods for Normal and Degenerating Myelin in the Central and Peripheral Nervous Systems," *Journal of Histochemistry*, vol. 30, no. 2, pp. 87-106, 2013, doi: 10.1179/his.2007.30.2.87.
- [61] L. Muratori, G. Ronchi, S. Raimondo, M. G. Giacobini-Robecchi, M. Fornaro, and S. Geuna, "Can regenerated nerve fibers return to normal size? A long-term post-traumatic study of the rat median nerve crush injury model," *Microsurgery*, vol. 32, no. 5, pp. 383-7, Jul 2012, doi: 10.1002/micr.21969.
- [62] P. O. Rujitanaroj *et al.*, "Controlling fibrous capsule formation through long-term down-regulation of collagen type I (COL1A1) expression by nanofiber-mediated siRNA gene silencing," (in eng), *Acta Biomater*, vol. 9, no. 1, pp. 4513-24, Jan 2013, doi: 10.1016/j.actbio.2012.09.029.
- [63] K. Basu, S. Appukuttan, R. Manchanda, and A. Sik, "Difference in axon diameter and myelin thickness between excitatory and inhibitory callosally projecting axons in mice," (in eng), *Cereb Cortex*, vol. 33, no. 7, pp. 4101-4115, Mar 21 2023, doi: 10.1093/cercor/bhac329.
- [64] A. R. Costa, R. Pinto-Costa, S. C. Sousa, and M. M. Sousa, "The Regulation of Axon Diameter: From Axonal Circumferential Contractility to Activity-Dependent Axon Swelling," (in eng), *Front Mol Neurosci*, vol. 11, p. 319, 2018, doi: 10.3389/fnmol.2018.00319.
- [65] P. Long and G. Corfas, "Neuroscience. To learn is to myelinate," (in eng), *Science*, vol. 346, no. 6207, pp. 298-9, Oct 17 2014, doi: 10.1126/science.1261127.
- [66] Z. Rao *et al.*, "Decellularized nerve matrix hydrogel scaffolds with longitudinally oriented and size-tunable microchannels for peripheral nerve regeneration," *Materials Science and Engineering: C*, vol. 120, p. 111791, 2021/01/01/ 2021, doi: <https://doi.org/10.1016/j.msec.2020.111791>.
- [67] S. Sornkamnerd, M. K. Okajima, and T. Kaneko, "Tough and Porous Hydrogels Prepared by Simple Lyophilization of LC Gels," *ACS Omega*, vol. 2, no. 8, pp. 5304-5314, 2017/08/31 2017, doi: 10.1021/acsomega.7b00602.
- [68] R. Abka-Khajouei, L. Tounsi, N. Shahabi, A. K. Patel, S. Abdelkafi, and P. Michaud, "Structures, Properties and Applications of Alginates," (in eng), *Mar Drugs*, vol. 20, no. 6, May 29 2022, doi: 10.3390/md20060364.
- [69] J. George, C.-C. Hsu, L. T. B. Nguyen, H. Ye, and Z. Cui, "Neural tissue engineering with structured hydrogels in CNS models and therapies," *Biotechnology Advances*, vol. 42, p. 107370, 2020/09/01/ 2020, doi: <https://doi.org/10.1016/j.biotechadv.2019.03.009>.

- [70] Y. Liu, X. Zhang, C. Xiao, and B. Liu, "Engineered hydrogels for peripheral nerve repair," (in eng), *Mater Today Bio*, vol. 20, p. 100668, Jun 2023, doi: 10.1016/j.mtbio.2023.100668.
- [71] Z. Liu *et al.*, "Low-Stiffness Hydrogels Promote Peripheral Nerve Regeneration Through the Rapid Release of Exosomes," (in eng), *Front Bioeng Biotechnol*, vol. 10, p. 922570, 2022, doi: 10.3389/fbioe.2022.922570.